UNIVERSITY OF BELGRADE

FACULTY OF MEDICINE

Nataša Z. Janović

ASSOCIATION OF

NASAL SEPTAL DEVIATION TYPES

WITH OBSTRUCTION SYMPTOMS SEVERITY

AND CHARACTERISTICS OF

NASAL AIRFLOW DYNAMICS

Doctoral Dissertation

Belgrade, 2020

УНИВЕРЗИТЕТ У БЕОГРАДУ

МЕДИЦИНСКИ ФАКУЛТЕТ

Наташа З. Јановић

ПОВЕЗАНОСТ ТИПОВА

ДЕВИЈАЦИЈЕ НОСНЕ ПРЕГРАДЕ

СА ТЕЖИНОМ ОПСТРУКЦИОНИХ СИМПТОМА

И КАРАКТЕРИСТИКАМА ПРОТОКА ВАЗДУХА

КРОЗ НОСНУ ДУПЉУ

докторска дисертација

Београд, 2020

PhD advisor:

Full Professor Marija Đurić, M.D., Ph.D.

University of Belgrade – Faculty of Medicine, Institute of Anatomy

Members of the evaluation committee:

1. Full Professor Tatjana Pekmezović, M.D., Ph.D.

   University of Belgrade – Faculty of Medicine, Institute of Epidemiology

2. Full Professor Dragan Mašulović, M.D., Ph.D.

   University of Belgrade – Faculty of Medicine, Clinical Center of Serbia, Department of Radiology

3. Full Professor Milovan Dimitrijević, M.D., Ph.D.

   University of Belgrade – Faculty of Medicine, Clinical Center of Serbia, Department of Otorhinolaryngology and Maxillofacial Surgery

4. Associate Professor Mirjana Stamenić, Ph.D.

   University of Belgrade – Faculty of Mechanical Engineering, Department of Process Engineering

5. Associate Professor Ivana Živanović-Mačužić, M.D., Ph.D.

   University of Kragujevac – Faculty of Medical Sciences, Department of Anatomy

Date of public defense: _____

Ментор:

Проф. Др Марија Ђурић, редовни професор

Универзитет у Београду – Медицински факултет, Институт за Анатомију

Чланови комисије за оцену и одбрану докторске дисертације:

1. Проф. Др Татјана Пекмезовић, редовни професор

    Универзитет у Београду – Медицински факултет, Институт за епидемиологију

2. Проф. Др Драган Машуловић, редовни професор

    Универзитет у Београду – Медицински факултет, Клиника за радиологију Клиничког Центра Србије

3. Проф. Др Милован Димитријевић, редовни професор

    Универзитет у Београду – Медицински факултет, Клиника за оториноларингологију и максилофацијалну хирургију Клиничког Центра Србије

4. Проф. Др Мирјана Стаменић, ванредни професор

    Универзитет у Београду – Машински факултет, Катедра за процесну технику

5. Проф. Др Ивана Живановић-Мачужић, ванредни професор

    Универзитет у Крагујевцу – Факултет медицинских наука, Катедра за Анатомију

Датум јавне одбране дисертације: _____

Abstract

ASSOCIATION OF NASAL SEPTAL DEVIATION TYPES WITH OBSTRUCTION SYMPTOMS SEVERITY AND CHARACTERISTICS OF NASAL AIRFLOW DYNAMICS

Aim: To investigate the association between the nasal septal deviation (NSD) morphology with nasal airway obstruction (NAO) symptom severity and the nasal airflow parameters.

Methods: The study included 225 patients with diagnosed NSD. The Nasal Obstruction Symptom Evaluation (NOSE) questionnaire was validated and cross-culturally adapted for the Serbian population and applied for the NAO assessment. Patients were examined by computed tomography (CT). CT images were used to classify NSD according to Mladina's classification and generate eight 3D computational models of the nasal cavity (one model without NSD, seven models representing each Mladina's NSD type). Inspiration was simulated by computational fluid dynamics (CFD) method and analyzed through CFD parameters (airflow partitioning, velocity, wall shear stress, pressure, nasal resistance (NR), heat flux (HF), turbulent kinetic energy (k), and airflow pattern). The obtained data were statistically analyzed.

Results: Although NOSE scores differed between patients with various Mladina's NSD types, the differences were not confirmed as statistically significant (B=0.837, p=0.261). There was no significant link between NSD types and NAO severity after applying additional morphology-based NSD classifications. CFD analysis showed that Mladina's NSD types induce various side asymmetry in all CFD parameters. CFD parameters that significantly correlated with the NOSE scores were: side asymmetry in NR (R=0.762, p=0.028), HF on the narrow nasal passage (R=-0.732, p=0.039), and ipsilateral k (R=-0.723, p=.043).

Conclusions: NSD morphology could not predict NAO severity. Side asymmetry in NR, reduction in HF and k in the narrow nasal passage may contribute to the NSD-related NAO perception.

Key words: Nasal septal deviation; Nasal airway obstruction; NOSE questionnaire; Computed tomography; Computational fluid dynamics; Mladina's classification system.

Scientific field: Medicine

Scientific subfield: Skeletal biology

Сажетак

ПОВЕЗАНОСТ ТИПОВА ДЕВИЈАЦИЈЕ НОСНЕ ПРЕГРАДЕ СА ТЕЖИНОМ ОПСТРУКЦИОНИХ СИМПТОМА И КАРАКТЕРИСТИКАМА ПРОТОКА ВАЗДУХА КРОЗ НОСНУ ДУПЉУ

Циљ: испитати повезаност типова девијације носне преграде (ДНП) са тежином опструкционих симптома и параметрима протока ваздуха кроз носну дупљу.

Метод: У студији је учествовало 225 пацијената са дијагностикованом ДНП. Упитник "Nasal Obstruction Symptom Evaluation (NOSE)" је валидиран и културално адаптиран за српску популацију и примењен за процену тежине опструкционих симптома. Снимци пацијената са апарата за компјутеризовану томографију (КТ) коришћени су за класификацију ДНП по Младининим критеријумима и за израду осам компјутерских модела носне дупље (један модел без ДНП, седам модела за сваки тип ДНП по Младини). Методом компјутеризоване динамике флуида (КДФ) симулирано је удисање на моделима и анализирани су параметри протока ваздуха кроз нос (дистрибуција удахнутог ваздуха између десне и леве стране, брзина, смичући напон, притисак, отпор, топлотни флукс (ТФ), турбулентна кинетичка енергија (ТКЕ) и образац протока). Добијени подаци су анализирани одговарајућим статистичким тестовима.

Резултати: Иако су уочене разлике у NOSE скоровима међу Младининим типовима ДНП, исте нису биле статистички значајне (B=0.837, p=0.261). Такође није детектована статистичка веза између NOSE скорова и типова ДНП класификованих према другим критеријумима. КДФ анализа је показала постојање разлика у свим КДФ параметрима између Младининих типова ДНП. КДФ параметри који су значајно статистички повезани са NOSE скоровима су асиметрија у отпору између десне и леве стране (R=0.762, p=0.028), ТФ (R=-0.732, p=0.039) и ТКЕ (R=-0.723, p=.043) на страни сужења.

Закључак: Није могућно предвидети тежину опструкционих симптома на основу морфологије ДНП. Асиметрија у отпору између страна носне дупље узрокована ДНП, редукција ТФ и ТКЕ на страни сужења могу бити одговорни за осећај опструкције.

Кључне речи: Девијација носне преграде; Носна опструкција; NOSE упитник; Компјутеризована томографија; Компјутеризована динамика флуида; Младинина класификација.

Научна област: Медицина

Ужа научна област: Биологија скелета

TABLE OF CONTENTS

Chapter   Page

1. INTRODUCTION

1.1. The nasal airway - anatomical background

The nose is a part of the upper airways with exceptionally complex geometry. It is divided into two approximately symmetrical nasal passages by the vertical mid-sagittal plate - the nasal septum. The anterior part of the nasal passages is enclosed by a pyramid-shaped structure, termed the external nose, which protrudes in the midline of the midface (Figure 1A). It is constructed from the paired nasal bones, pared upper and lower lateral, i.e. major alar cartilages, skin, and soft tissue (Standring et al., 2008). There are two openings on the base of the external nose, termed nostrils, through which the nasal passages communicate with the external environment. The rest of the nasal passages are placed between skull bones. Three paired bony nasal turbinates (the superior, middle, and inferior) protrude from the lateral nasal wall into nasal passages. Their medial surfaces and the lateral surface of the nasal septum enclose the common nasal meatus (Figure 1B) (Standring et al., 2008). Inferior and lateral to each turbinate, there are grooved parts of the nasal passages termed the inferior, middle, and superior nasal meatus (Figure 1B) (Standring et al., 2008). These nasal meatuses communicate with the nasopharynx through the posterior nasal openings - the choanae. All internal nasal structures are lined with ciliated and highly vascularized mucosa, rich in mucosal glands and goblet cells (Shimzu, 2013). In the submucosa of the anterior part of the nasal septum and the inferior turbinate lies erectile tissue composed of well-developed venous sinuses plexuses (Sahin-Yilmaz et al., 2011).

Figure 1. A. The structure of the external nose. B. Coronal section image through the nasal cavity (taken from Netter, 2004).

1.2. The nasal septum - anatomy

The nasal septum is constructed of various parts that differ in size, shape, and histological structure fit together like a mosaic (Figure 2). It is constructed from membranous, cartilaginous, and bony tissue (Lang, 1989). The membranous septum is the anterior part of the nasal septum (Lang, 1989; Standring et al., 2008). It is placed between the nostrils and composed of a fibro-fatty tissue (Lang, 1989). The cartilaginous part of the septum that lies posterior to the membranous part is made of the quadrangular cartilage (Figure 2) (Lang, 1989; Standring et al., 2008). The greatest part of the nasal septum, the bony septum, is composed of the vomer posteroinferiorly and the perpendicular plate of the ethmoid bone anterosuperiorly (Figure 2) (Lang, 1989; Standring et al.,

2008). To a minor extent, other bones also contribute to the construction of the bony septum: the nasal bones, the frontal bone, the sphenoid bone, the maxilla, and the palatine bones (Figure 2) (Lang, 1989; Standring et al., 2008).
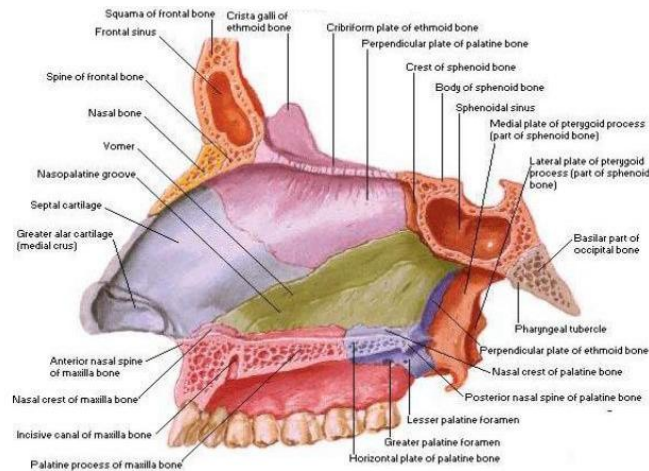
Figure 2. Structure of the nasal septum (taken from Netter, 2004).

1.3. Physiology of the nasal airflow

At rest, humans respire dominantly through the nose. A daily rate of inhaled air during calm breathing is about 10,000 liters (normal breathing frequency is 12-15 breaths per minute for adults, and the lungs' vital capacity is commonly 0.5L) (Barrett et al., 2016). One of the nasal cavity's main tasks is to prepare inhaled air for lungs and alveolar gas exchange. Therefore, the air has to be purified, warmed, and humidified. Other essential functions of the nose are olfaction and immune defense.

Prerequisites for the inhaled air's adequate filtration and conditioning are large nasal mucosal surface area, narrow airflow passages, sufficient contact time between the air and the mucosa, and turbulent airflow formation and regulation (Mlynski, 2013). The nasal septum and the turbinates provide a large nasal mucosal surface area. The presence of narrow - slit-like airflow channels formed by these structures creates an essential spatial precondition for optimal air - mucosa contact. During calm breathing, airflow is predominantly laminar (Lang et al., 2003). A thin layer of air closest to the nasal cavity walls meets nasal mucosa and receives heat and moisture from it, while the central part of airflow remains isolated (Mlynski, 2013). The simultaneous presence of turbulent airflow behavior allows more effective air conditioning and filtration. Namely, the air mixes the central part of the airstream with the peripheral air layer allowing all streaming molecules to meet nasal mucosa and, subsequently, adequate heat and moisture exchange (Mlynski, 2013). Optimally, the nose warms and humidifies inhaled air to almost 98% of alveolar conditions (Wolf et al., 2004). The airflow's turbulent behavior also promotes more efficient air filtration by depositing most of the air pollutants, dust, and germs to the nasal mucosa. Particles trapped in the mucus covering the mucosal surface are transported via ciliary activity toward the nasopharynx and the digestive system (Even-Tzur et al., 2008).

The complex anatomy of the nasal cavity strongly supports airflow dynamics. The nasal airway geometry enables bend, nozzle, and diffuser effects that trigger specific airflow patterns in different parts of the nasal airway (Figure 3) (Mlynski et al., 2001). Good configuration of the airstream is essential for achieving efficient nasal physiological functions (Mlynski et al., 2001; Clement & Gordts, 2005). The initial parts of the nasal cavity (the nasal vestibule and the nasal isthmus) have a curved tube shape, which diameter gradually narrows toward the isthmus nasi (the

narrowest part of the nasal cavity). Curved tube redirects the airflow for 30° to 40° toward the turbinates area (bend effect) (Mlynski et al., 2001). A gradual decrease in cross-section of the same area modifies the inhaled air's turbulent behavior into laminar and increases flow velocity, mainly through the isthmus nasi (nozzle effect) (Mlynski et al., 2001). An abrupt increase in cross-sectional area in the anterior nasal cavum (the area between the isthmus nasi and the head of the middle turbinate) naturally causes a transition from laminar to turbulent airflow and deceleration of the flow (diffuser effect) (Mlynski et al., 2001). In the turbinate area, the lower air velocity and swirling of the air allow prolonged air-mucosa contact and consequent optimal heat and moisture exchange (Mlynski, 2013). In the choana region, the airflow pattern becomes laminar again due to a decrease in the cross-section area (nozzle effect) (Mlynski et al., 2001). Eventually, in the nasopharynx, purified and almost fully saturated airstreams converge into single bulk of air with redirection of flow for 90° toward the lower airways (bend effect) (Mlynski et al., 2001; Mlinski, 2013).
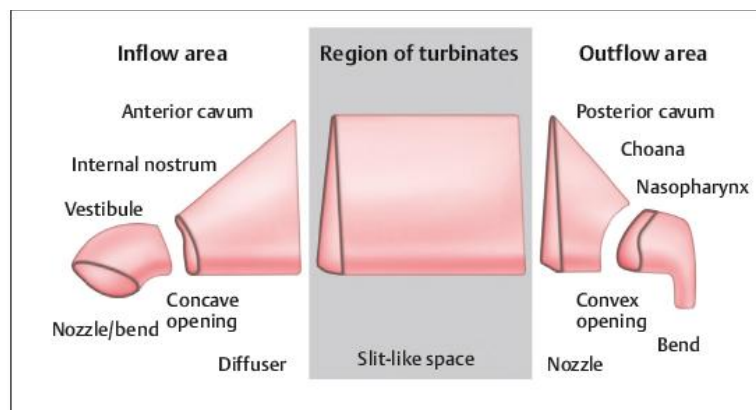
Figure 3. Schematic representation of structural elements of the nose
(taken from Behrbohm, 2015)

The crucial morphological structure for turbulence formation and regulation is erectile tissue located in the anterior part of the nasal septum and the head of the inferior turbinate (Cauna, 1982; Mlynski et al., 2001). The erectile tissue is normally subjected to reciprocal, spontaneous, and cyclic vasodilatation and vasoconstriction that causes reversible changes of the anterior nasal cavum diameter. This phenomenon, known as the nasal cycle, induces periodic shifting of the dominant breathing route between the right and left nasal passage (Kayser, 1895; Stoksted, 1953). The changes in the anterior nasal cavum diameter associated with the nasal cycle create the conditions for the emergence of turbulence and alterations in nasal airflow resistance (Mlynski et al., 2001). During the "working" phase of the nasal cycle, erectile tissue decongestion and subsequent unilaterally enlarged cross-sectional area of the anterior nasal cavum cause the turbulence intensity elevation and the airflow resistance decrease (Lang et al., 2003). These conditions allow adequate cleaning and conditioning of the inhaled air on the dominant breathing side (Lang et al., 2003). Simultaneously, erectile tissue congestion in the contralateral nasal passage (the "resting" phase of the nasal cycle) reduces the anterior nasal cavum diameter inducing mainly laminar flow patterns and an increase in airflow resistance (Lang et al., 2003). Regardless of the nasal cycle phase, the overall hydraulic diameter of the nasal passages, nasal respiratory work, and total nasal airflow resistance normally remain constant (Cole, 1989; Lang et al., 2003). The nasal cycle-related unilateral turbulence "switch on" and "switch off" is also essential for maintaining the thermal and moist gradients between mucosa and inhaled air. During the "resting" phase, the nasal mucosa recovers from the turbulent airflow's dehydrating effect and regains thermal energy and moisture (Beule, 2010). Therefore, the critical requirement for the inhaled air's continuous conditioning is the accumulation and storage of thermal energy and moisture during the "resting" phase for the upcoming "working" phase.

Furthermore, the airflow's turbulent behavior was also proven as a crucial factor in nasal patency perception due to its impact on the nasal mucosal cooling (Lindemann et al., 2004; Sozansky & Houser, 2014). Swirling enables the "cold" air from the airstream center to get into contact with mucosa by disrupting the already warmed thin air layer near the mucosal wall (Mlynski et al., 2001). When the "cold" air meets nasal mucosa, the temperature of the epithelial lining fluid decreases as well as the epithelial membrane permeability. This causes signal generation in the menthol sensitive (TRPM8) receptors (Baraniuk, 2011). The arrival of a "cold" impulse into the brainstem is perceived as a patent nasal passage, whereas lack of this impulse evokes the opposite sensation - nasal airway obstruction (NAO) (Baraniuk, 2011).

1.4. Nasal septal deviation: definition and classification

Nasal septal deviation (NSD) is an anatomical variation of the septal plate, including deflection from the midline and/or deformation of the septal shape (Mladina, 1990). The prevalence of NSD in the literature varies between 20% and 90% depending on the applied examination techniques, differences in the targeted population, age groups, and application of different classification systems (Lang, 1989; Smith et al., 2010; Mohebbi et al., 2012; Taghiloo & Halimi, 2019). Available literature suggests a slight gender difference in NSD prevalence, commonly diagnosed in males than in females (Mladina et al., 2008).

Table 1. The most frequently used classifications of the NSD

Classification of NSD	NSD type	Diagnostic criteria
Mladina's classification	I	vertical deviation in the nasal valve region that does not change physiologic valve angle (15˚)
	II	vertical deviation in the nasal valve region that change physiologic valve angle (<15˚)
	III	deviation inside the nasal cavity at the level of the head of the middle turbinate
	IV	bilateral deviation with the anterior curve in the region of the nasal valve and posterior curve more inside in the nasal cavity
	V	bony spur with straight septum
	VI	deviation parallel to the horizontal plate with basal septal crest and "gutter" at the opposite side
	VII	combination of previous types
Guyuron's classification	I	tilt deformity of the nasal septum
	II	deviation in the form of letter "C" in the anteroposterior direction
	III	deviation in the form of letter "C" in the cephalocaudal direction
	IV	deviation in the form of letter "S" in the anteroposterior direction
	V	deviation in the form of letter "S" in the cephalocaudal direction
	VI	nasal septum with localized deviations or large spurs
NSD location-based classification	caudal	nasal septal deviation in front of the head of the inferior turbinate
	anterior	NSD between anterior edges of the inferior turbinate and the middle turbinate
	media	NSD between anterior and posterior edge of the middle turbinate
Structure-based classification	cartilaginous	deviation of the cartilaginous part of the nasal septum
	combined	deviation of the cartilaginous and bony part of the nasal septum
	bony	deviation of the bony part of the nasal septum
NSD angle-based classification	mild	deviation with the maximal angle from 0˚ to 9.99˚
	moderate	deviation with the maximal angle from 10˚ to 14.99˚
	severe	deviation with the maximal angle >15˚

Many NSD classification systems are described in the literature, each focusing on some different aspects of NSD morphology (Table 1). The NSD classification proposed by Mladina is considered the most detailed (Mladina et al., 2008). This comprehensive and anatomically based classification divides NSD into seven types that include complicated morphological variants of the nasal septum frequently neglected by other simplified classifications (Mladina et al., 2008). Guyuron's classification consists of six different types of NSD that require diverse surgical approaches (Guyuron et al., 1999). The classification used by Liu et al. (2012) contains three groups of deviation (caudal, anterior, and media) depending on the location of the most prominent point of the NSD. Another classification based on which septal structure is deformed categorizes NSD into cartilaginous, bony, and combined cartilaginous-bony type. According to the maximal NSD angle, classification divides NSD into mild, moderate, and severe (Savovic et al., 2014; Serifoglu et al., 2017). However, none classification is widely accepted and routinely used in everyday Ear, Nose, and Throat (ENT) practice.

1.5. Symptoms and therapy of the NSD

NSD is the leading structural cause of nasal airway obstruction (NAO). Patients with NSD may also experience additional symptoms such as sleep disturbance, daytime somnolence, fatigue, altered sense of smell, nose bleeding, and headache (O'Reilly et al., 1996; Cuddihy & Eccles, 2003; Chen et al., 2009; Liu et al., 2012; Gunbey & Karabulut, 2014), which may also contribute to the altered quality of life. Therefore, surgical correction of the nasal septum or septoplasty is considered the definitive therapy of NSD related NAO.

Approximately 95,000 and 260,000 septoplasties are performed each year in European countries and the United States, respectively (Baumann, 2010; Bhattacharyya, 2010; Van Egmond et al., 2015; Thomas et al., 2016). Although septoplasties are performed for thousands of years (first recorded on Eberes Papyrus, 3500 BC, Egypt), there is still a knowledge gap in this surgery field (Hinderer, 1971; Van Egmond et al., 2015). The primary issue is the lack of a diagnostic tool that could estimate NAO's level objectively and correlate well with patients' symptoms and clinical findings (Andre et al., 2009). Currently, available clinical methods, e.g. acoustic rhinometry, rhinomanometry, and peak nasal inspiratory flow, have been provided conflicting results that brought their objectivity for assessing the NSD-NAO relationship into question. Additionally, lack of strong evidence base for selection of septal surgery candidates, frequent reoperations, and dissatisfaction with surgery outcomes (up to 35%) cast a shadow on septoplasty effectiveness (Becker et al., 2008; Aziz et al., 2014; Van Egmond et al., 2015; Delaney, 2018). Thus, in the absence of internationally accepted guidelines, the decision for septoplasty is solely based on the ENT surgeon's experience.

The self-assessment of NAO severity through a health-related-quality-of-life questionnaire plays an important role in evaluating the NAO burdensome. The Nasal Obstruction Symptom Evaluation (NOSE) questionnaire is specifically designed to evaluate the quality of life in patients with NAO (Table 2) (Stewart et al., 2004). The NOSE questionnaire consists of five obstruction-related questions that measure the severity of complaints experienced during the last month (Stewart et al., 2004). Answer to each question is scored using 5-point Likert's scale system (0 - not a problem, 1 - very mild problem, 2 - moderate problem, 3 - fairly bad problem, and 4 - severe problem) (Stewart et al., 2004). The initial score is multiplied by 5 so that the final score may range from 0 (absent NAO) to 100 (the most severe NAO). It has been confirmed as valid, reliable, and sensitive to change in a patient's clinical status (Stewart et al., 2004). Up to date, many countries validated and cross-culturally adapted the NOSE questionnaire in order to apply it in everyday clinical practice and research (Bezerra et al., 2011, Marro et al., 2011; Mozzanica et al., 2013; Dong et al., 2014; Lachanas et al., 2014; Larrosa et al., 2015; Urbančič et al., 2016; Van Zijl et al., 2017; Amer et al., 2017).

Table 2. The Nasal Obstruction Symptom Evaluation (NOSE) instrument
by Stewart et al. (2004)

Over the past <u>1 month</u>, how much of a <u>problem</u> were the following conditions for you?					
	Please <u>circle</u> the most correct response				
	Not a problem	*very mild problem*	*moderate problem*	*fairly bad problem*	*severe problem*
1. Nasal congestion or stuffiness	0	1	2	3	4
2. Nasal blockage or obstruction	0	1	2	3	4
3. Trouble breathing through my nose	0	1	2	3	4
4. Trouble sleeping	0	1	2	3	4
5. Unable to get enough air through my nose during exercise or exertion	0	1	2	3	4

1.6. Association between NSD morphology and nasal obstruction

In the era of evidence-based medicine, researchers aim to find a diagnostic test that could serve as an objective indicator of the NSD-related NAO severity and strongly support the clinical decision that the patient should be treated surgically. Initially, many studies were focusing on the connection between NSD morphology and NAO symptoms. Although the anterior rhinoscopy and nasal endoscopy are the gold standards for clinical evaluation of NSD, these methods are not measuring techniques and, more importantly, depend on clinicians' experience (Sedaghat et al., 2014; Wotman & Kacker, 2016). Inter-observer variability related to the application of these technique should affect the determination of the precise NSD location, the NSD angle, and consequently the clinical impact of the NSD (Suh et al., 2008; Aziz et al., 2014). The particular disadvantage of these techniques is posterior NSD misjudgment because posterior parts of the septum could not be seen by anterior rhinoscopy, while nasal endoscopy often underestimates posterior deviations (Lebowitz et al., 2001; Mladina et al., 2008). In addition, a small variation in endoscope insertion angle into nasal cavity might affect endoscopic findings and compromise repeatability and accuracy of the NSD assessment (Suh et al., 2008; Lee et al., 2013).

Another technique that was also used to estimate the geometry of the nasal passages and the NSD was acoustic rhinometry. While acoustic wave reflections may evaluate anterior diameter of the nasal passages with high sensitivity, estimation of the deep portions of the nasal passages again appeared as less accurate (Aziz et al., 2014). Namely, this technique tends to overestimate the diameter of the posterior nasal passages (behind the ostiomeatal complex) (Cakmak et al., 2005; Tarhan et al., 2005), as well as the decongestive effect on the nasal mucosa (Cankurtaran et al., 2007). Furthermore, studies that applied acoustic rhinometry reported a discrepancy between acoustic rhinometry and clinical findings in NSD patients (Mamikoglu et al., 2000) and a low correlation with patient-reported NAO severity (Kahveci et al., 2012; Prus M et al., 2017).

Recent computed tomography (CT) analysis of the NSD morphology appeared as a promising method to provide an objective parameter that could explain the severity of NAO symptoms. Such expectations were based on many CT advantages that include objectivity, detailed insight into the septum morphology, reproducibility, and the possibility to measure various parameters directly on the CT station. Currently, third-party payors in some Western countries request CT imaging to confirm NAO severity in NSD patients before authorizing financial support for septoplasty. However, the link between CT-assessed NSD morphology and NAO severity is still not clear enough. In the study of Lee et al. (2013), a significant correlation was revealed between NSD angle and NAO symptoms only at the ostiomeatal unit level. A similar link was found

between NAO symptoms and the cross-sectional areas of the nasal passages at the ostiomeatal unit and choana levels. CT parameters measured by Lee et al. (2013) did not show any association with NOSE scores at other sites throughout the nasal cavity. Savovic et al. (2014)noticed that an NSD angle greater than 10° significantly correlates with NAO perception at the deviation side. By contrast, Ardeshirpour et al. (2016) argued against the utility of CT imaging for NSD morphology assessment because they failed to detect any connection between NOSE scores and maximal NSD angle and location of NSD (in the anterior, middle, and posterior segment).

Regardless of the contradictory results of the previous CT studies, the authors considered the NSD angle and cross-sectional area of nasal passages as the only CT parameters relevant for NAO. The full potential of the CT imaging to display detailed morphology of NSD seemed to be underutilized. Namely, other morphological characteristics of NSD such as single or double curve, presence of the spur, which septal structure is affected by deviation (bone or cartilage) were not analyzed in the context of the NAO severity. Therefore, it is still unclear whether some of the abovementioned morphological characteristics of the NSD, if any, could serve to predict NAO severity.

1.7. Impact of NSD on nasal airflow patterns and NAO perception

The presence of NSD disturbs the symmetry of the nasal passages and makes nasal airway geometry even more complicated. This fact leads to a conclusion that NSD could induce atypical airflow patterns and consequently impair the nasal function and nasal patency perception. However, there is still a puzzling question of why structurally severe NSD may be symptomless, and, by contrast, why some patients with a seemingly negligible NSD may suffer from severe NAO. A new light was recently shed on the intriguing association between NSD and subjective perception of NAO severity when the research direction was changed from NSD morphology to physical aspects of the nasal airflow. Rhinomanometry (RMM) and computational fluid dynamics (CFD) were techniques that provided new objective parameters related to the nasal airflow that could be correlated with NAO severity in NSD patients.

Rhinomanometry measures the nasal airflow and pressure throughout the nasal airway, allowing assessment of the nasal airflow resistance (NR) (Clement, 1984). Clinical RMM studies found increased NR at the deviation side, which was in accordance with experimental studies (Naito et al., 1990; Grutzenmacher et al., 2006; Andre et al., 2009; Haavisto & Sipila, 2013). Besides, such an increase in NR was site-dependent (Cole et al., 1988). Even a small deflection of the nasal septum at the internal nasal valve (INV) region harshly raised NR, whereas more severe deformations inside the bony cavum minimally affected NR (Cole et al., 1988; Dinis & Haider, 2002). However, the diagnostic value of the RMM in NAO severity estimation is limited (Andre et al., 2009). Although considered as an objective tool for NAO evaluation, inconsistent RMM results in repeated measurements indicated poor reliability and reproducibility of this technique (Courtiss & Goldwyn, 1983; Clement & Gordts, 2005). Moreover, many studies demonstrated poor connection of RMM-derived NR with NAO symptoms (Naito et al., 1988; Tomkinson & Eccles, 1996; Bermuller et al., 2008; Mlynski & Beule, 2008; Baumann, 2010).

Application of a more advanced method, i.e. CFD, provides a set of new variables that reflect nasal airflow patterns more reliably and could explain NAO symptom severity. CFD method is adopted from mechanical engineering and has already been used successfully in cardiovascular physiology and pathology (Goubergrits et al., 2012; Goubergrits et al., 2013). The method is based on physical conservation laws (mass, momentum, and energy) and uses computer-assisted numerical calculations and mathematical algorithms to resolve and analyze fluid flow in complicated geometries such as nasal airspace (Leong et al., 2010; Leite et al., 2019). CFD allows breathing simulations on anatomically realistic three-dimensional (3D) computational models of the nasal airspace and precise spatial visualization and analysis of the airflow patterns in the entire

nasal cavity and the selected segment. CFD is a valid and reliable method for nasal airflow evaluation, confirmed in experimental and RMM studies (Garcia, 2007; Zachow et al., 2009). CFD based airflow analysis provides a set of airflow components such as velocity, pressure, turbulent kinetic energy, wall shear stress, temperature, heat flux, and flow partitioning. Up to date, the CFD method has been used to study characteristics of the physiologic airflow pattern, alternation of airflow patterns pre and postsurgery, odorant transport, and drug delivery.

Only a few papers in the literature are dealing with the NSD effects on the nasal airflow (Liu et al., 2012; Kim et al., 2014), whereas the majority of CFD studies investigated pre and post septoplasty airflow changes (Rhee et al., 2011; Rhee et al., 2012; Kimbel et al., 2012; Kimbel et al., 2013). Nevertheless, more or less irregular and asymmetrical airflow pattern was noticed in nasal cavities with NSD. Novel studies recognized middle airflow and heat flux as CFD-derived airflow parameters that correlated well with subjective nasal patency (Kimbell et al., 2013; Zhao & Jiang, 2014) while conflicting results were obtained for CFD-derived nasal resistance (Kim et al.; 2014). Generally, all these studies investigated only simple nasal septum morphologies (plain curvature), deliberately omitting to model complicated septum geometries such as spur and double-curved nasal septum. Therefore, the exact relationship between NAO symptoms' presence and severity in different morphological NSD types and resulting airflow dynamics still is not clear enough. Some studies used CT images of a cadaver to make a 3D model, neglecting postmortem tissue shrinkage and a consequent increase of the nasal cavity diameter (Ozlugedik et al., 2008). Moreover, some authors did not pay attention to nasal cycle effects on the airflow dynamics (Radulsco et al., 2019). In contrast, others emphasized the importance of applying nasal decongestants before the CT examination to eliminate nasal mucosal swelling caused by the nasal cycle (Hildebrandt et al., 2013).

2. RESEARCH GOALS

The goals of this research were the following:

1. to conduct cross-cultural adaptation and validation of the Nasal Obstruction Symptom Evaluation (NOSE) questionnaire for Serbian population in order to use it to evaluate quality of life in patients with NAO,

2. to estimate the prevalence of the NSD in the Serbian population, and the prevalence of each NSD type according to Mladina's classification system,

3. to estimate the severity of the nasal obstruction symptoms using the NOSE scale among patients with different NSD types,

4. to explore the association between NOSE scores and various morphological types of NSD classified by the five classification systems commonly applied in the clinical practice and research,

5. to develop eight 3D computer models of the nasal cavity (one model with the straight nasal septum of a symptomless patient and seven models representing each Mladina's NSD type) and to simulate inspiration using computational flow dynamics (CFD).

6. to analyze CFD-based nasal airflow characteristics in straight septum model and seven NSD models quantitatively (airflow partitioning, velocity, pressure, nasal resistance, wall shear stress, temperature - heat flux, and turbulent kinetic energy) and qualitatively (presence of laminar and turbulent flow, vortices).

7. to explore the association between NOSE scores and relevant quantitative airflow parameters (nasal resistance, heat flux, turbulent kinetic energy) calculated in eight 3D nasal cavity models.

3. MATERIALS AND METHODS

3.1.Ethical approval

The study was approved by the Ethic Committee of the Faculty of Medicine, No. 29/V-1. All procedures performed in this research involving human participants were in accordance with the institutional and national research committee's ethical standards and with the 1964 Helsinki declaration and its later amendments or comparable ethical standards.

3.2.Study design

All parts of this research were designed as a prospective. Study participants were recruited at the Department of Diagnostic Radiology, Faculty of Dental Medicine, University of Belgrade, in order to obtain the most representative sample of the general population and due to the high frequency of head and neck CT examinations. All participants were older than 18 years and gave written informed consent for participation in the study.

3.3. Cross-cultural adaptation and validation of the NOSE scale into the Serbian language

3.3.1. Cross-cultural adaptation process

Written consent to perform a cross-cultural adaptation of the NOSE scale into the Serbian language was obtained from the author of the original version of the questionnaire. Standard techniques for cross-cultural adaptation and validation of the health-related-quality-of-life instruments were applied (Beaton et al., 2000; Sousa & Rojjanasrirat, 2011; Lauffer et al., 2013). Two independent Serbian native-speakers with academic knowledge of English performed forward translations. Both translated versions were reconciled into a single version by an expert committee. Subsequently, two persons performed independent back translations of this version of the questionnaire. The first person was an English native speaker with a medical education, who was also fluent in the Serbian language. Another person was a bilingual speaker, the English teacher whose first language is Serbian. None of the back translators had insight into the original scale. These versions were further adjusted into a single version. The expert board reviewed all reports once again and created the pre-final version of the scale. This version was pretested on a group of 30 randomly selected patients. Each patient completed the pre-final version of the NOSE-s scale. According to the technique suggested by Reichenheim & Moraes (2007), the meaning of each question was explored by asking patients to rephrase them. Proper understanding and approval of the instrument was surveyed by achieving more than 90 percent of understanding (Reichenheim & Moraes, 2007). Thus, the final version of the Serbian NOSE scale (NOSE-s) scale was created (Table 3).

3.3.2. NOSE-s scale validation

A general rule of thumb was applied as a standard procedure for determining sample size for psychometric validation of the NOSE-s scale (Stewart et al., 2004; Sousa & Rojjanasrirat, 2011; Lachanas et al., 2014; Urbančič et al., 2016; Van Zijl et al., 2017;). This rule requires the inclusion of10 subjects per question of the scale (Sousa & Rojjanasrirat, 2011). Since the NOSE scale

contains five questions, 50 participants constituted the study group and the control group, respectively (100 participants in total). Participants for each group were gathered consecutively and sex- and age-matched. The NOSE-s scale was self-administrated in order to avoid possible investigator influence on patients' responses. The time needed to complete the questionnaire was measured for each patient.

Table 3. The Serbian version of the Nasal Obstruction Symptom Evaluation (NOSE-s) scale

У последњих <u>месец дана</u>, колики <u>проблем</u> су Вам представљале следеће тегобе? Молимо Вас да <u>заокружите</u> одговор који најбоље описује Ваше тегобе		*Без тегоба*	*Веома благе тегобе*	*Средње изражене тегобе*	*Изражене тегобе*	*Веома изражене тегобе*
1.	Осећај запушености носа	0	1	2	3	4
2.	Осећај непроходности носа	0	1	2	3	4
3.	Отежано дисање кроз нос	0	1	2	3	4
4.	Лош сан	0	1	2	3	4
5.	Отежано дисање кроз нос приликом изражене физичке активности	0	1	2	3	4

The study group was selected among patients clinically diagnosed with NSD by an ENT specialist and referred to the CT examination of the nose and paranasal sinuses. These patients had symptoms of chronic NAO persisting four weeks after the trial of medical therapy. Patients with a history of surgery (septoplasty, septorhinoplasty, septoplasty combined with a paranasal sinus surgery), craniofacial syndromes, facial bone trauma, adenoid hypertrophy, sleep apnea syndrome, acute or chronic sinusitis, sinonasal malignancy, radiotherapy of the head and neck, and uncontrolled asthma, were not included in the study.

Patients enrolled in the control group were referred to the CT examination of the head and neck due to other non-rhinologic diagnoses. These patients did not complain of any rhinological symptoms and had no NSD, which was confirmed by CT scans. None of these patients had a history of facial anomalies, facial trauma, and/or sinonasal malignancy.

The test-retest procedure was carried out among 30 randomly selected patients from the study group within two weeks. Forty patients from the study group underwent septoplasty, while ten patients refused surgical intervention. Three months after surgery, 33 patients completed the NOSE-s questionnaire again. The rest of the seven patients were lost to follow-up.

3.4. The NSD prevalence in the Serbian population

The NSD prevalence was estimated on 386 participants. The sample size was calculated according to standard method for prevalence studies using the following formula (Daniel, 1999; Naing et al., 2006):

$$n = Z^2 P (1 - P)/d^2$$

where n is a sample size, Z is the level of confidence (Z value is 1.96 for the level of confidence of 95%), P is the expected prevalence, and d is the precision (the value of 0.05 was recommended if the expected prevalence is between 10% and 90%). Since the prevalence of the NSD varies in different studies from 19.4% to 89.2%, we used the value of 0.5 (50%) because it gives the largest sample size.

Selection of participants was performed among patients who were referred to the CT examination of the head and neck region. The following inclusion criteria were applied: CT scanning includes the whole nasal cavity in the field of view, the absence of facial anomalies, negative history of facial trauma, nasal surgery, and sinonasal malignancies.

All patients were examined by the same CT devise Siemens Somatom Sensation 16 (Munich, Germany). Intranasal decongestants were administered 15 min before the CT examination to minimize the nasal cycle's effect on the geometry of the nasal passages. During the CT examination, patients were lying in a supine position. Regardless of the examination protocol and the examined head and neck region, native scans through the nasal cavity were reconstructed from raw CT data in 0.75 mm thick axial sections parallel to the hard palate using bone window settings. Obtained axial CT images of the nasal cavity were then imported into multiplanar reformation software, which was used to analyze nasal septum morphology in the axial and frontal plane simultaneously. Analyses were performed directly on the Siemens CT workstation.

The presence of the NSD was recorded and classified according to Mladina's classification system. The distinction between Mladina's NSD type 1 and 2 was based on the internal nasal valve (INV) angle degree. The INV angle was measured as follows. The plane parallel to the superior border of the cartilaginous nasal dorsum was set on the mid-sagittal CT image (Figure 4A). Perpendicular to this plane, the coronal oblique plane was set running through the INV region. The section image closest to the head of the inferior nasal turbinate was selected as a reference image for the INV angle measurement (Figure 4B). The angle was measured between the nasal septum and the lateral nasal wall.
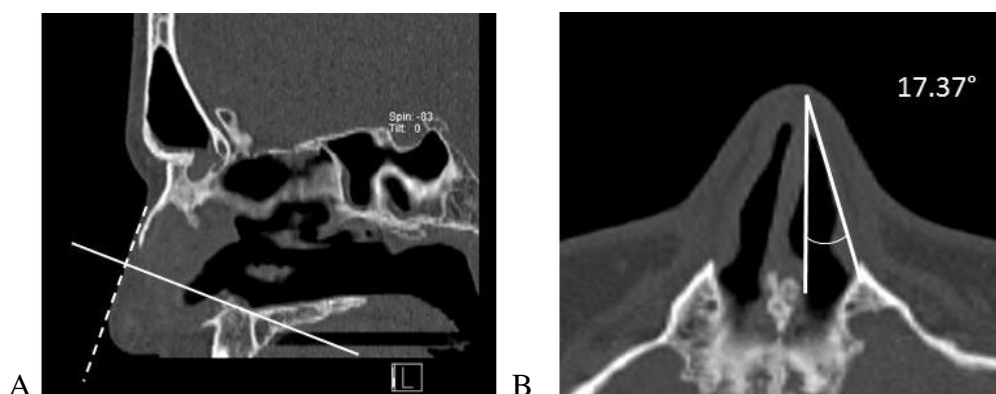
Figure 4. CT method applied for the INV angle measurement. A. The dashed line on the mid-sagittal CT image fits the superior border of the cartilaginous nasal dorsum. An oblique coronal section perpendicular to the dashed line was set for the INV angle measurement. B. The INV angle measurement demonstration on the representative CT image.

3.5. Estimation of nasal obstruction symptoms severity

In order to investigate the association between NAO severity and NSD morphology, additional exclusion criteria were applied for participants with CT confirmed NSD. Patients who had a history and/or CT finding of any condition that may cause NAO were excluded from the initial study group. These conditions included: anatomical variations of the nasal cavity structures (e.g. paradoxical middle turbinate, concha bullosa), turbinate hypertrophy, rhinosinusitis, nasal polyps, adenoid hypertrophy, asthma, chronic obstructive lung disease. Therefore, the study group was reduced to 225 patients.

These patients fulfilled the NOSE-s questionnaire and self-assessed severity of the nasal obstruction experienced in the last month. The total NOSE score was calculated as a sum of the five-question responses multiplied by 5.

Besides Mladina's classification, NSDs of 225 patients were additionally classified according to the criteria of the other four classification systems listed in Table 1. These classifications were selected from the literature due to their frequent use in clinical researches and easy applicability on the CT. Since these classifications consider NSD from different aspects, various anatomical details of the deviated nasal septum that potentially could cause NAO symptoms were incorporated in the analysis.

Considering that one of the applied classifications is based on the NSD angle (Table 1), the maximum degree of the angle was measured on CT images according to the method applied in previous studies (Figure 5) (Savovic et al., 2014; Ardeshirpour et al., 2016). The angle was measured between the line connecting the crista galli with the nasal crest and another line that was drawn from the crista galli to the greatest deflection point of the NSD. For double-curved NSD, a greater value was taken into account.
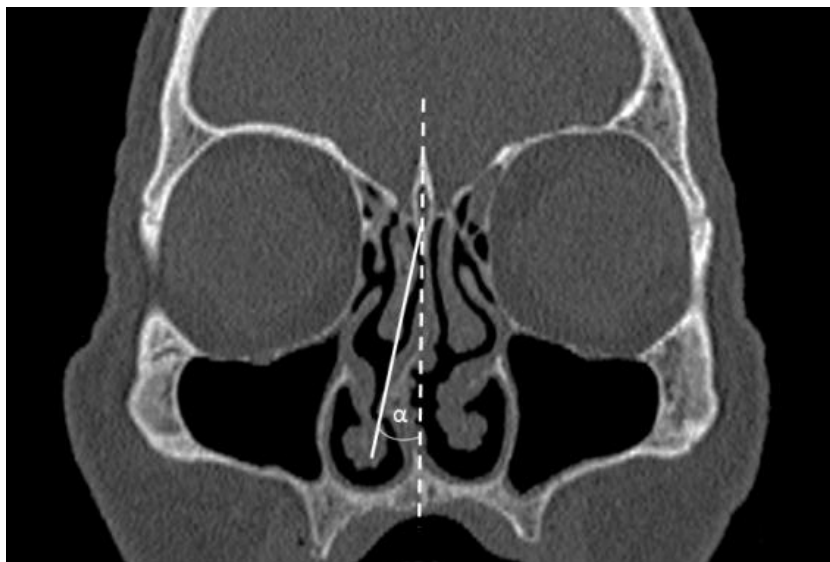
Figure 5. Measurement of the maximum NSD angle on coronal CT image.

3.6. Development of 3D computer models of the nasal cavity

3.6.1. Extraction of the nasal airspace from CT images

The development of 3Dcomputer models of the nasal cavities from CT images and CFD analyses were performed at the Department for Process Engineering and Department of Fluid Mechanics, Faculty of Mechanical Engineering, University of Belgrade. Eight 3D computational models were created from 0.75 mm thick CT scans. The first model represented the nasal cavity of a symptomless patient with a straight septum, while the other seven models were the most representative cases for each Mladina's NSD type (Figure 6). Types 1, 2, 3, and 5 were left-sided, whereas the type 6 NSD was right-sided. Type 4 had a right-sided anterior and left-sided posterior curvature. Type 7 was a combination of right-sided type 2 and left-sided type 5.
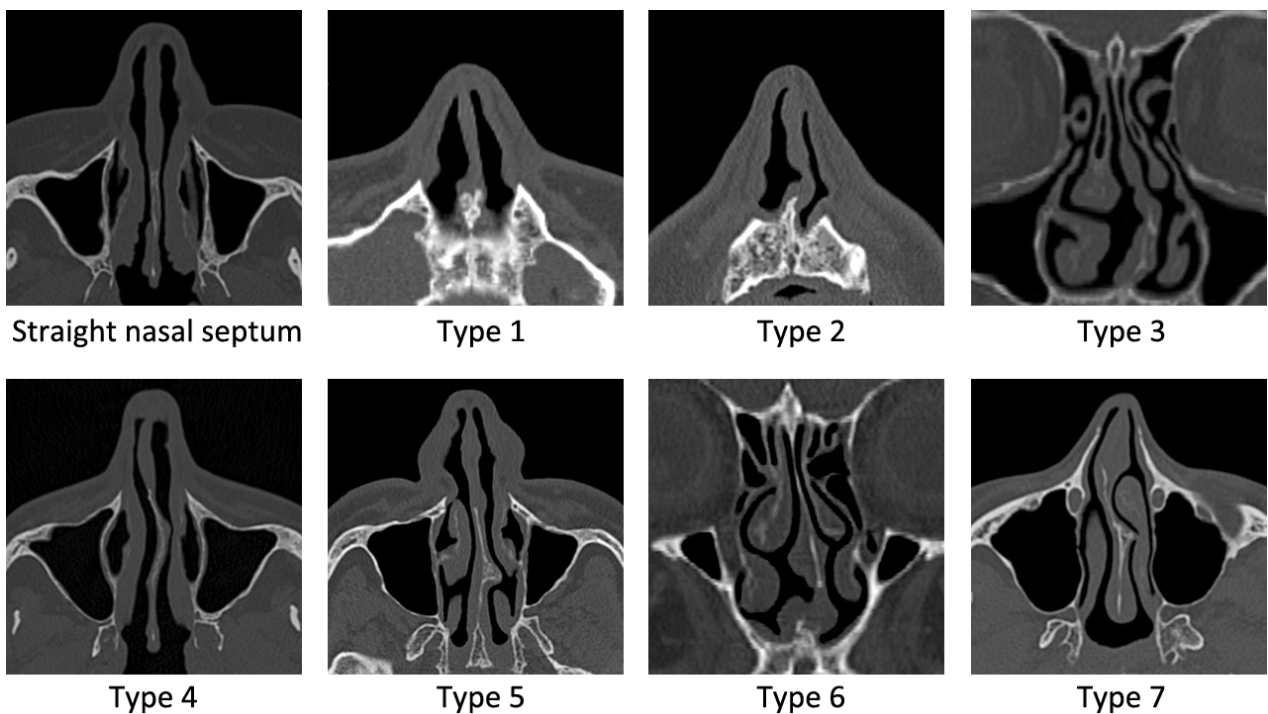
Figure 6. CT images of patients with the straight nasal septum and seven Mladina's NSD types selected for generation of 3D computer modeling

DICOM files were imported into 3D Slicer software (4.1.2, open-source, National Institute of Health) to generate anatomically accurate geometry of the nasal cavity and paranasal sinuses (Figure 7). The nasal and paranasal airspace was extracted automatically by selecting pixels with Hounsfield Units ranging from -1024 to -512.12. A segment editor was used to delineate nasal passages. Pixels selected outside the nasal passages and paranasal spaces were removed manually. The final 3D models included nasal passages from the nostrils to the oropharynx and were saved in *.stl files (Figure 7).

.dicom files

CT Siemens Somatom Sensation 16

*.stl file

3D Slicer software
(4.1.2., open-source, National Institute of Health)

ICEM CFD® software
(ANSYS, InC., Canonsburg, PA, USA, version 11.0)

S4   S5   S3   S2   S1   S6   S7   S8   S*

CAD CAM
software
(CATIA V5R21,
Academic licensed)

cfMesh application
OpenFOAM software
(version foam-extend 4.1)
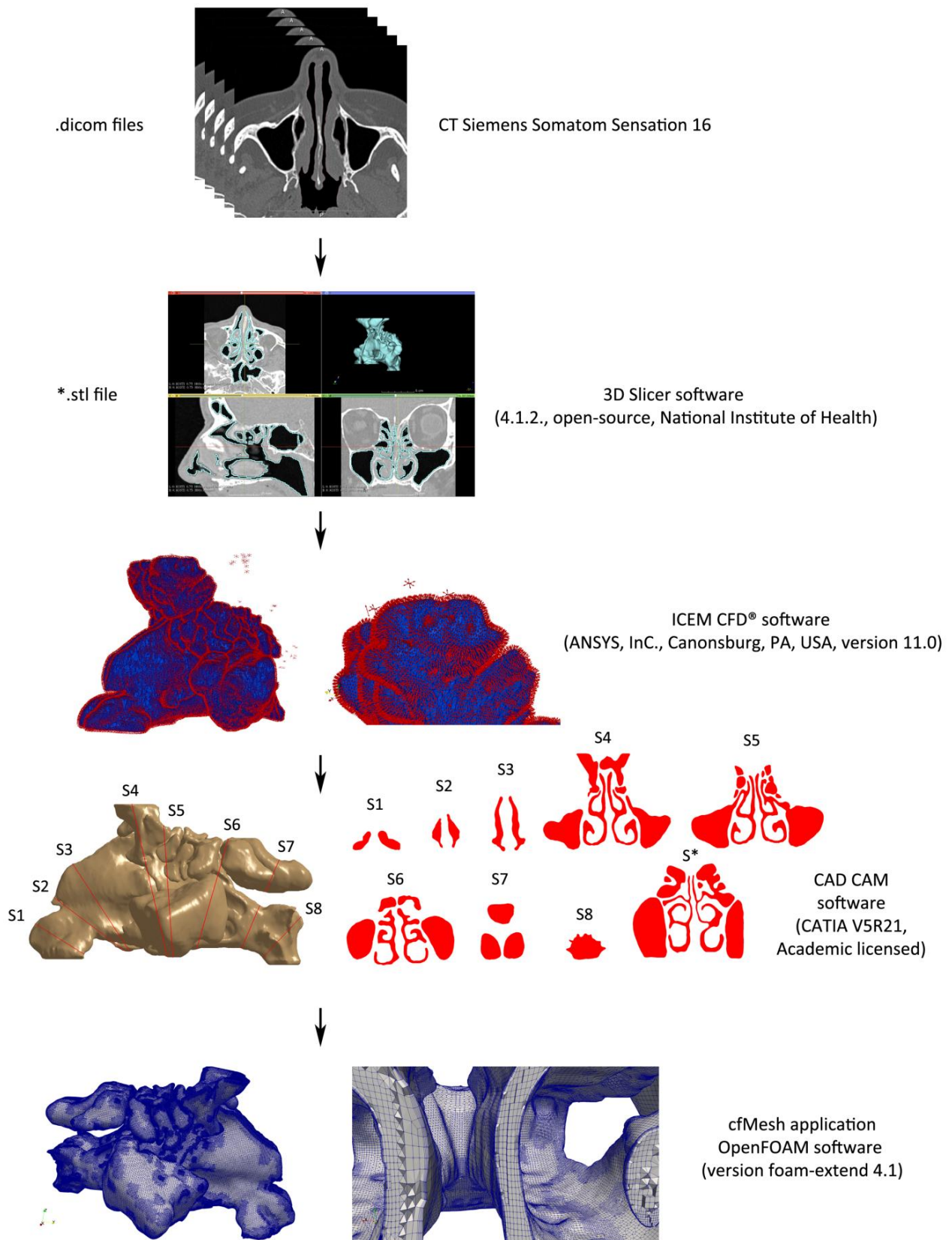
Figure 7. Steps in the generation of 3D computer models of the nasal cavity from CT images

The initial *.stl files generated in 3D Slicer software were imported in ICEM CFD® software (ANSYS, InC., Canonsburg, PA, USA, version 11.0) in order to refine the geometry of 3D models before mesh generation (Figure 7). The geometry refinement included detection and deletion of small volumes outside the nasal cavities, surface smoothing, and deletion of multiple vertices and edges.

Before mesh generation, eight section planes perpendicular to the airstream were defined through the nasal passages to comprehensively evaluate local changes in airflow parameters (Figure 7). The plane selection was made by CAD-CAM software (CATIA V5R21, Academic licensed). The following section planes were selected: (1) 1 cm from the nostrils, (2) the narrowest part of the INV region, (3) the head of the inferior turbinate, (4) the head of the middle turbinate, (5) ostiomeatal unit, (6) the head of the superior turbinate, and (7) choanae. In type 5 and type 7 NSD models, an additional cross-section was set at the most prominent point of the bony spur (section S* in Figure 7).

3.6.2. Mesh generation

Stereolithography (*.stl) files were imported into the cfMesh application within OpenFOAM software (version foam-extend 4.1) for automatic mesh generation (Juretic, 2015). Numerical meshes for all 3D models consisted mostly of hexahedral elements, with three layers of boundary cells parallel to the cavity walls (boundary layer cells). The maximum length of the cell edge inside the domain is set to 7 mm. The distance of 0.5 mm from the wall is chosen as the characteristic size of the first boundary layer cell (Figure 7).The total number of cells for all 3D models was around 5.5 million.

3.7. Computational simulation of the nasal airflow

3.7.1. Mathematical modeling of the nasal airflow

Since the air velocities inside the nasal cavity are generally very small, density variations are also small, so that the flow is usually assumed as incompressible (ρ = const). The Boussinesq approximation was used in the momentum equation for the computation of the temperature field. Concerning that this approximation is valid for small density variations, it had no effect on the flow field in developed 3D nasal cavity models. The mathematical basis of the flow applied in this research was defined by the following equations.

The incompressible flow was fully determined with continuity and momentum equation,

$$\nabla \times \vec{U} = 0 \tag{1}$$

$$\frac{\partial \rho \vec{U}}{\partial t} + \nabla \times \left(\rho \vec{U} \vec{U} \right) = -\nabla p + \rho \vec{g} + \nabla \times \left[2\mu_{\text{eff}} \vec{S}(\vec{U}) \right] \tag{2}$$

where $\vec{U}$ is the velocity field, p is the pressure field, ρ is the density field, and $\vec{g}$ is the gravitational acceleration. The effective viscosity is a sum of molecular and turbulent viscosity, $\mu_{\text{eff}} = \mu + \mu_t$, while $\vec{S}$ is the rate of the strain tensor, defined as

$$\vec{S} = \frac{1}{2} \left[\nabla \vec{U} + (\vec{U})^T \right]$$

Effects of turbulence were incorporated in turbulent viscosity, which was determined from auxiliary equations. In the case of laminar flow $\mu_t = 0$, and $\mu_{\text{eff}} = \mu$.

Since equations (1) and (2) can be additionally simplified in the case when gravitational acceleration and density are constant, gravitational force can be expressed as the gradient of a scalar function

$$\rho \vec{g} = \nabla(\rho \vec{g} \times \vec{r})$$

where $\vec{r}$ is the position vector. This term now can be joined with a pressure gradient term,

$$\nabla p - \rho \vec{g} = \nabla(p - \rho \vec{g} \times \vec{r})$$

A further standard procedure in all incompressible solvers is to divide the equation (2) with density and to end up with the following system of the equations

$$\nabla \times \vec{U} = 0 \tag{3}$$

$$\frac{\partial \rho \vec{U}}{\partial t} + \nabla \times (\vec{U}\vec{U}) = -\nabla p^* + \rho \vec{g} + \nabla \times (v_{\text{eff}} \nabla \vec{U}) \tag{4}$$

where $p^* = p/\rho + \rho \vec{g} \times \vec{r}$ is kinematic pressure and $v_{\text{eff}} = v + v_t$ kinematic effective viscosity. Therefore, the value of the density was not used in the computations.

The procedure in the Boussinesq approximation was then applied. This approximation is valid when the variation of the density induced by the temperature change is small, which is the case in the flow considered. The reference density ρ_0 at the ambient temperature T_0 was denoted. In each term in the equation (2), ρ was replaced with ρ_0, except in the gravitational term. After division with ρ_0 the following equations were:

$$\frac{\partial \vec{U}}{\partial t} + \nabla \times (\vec{U}\vec{U}) = -\frac{1}{\rho_0}(\nabla p - \rho \vec{g}) + \nabla \times (v_{\text{eff}} \nabla \vec{U}) \tag{5}$$

The pressure gradient and gravity term in momentum equation (5) were further rearranged in the following form

$$-\nabla\left(\frac{p}{\rho_0}\right) + \left(\frac{\rho}{\rho_0}\right)\vec{g} = -\nabla\left(\frac{p - \rho \vec{g} \times \vec{r}}{\rho_0} + \frac{\rho \vec{g} \times \vec{r}}{\rho_0}\right) + \left(\frac{\rho}{\rho_0}\right)\vec{g} = -\nabla p_{rgh} - (\vec{g} \times \vec{r})\nabla\left(\frac{\rho}{\rho_0}\right)$$

where $p_{rgh} = (p - \rho \vec{g} \times \vec{r})/\rho_0$ is modified pressure. The final form of the momentum equation was

$$\frac{\partial \vec{U}}{\partial t} + \nabla \times (\vec{U}\vec{U}) = -\nabla p_{rgh} + \nabla \times (v_{\text{eff}} \nabla \vec{U}) - (\vec{g} \times \vec{r})\nabla\left(\frac{\rho}{\rho_0}\right) \tag{6}$$

which had the same form as the momentum equation (4) for incompressible flow, with one additional source term. The density ρ in that term was calculated using the equation

$$\rho = \rho_0[1 - \beta(T - T_0)] \tag{7}$$

where β is the volumetric expansion coefficient, for which it was assumed a constant value. For air at ambient condition, this value is $\beta = 3 \times 10^{-3} K^{-1}$.

Finally, the temperature was determined from the energy equation, which had the form

$$\frac{\partial T}{\partial t} + \nabla \times (\vec{U}T) = \nabla \times (\alpha_{\text{eff}}\, T) \tag{8}$$

where $\alpha_{\text{eff}} = \alpha + \alpha_t$ effective thermal diffusivity. Values of turbulent thermal diffusivity was determined as a ratio of turbulent viscosity and turbulent Prandtl number $\alpha_t = v_t / Pr_t$. A constant value of turbulent Prandtl number of 0.85 was assumed.

3.7.2. Numerical modeling of the nasal airflow and boundary conditions

The inlet was set at the nostrils, while the outlet was placed in the nasopharynx (Figure 8). Breathing at rest was simulated by applying a constant inspiratory flow rate of 125 mL/s at the nostrils (inlet) with zero gradients at the nasopharynx (outlet) (Hall, 2005).
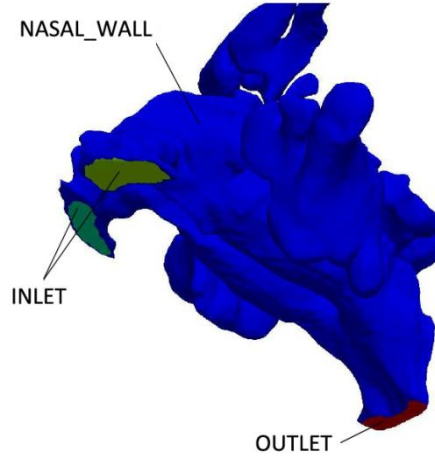
Figure 8. The geometry of the 3D model with the designated boundary surface

For all numerical computation open-source CFD code OpenFOAM was used, which is based on the finite volume method (Moukalled et al., 2016). This method was applied for the discretization of spatial domain in a finite number of volumes (cells) and discretization of conservation equations (continuity, momentum, and energy) that provided a large number of algebraic equations solved on the computer.

Solver named *buoyantBoussinesqSimpleFoam* was used for the computations and equations that were numerically solved as described in the previous subsection. Since the flow was considered a steady, SIMPLE algorithm was applied for pressure-velocity coupling. A laminar-transient-turbulent flow (k-ω SST model) was computed in all 3D models (Menter, 1994). Boundary conditions for flow variables are summarized in Table 4. A fixed volumetric flow rate of 125 mL/s was prescribed at the inlet surface. The uniform velocity distribution on the inlet surface was calculated simply by dividing the flow rate by the inlet surface area. The walls of the nasal cavity were assumed rigid with a no-slip condition. FixedFluxPressure boundary condition sets the pressure gradient to the provided value such that the flux on the boundary is that specified by the velocity boundary condition. The value of temperature at the inlet was set at T = 293 K (20˚C), while the nasal mucosal temperature of T = 307 K (34˚C) was set over the entire wall surface (Lindemann et al., 2004). Values of turbulent kinetic energy k and specific rate of dissipation ω were calculated from the prescribed intensity of the turbulence at the inlet (2%) and the value of mean velocity.

18

Table 4. Boundary conditions

	INLET	OUTLET	NASAL_WALL
U	flowRateInletVelocity	zeroGradient	noSlip ($U = 0$)
p_{rgh}	fixedFkuxPressure	fixedValue	zeroGradient
T	fixedValue	zeroGradient	zeroGradient
k	fixedValue	zeroGradient	kWallFunction
ω	fixedValue	zeroGradient	omegaWallFunction

Second order accuracy with limitedLinear discretization scheme was used for the convective term in the momentum equation, while second order linearUpwind scheme was used for convective terms in transport equations for k and ω. It was assumed that a converged solution is obtained when values of normalized residuals for all quantities fall below 10^{-5}.

3.8. CFD analysis of the airflow parameters

After CFD simulations were run, the nasal airflow characteristics in the straight septum model and seven NSD models were analyzed quantitatively, semiquantitatively, and qualitatively.

Quantitative evaluation of nasal airflow characteristics was performed by calculating the following CFD-based airflow parameters: *airflow partitioning* (in %), *velocity* (U, m/s), *pressure* (p, in Pa), *wall shear stress* (τ, in Pa), *nasal resistance* (NR, in Pa·s/mL), *temperature - heat flux* (HF, in W/m^2), and *turbulent kinetic energy* (k, in m^2/s^2).

Airflow partitioning was calculated in each model as a percentage of the total inhaled air flowing through the right and left nasal passage, respectively.

Airflow velocity was analyzed by calculating the maximum velocity values inside the right and left nasal passage.

Wall shear stress was analyzed by identifying the nasal cavity wall segment subjected to the highest shear stress and calculating its maximum values. This parameter corresponds to the tangential force produced by air acting on the mucosal surface.

The mean *pressure* value was measured at all sections along the nasal passages bilaterally in order to analyze the pressure drop pattern. Obtained pressure values were used to calculate CFD-derived *nasal resistance* (CFD-NR). Unilateral CFD-NR was calculated for the right and left nasal passage, respectively, using a standard equation

$$NR = \Delta p / Q$$

where Δp represents a transnasal pressure drop between the inlet and choanae, and Q is a flow rate of 125 mL/s (Kimbell et al., 2012; Borojeni et al., 2020). Side differences in the CFD-NR were calculated by the equation

$$NR = NR_{left} - NR_{right} \; .$$

Temperature values obtained during CFD simulations were used to compute *heat flux* bilaterally in all cross-sections. This parameter is an indicator of local changes in mucosal cooling. A standard equation used for heat flux calculation was

$$\emptyset = -k\nabla T$$

where $\emptyset$ is heat loss over the nasal mucosa during inspiration (W/m^2), k is the specific heat of the air and has a constant value of 0.0268 W/(m·K), and ∇T is temperature gradient at the wall (Sullivan et al., 2014; Borojeni et al., 2020).

Turbulent kinetic energy was evaluated by measuring the maximum k values in both nasal passages at predefined cross-sections.

Airflow velocity and turbulent kinetic energy were also evaluated semiquantitatively by illustrating their local profiles at each cross-section on a color-coded scale. The red color in the scale represented high values of the CFD parameter, whereas the blue color corresponded to its low values.

The nasal airflow pattern in eight 3D models was also analyzed qualitatively by detecting the direction of the streamlines and the presence of laminar airflow and vortices.

3.9. Statistical analysis

Statistical analyses were performed in SPSS Statistical Software 17.0 (SPSS, Inc., Chicago, IL, USA). Data were analyzed by appropriate descriptive and analytical methods. The Kolmogorov-Smirnov test assessed the normality of numerical data distribution.

For the NOSE scale validation process, internal consistency was assessed by Cronbach's alpha coefficient. A value higher than 0.81 was considered satisfactory (Aday, 1996). Test-retest reliability was evaluated by the Goodman-Kruskal gamma coefficient. Discriminant validity between groups was evaluated by the Mann–Whitney U test. Spearman's coefficient (r) was used to correlate item-item and item-total score. The statistically significant degree of correlation was considered if the coefficient r was higher than or equal to 0.40. In order to evaluate the response sensitivity of the questionnaire, the standardized response mean was computed by dividing the mean score change by the standard deviation of the change. A value of approximately 0.2 demonstrated low sensitivity to change, while a value of 0.5 demonstrated a moderate sensitivity, and 0.8 demonstrated high sensitivity to change.

The total NSD prevalence and the prevalence of each NSD type were presented in frequencies. The Chi-square test evaluated the gender-related difference in NSD prevalence. Data related to the NOSE scores and NSD angle were analyzed by the mean, standard deviation (SD), median, minimum, and maximum. Linear regression analysis was used to explore the relationship between the total NOSE scores, five NSD classifications, and the angle of NSD. In order to investigate whether some NSD types are more likely characterized by particular nasal obstruction symptoms (single NOSE scale items), binomial logistic regression analysis was applied. For the necessity of this analysis, Likert's grading of NOSE scale items was simplified and observed in light of experience (1) or does not experience (0) symptom. Afterward, every item was analyzed with each type of NSD according to five NSD classification systems. The association between septal spur induced nasal passage partitioning, and nasal obstruction (total NOSE score and single items) was also analyzed by the same regression models.

Spearman's correlation analysis explored the association between the following parameters: mean NOSE scores and side differences in CFD-NR, airflow partitioning and CFD-NR, mean NOSE scores and the maximum k values at each cross-section level, mean NOSE scores and heat flux at each cross-section level, and the maximum k values and heat flux within cross-sections at the side of NSD.

The level of significance for all statistical tests was set at 0.05.

4. RESULTS

4.1. NOSE-s scale

The final version of the NOSE-s scale is displayed in Table 3. The mean time required to fulfill the questionnaire was 2.5 ± 0.5 min and 2.0 ± 0.5 min for the study group and control group, respectively.

The internal consistency analysis demonstrated good reliability of the NOSE-s questionnaire at the level of Cronbach's alpha coefficient of 0.81. The mean time between test-retest administrations was 11.4 days (5 - 14 days). The obtained value of Goodman-Kruskal gamma coefficient of 0.83 (p<0.001) suggested a good test-retest reliability. Test reproducibility was presented by a standardized response mean of 0.18, which confirmed low sensitivity to change after retesting.

Average scores for each item obtained in both groups are shown in Table 5. All values (single items and the total score) were significantly higher in patients from the study group when compared to the control group (p<0.001), which demonstrated excellent inter-group discrimination.

Table 5. Comparison of item and total scores between groups (items presented as mean ± standard deviation; range of patients' responses shown in parentheses).

Item	Study group	Control group	p value
Nasal congestion	2.0 ± 1.1 (0-4)	0.2 ± 0.4 (0-2)	<0.001
Nasal obstruction	1.8 ± 1.1 (0-4)	0.1 ± 0.4 (0-2)	<0.001
Trouble breathing	1.6 ± 1.2 (0-4)	0.1 ± 0.1 (0-1)	<0.001
Trouble sleeping	0.9 ± 1.1 (0-4)	0	<0.001
Trouble breathing during exercise	2.5 ± 1.3 (0-4)	0.2 ± 0.5 (0-2)	<0.001
Total raw score	8.9 ± 4.4	0.6 ± 0.8	<0.001
Total score x 5	44.3 ± 22.3	2.9 ± 3.9	<0.001

Table 6 displays the construct validity of the NOSE-s questionnaire assessed through inter-item and item-total correlation coefficients. The item "Nasal congestion or stuffiness" correlated significantly only with the item "Nasal blockage or obstruction" (r=0.646). The item "Nasal blockage or obstruction" correlated significantly with all other items except with the "Trouble sleeping" (r=0.310). Moreover, the item "Trouble breathing" was significantly associated with all but the first item ("Nasal congestion or stuffiness") (r=0.368). The fourth item ("Trouble sleeping") correlated significantly with the "Trouble breathing" (r=0.466) and not with other items. Finally, the item "Trouble breathing during exercise" was not significantly associated with items "Nasal congestion or stuffiness" (r=0.386) and "Trouble sleeping" (r=0.383). Additionally, each item correlated significantly with the total score.

Table 6. Inter-item and item-total correlations (Spearman's correlation coefficient)

	Nasal congestion	Nasal obstruction	Trouble breathing	Trouble sleeping	Trouble breathing during exercise
Nasal congestion					
Nasal obstruction	0.646				
Trouble breathing	0.368	0.611			
Trouble sleeping	0.170	0.310	0.466		
Trouble breathing during exercise	0.386	0.537	0.673	0.383	
Total score	0.653	0.776	0.852	0.571	0.811

The preoperative NOSE score of the patients that underwent septoplasty was 52.38 ± 16.5. Three months after septoplasty, a mean NOSE-s score in patients was 19.2 ± 12.8. A calculated standardized response mean of 1.7 showed high sensitivity to change.

4.2. The prevalence of NSD in the Serbian population

Among the initial study group of 386 patients, 153 (39.6%) were males, and 233 (60.4%) were females. The mean age was 55.08 ± 16.09 years for the whole group. The mean age for the male and female subgroup was 54.80 ± 16.53 years and 55.26 ± 15.84 years, respectively.

The estimated prevalence of NSD was 92.7% (358/386). The prevalence of each type of NSD, according to Mladina's classification system in the study group, is presented in Table 7. The most prevalent NSD type was type 7 (34.9%). Types 5 and 3 were also frequent, with percentages of 24.9% and 23.7%, respectively. The least frequent type was type 2 (0.6%). The Chi-square test showed no significant difference in NSD prevalence among genders (Pearson Chi-Square 1.545, p=0.214).

Table 7. Prevalence of Mladina's NSD types in 358 patients with NSD

Type of NSD	Number of patients (%)
Type 1	11 (3.1%)
Type 2	2 (0.6%)
Type 3	85 (23.7%)
Type 4	40 (11.2%)
Type 5	89 (24.9%)
Type 6	6 (1.7%)
Type 7	**125 (34.9%)**
Total	358 (100%)

In the study group of 225 patients, there were 85 (36.4%) males and 143 (63.6%) females. Patient's mean age in this group were 59.52 ± 14.59 years (60.33 ± 14.73 years in male and 59.06 ± 14.55 years in female). Table 8 displays the prevalence distribution of various NSD types according to five classification systems applied in 225 patients. In the case of Mladina's classification, the similar prevalence distribution of NSD types was noted as in the initial study group of 386 patients. The most common was type 7, while the least frequent was type 2. The NSD type with "localized deviation or large spur" was the most prevalent in Guyuron's classification with 121 (53.8%). When concerning the location of the most prominent point of NSD, the largest number of NSDs was classified in the "media" type (58, 25.8%). The bony part of the septum was the most affected by deviation. This NSD type was registered in 112 (49.8%) patients.

Table 8. The prevalence of NSD types according to five classification systems and NOSE scores (mean ± SD, median, minimum, and maximum) in 225 patients

Classification of NSD	NSD type	NSD prevalence (n, %)	Total NOSE scores		
			mean ± SD	median	min.-max.
Mladina's classification	I	4 (1.8%)	20.0 ± 15.8	17.5	5 - 40
	II	2 (0.9%)	**45.0 ± 28.3**	45	25 - 65
	III	53 (23.6%)	13.7 ± 17.5	10	0 - 85
	IV	25 (11.1%)	17.0 ± 19.0	5	0 - 70
	V	59 (26.2%)	18.4 ± 17.9	15	0 - 85
	VI	5 (2.2%)	14.0 ± 10.8	15	0 - 30
	VII	**77 (34.2%)**	19.6 ± 19.9	15	0 - 85
Guyuron's classification	I	11 (4.9%)	**24.6 ± 19.6**	25	0 - 65
	II	27 (12.0%)	22.9 ± 21.8	15	0 - 85
	III	42 (18.7%)	10.4 ± 13.4	5	0 - 60
	IV	18 (8.0%)	15.8 ± 19.9	5	0 - 70
	V	6 (2.7%)	18.3 ± 18.9	7.5	5 - 45
	VI	**121 (53.8%)**	18.8 ± 18.8	15	0 - 85
NSD location based classification*	*caudal*	6 (2.7%)	**28.3 ± 21.8**	25	5 -65
	anterior	6 (2.7%)	14.2 ± 18.8	5	0 - 45
	media	**58 (25.8%)**	15.5 ± 18.2	10	0 - 85
Structure based classification	*cartilaginous*	11 (4.9%)	**21.8 ± 18.5**	15	0 - 65
	combined	102 (45.3%)	19.0 ± 19.6	10	0 - 85
	bony	**112 (49.8%)**	16.2 ± 17.8	10	0 - 85
NSD angle based classification**	*mild*	**161 (71.6%)**	**18.2 ± 18.8**	15	0 - 85
	moderate	48 (21.3%)	18.0 ± 19.4	10	0 - 70
	severe	11 (4.9%)	14.6 ± 16.3	10	0 - 50

* - this classification does not include NSD types with double-curved septum and spurs,
** - the angle could not be precisely measured in five patients due to various CT artifacts.

The estimated angle of NSD in the study group of 225 patients ranged from 2.5° to 22.6°, with a mean value of 8.6° ± 3.4. When NSD was classified according to the angle degree, the majority of NSD corresponded to the "mild" category (Table 8). Table 9 shows descriptive statistical parameters of NSD angle between patient groups with (NOSE score>0) and without (NOSE score=0) NAO symptoms. Interestingly, the mean NSD angle was slightly higher in the group of patients who did not complain of NAO (Table 9).

Table 9. The angle of NSD in patients with and without nasal obstruction

Nasal obstruction	Number of patients (%)	The angle of the NSD		
		mean ± SD	*median*	*min - max*
Absent (total NOSE score = 0)	58 (25.8%)	9.1° ± 3.8	8.8°	2.9° - 22.6°
Present (total NOSE score > 0)	167 (74.2%)	8.5° ± 3.2	8.1°	2.5° - 22.4°

4.3. NOSE scores

Descriptive statistical data of the NOSE scores for each NSD type within five classifications are displayed in Table 8. Regardless of the applied classification, patients with various NSD types showed apparent differences in mean NOSE scores. Considering the first four classifications, the highest NOSE scores were recorded in the NSD types located in the anterior segment of the septum. The worst mean NOSE score of 45.00 ± 28.28 was detected in Mladina's type 2 NSD (Table 8). Interestingly, in angle-based NSD classification, patients with smaller NSD angle had higher NOSE scores, whereas patients with greater NSD angle reported less severe NAO (Table 8). As confirmed by the Kolmogorov-Smirnov test, the NOSE score data distribution was not normal ($p<0.001$).

4.4. Association between NOSE scores, NSD type, and NSD angle

Linear regression analysis did not find a statistically significant influence of the NSD angle on the NAO subjective perception (B=-0.122 (-0.859 - 0.615) for 95% confidence interval, p=0.745).

The results of the linear regression analysis showed that there was no statistically significant influence of any of the NSD classification type on total NOSE scores (Table 10). Table 11 presents the results of the binomial regression analysis. Similar to the total NOSE score, NSD classifications were not significantly associated with single NOSE items. Additionally, spurs partitioning of the nasal passages did not show a statistically significant effect on the nasal obstruction severity expressed by total NOSE scores and single NOSE items (Table 10 and 11).

Table 10. Linear regression analysis of total NOSE scores and NSD classifications including spurs

Nasal obstruction symptoms	Mladina's classification		Guyuron's classification		NSD location based classification		Structure based classification		NSD angle based classification		Spur touch/ or not lateral nasal wall	
	#B (95% C.I.for#B)	Sig.	#B (95% C.I.for#B)	Sig.	#B (95% C.I.for#B)	Sig.	#B (95% C.I.for#B)	Sig.	#B (95% C.I.for#B)	Sig.	#B (95% C.I.for#B)	Sig.
Total NOSE score	0.837 (-0.628 - 2.301)	0.261	0.081 (-1.339 - 1.501)	0.911	-0.366 (-3.311 - 2.580)	0.807	1.132 (-3.094 - 5.358)	0.598	-1.053 (-5.486 - 3.380)	0.640	3.680 (-2.262 - 9.623)	0.224

Table 11. Binomial logistic regression analysis of single NOSE items and NSD classifications including spurs

Nasal obstruction symptoms	Mladina's classification		Guyuron's classification		NSD location based classification		Structure based classification		NSD angle based classification		Spur touch/ or not lateral nasal wall	
	Exp(B) (95% C.I.for EXP(B))	Sig.	Exp(B) (95% C.I.for EXP(B))	Sig.	Exp(B) (95% C.I.for EXP(B))	Sig.	Exp(B) (95% C.I.for EXP(B))	Sig.	Exp(B) (95% C.I.for EXP(B))	Sig.	Exp(B) (95% C.I.for EXP(B))	Sig.
NOSE question 1 (Nasal congestion or stuffines)	1.073 (0.918 - 1.255)	0.376	0.982 (0.844 - 1.142)	0.810	1.078 (0.787 - 1.475)	0.641	1.130 (0.720 - 1.773)	0.595	0.889 (0.555 - 1.424)	0.624	1.780 (0.936 - 3.385)	0.078
NOSE question 2 (Nasal blockage or obstruction)	1.003 (0.856 - 1.176)	0.966	0.940 (0.807 - 1.095)	0.427	0.908 (0.662 - 1.247)	0.551	1.021 (0.647 - 1.611)	0.928	0.822 (0.505 - 1.336)	0.428	1.489 (0.788 - 2.814)	0.221
NOSE question 3 (Trouble breathing through my nose)	1.178 (0.999 - 1.389)	0.052	1.063 (0.908 - 1.244)	0.447	1.154 (0.829 - 1.605)	0.396	1.410 (0.878 - 2.264)	0.155	0.861 (0.525 - 1.411)	0.552	1.668 (0.878 - 3.167)	0.118
NOSE question 4 (Trouble sleeping)	1.019 (0.801 - 1.297)	0.875	1.039 (0.821 - 1.316)	0.748	0.818 (0.518 - 1.292)	0.389	0.791 (0.400 - 1.562)	0.499	1.494 (0.789 - 2.831)	0.218	0.795 (0.285 - 2.222)	0.662
NOSE question 5 (Trouble breathing during exercise)	0.992 (0.848 - 1.160)	0.919	1.006 (0.864 - 1.170)	0.942	0.914 (0.666 - 1.254)	0.577	0.912 (0.580 - 1.432)	0.688	0.866 (0.541 - 1.386)	0.548	0.829 (0.440 - 1.563)	0.562

4.5. The nasal airflow pattern in 3D models with different NSD types

4.5.1. Airflow partitioning

In the model of a symptomless patient without NSD, airflow was almost evenly distributed with a minimal difference between right and left nasal passages (Table 12). Side differences in airflow distribution in type 3, 4, 5, and 7 were similar to the model without NSD. There were more substantial alterations in the airflow partitioning between right and left nasal passages in the NSD type 6, 1, and 2 (Table 12). The greatest side difference in flow partitioning was observed in the type 2 NSD model.

Table 12. CFD-calculated parameters (airflow partitioning (%), maximum velocity (m/s), maximum wall shear stress (Pa), and CFD-NR (Pa/(mL/s)) for normal nasal cavity and seven Mladina's NSD types, separately for the left and right side.

3D model	Airflow partitioning (%)		Maximum velocity (m/s)		Maximum wall shear stress (Pa)		CFD-NR (Pa/(mL/s))		
	Left	*Right*	*Left*	*Right*	*Left*	*Right*	*Left*	*Right*	*ΔNR*
No NSD	45.83	54.17	1.2	1.5	0.17	0.20	0.0136	0.0152	-0.0016
NSD									
Type 1	43.37	56.63	1.5	0.9	0.23	0.10	0.0232	0.0088	0.0144
Type 2	34.71	65.29	1.5	1.3	0.25	0.12	0.0180	0.0068	0.0112
Type 3	53.39	46.61	1.5	1.5	0.21	0.17	0.0158	0.0126	0.0032
Type 4	51.96	48.04	1.1	1.5	0.09	0.25	0.0074	0.0194	-0.0120
Type 5	55.04	44.96	1.5	1.5	0.21	0.25	0.0160	0.0248	-0.0088
Type 6	55.91	44.09	1.8	1.3	0.25	0.18	0.0290	0.0266	0.0024
Type 7	45.19	54.81	2.5	2.2	0.25	0.25	0.0533	0.0101	0.0432

4.5.2. Airflow velocity

The airflow velocity profiles in eight 3D models were visualized for each cross-section in Appendix 1. All models showed generally higher velocity values at the central part of the nasal passages at all cross-sections (red areas) and decreased toward nasal walls (green and blue areas). The highest velocity values were recorded at the nasal valve region in all 3D models with airflow rate around 1.5 m/s in the straight septum model and the first five NSD types (Table 12). Slightly higher maximum airflow velocities of 1.8 m/s and 2.5 m/s were detected in types 6 and 7, respectively.

The distribution of velocity fields in the straight septum model was symmetrical between the right and left nasal passages. Air flowed predominantly through the central part of the nasal passages at the level of the middle meatus. The asymmetrical and gradual decrease in airflow velocity was observed bilaterally from nostrils to the nasopharynx (Figure 9 in Appendix 1).

In models with NSD, various degree of side asymmetry was recorded in the airflow velocity profile. The septal curvature in types 1, 2, 3, 6, and 7 caused more or less redirection of the high-velocity field toward the inferior nasal meatus (Figure 9 in Appendix 1). In the model with a

double-curved NSD (type 4), air constantly flowed faster throughout the nasal passage that was narrowed by the anterior septal curvature. However, in the opposite nasal passage, only a local elevation in airflow velocity was recorded at the site narrowed by the posterior curvature (Figure 9 in Appendix 1). A similar local increase in airflow velocity was registered in types 5 and 7 at the level of the tip of the spur (Figure 9 in Appendix 1).

4.5.3. Airflow pattern

Airflow patterns inside all 3D models were visualized via streamlines in Figure 10 (see Appendix 2). After passing the INV region, the most streamlines in the normal nasal cavity model were grouped into two main trajectories. The first high-velocity trajectory was directed toward the common nasal meatus at the middle turbinate level, while the second low-velocity trajectory was directed posterosuperiorly toward the olfactory region. The presence of the NSD more or less altered such regularity in streamline distribution. Except for the type 3 NSD, more irregular streamline dissipation was observed in the rest of the 3D models, particularly in the NSD type 2, 4, 6, and 7.

A predominant airflow pattern at the simulated airflow rate of 125 mL/s was laminar in all 3D models (Figure 10 in Appendix 2). The focal zones of air swirling in the anterior nasal cavum, known as anterior dorsal vortices, were visualized in NSD models 3, 4, 5, and 7. A small vortex was also detected at the bony spur's tip in the NSD type 5. However, in the NSD type 2, a relatively large atypical vortex was noted in the wider nasal passage inside the inferior nasal meatus.

4.5.4. Wall shear stress

The distribution of the wall shear stress magnitude in all 3D models is displayed in Figure 12 (see Appendix 3). In the normal nasal cavity without NSD, the distribution of wall shear stress was nearly symmetrical between the right and left nasal passages. The highest wall shear stress values were recorded in the INV region (Table 12), affecting a relatively small area, particularly the nasal isthmus (Figure 12).

The magnitude of wall shear stress in Mladina's seven NSD types showed more or less discrepancy concerning the side of NSD (Table 12). Wall shear stress values were constantly higher in the narrowed nasal passage in all 3D models. In contrast to the normal nasal cavity model, the greater wall area in the narrowed nasal passages was exposed to high wall shear stress, particularly walls around the inferior turbinate head and the nasal septum. This finding was the most accentuated in the NSD type 7 (Figure 12 in Appendix 3).

Side discrepancies in the maximum wall shear stress values followed the trend observed in the maximum airflow velocity (Table 12): the greater the airflow velocity value, the greater the wall shear stress, and vice versa.

4.5.5. Airflow pressure and CFD-derived nasal resistance

Figure 11 illustrates the transnasal pressure drop through the right and left nasal passage in eight 3D models. In the model without NSD, similar pressure values were recorded on both sides, showing a smooth in-phase decrease along the nasal passages. CFD-NR, in the same model, also exhibits minimal side differences (Table 12). Transnasal pressure drop pattern in type 3 and 6 NSD models resembled that of a normal nasal cavity, including a constant in-phase decrease in pressure, minimal side differences in mean pressure values (Figure 11), and similar CFD-NR on each side (Table 12). Transnasal pressure drop in type 5 was similar to type 3, although side differences in the

single pressure values in the anterior segments were slightly higher as well as the side difference in CFD-NR.
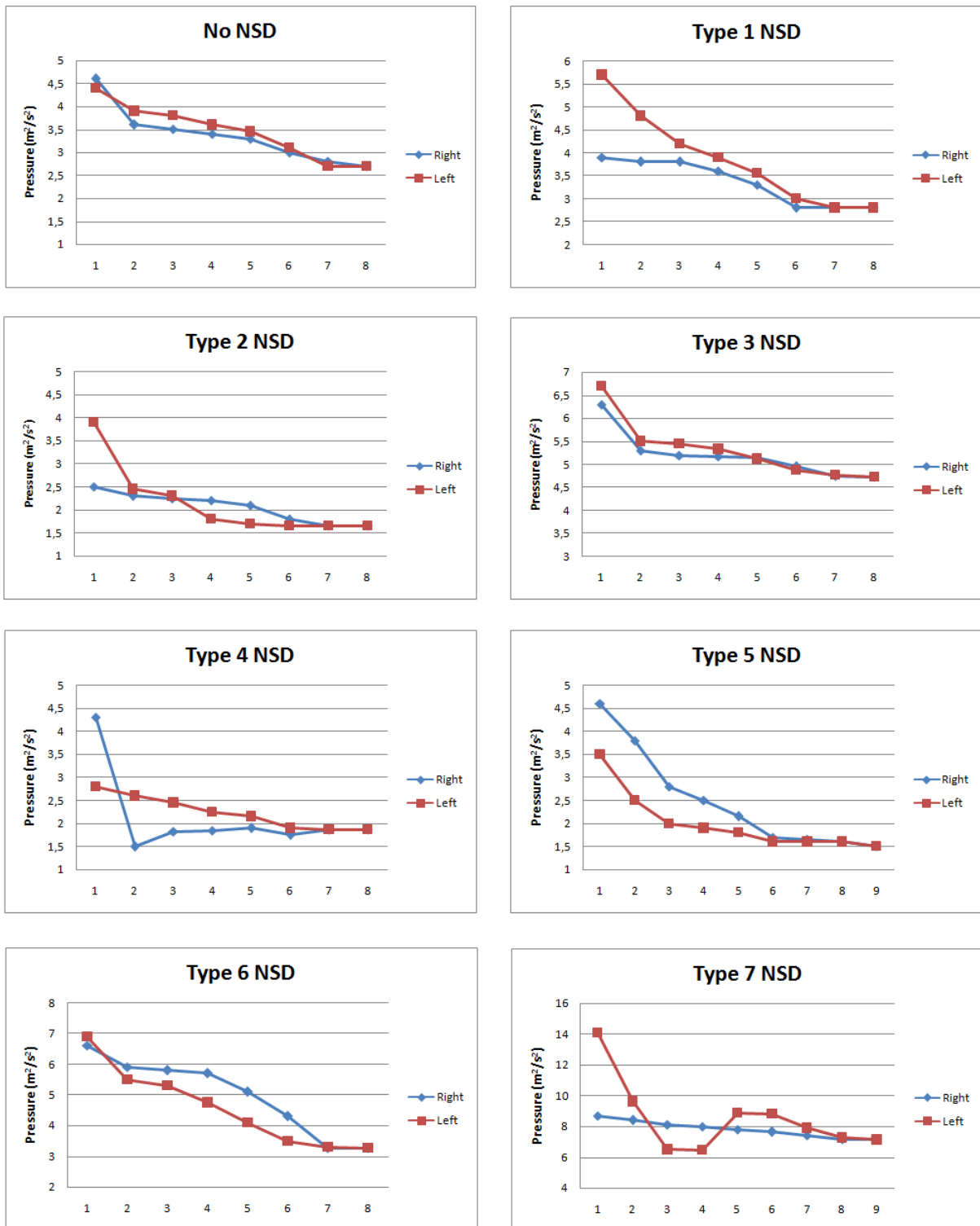
Figure 11. Comparative analysis of pressure drop through the right and left nasal passage in a straight septum model and seven Mladina's NSD models.

28

The appearance of pressure drop lines in other NSD models, however, revealed more accentuated side asymmetry in mean pressure values and CFD-NR (Table 12), including an out-of-phase pattern in a pressure drop (Figure 11). The largest side differences in the mean pressure values were observed in the anterior segments of the nasal cavity. In the segments behind, pressure continued to drop in-phase only in type 1. By contrast, types 2, 4, and 7 showed a steep initial drop in pressure at the narrow side, which subsequently increased to some extent in type 4 and 7. Almost a flat line in the pressure drop and low CFD-NR were noted in these three models in the opposite (wider) nasal passage. There were no detectable changes in the transnasal pressure drop at the site of the bony spur in type 5 and 7 (Figure 11, point 6 in NSD type 5 and 7).

4.5.6. Heat flux

Heat flux values through the right and left nasal passage were illustrated in Figure 13 for all 3D models. In the straight septum model, similar heat flux values were recorded bilaterally, showing a smooth in-phase decrease along the nasal passages. In NSD models, heat flux values recorded at the narrow nasal passage were represented with steeper lines when compared to the opposite wide side heat flux lines (Figure 13).

The steepest heat flux line on the narrow side was observed in type 2 NSD. Compared with the straight septum model, all NSD models showed more or less pronounced side asymmetry in heat flux values. The largest side difference was noticed in the type 2 NSD (Figure 13), continuously along the nasal cavity. Heat flux lines in types 3 and 4 NSD diverged from each other in posterior segments of the nasal passages. Similar side differences in heat flux values within posterior parts of the nasal passages were detected in the spur region of the NSD type 5 and 7 (Figure 13, point 6 in NSD type 5 and 7).

4.5.7. Turbulent kinetic energy

The turbulent kinetic energy (k) profiles for all 3D models were presented for each cross-section in Figure 14 (Appendix 4). Similar to airflow velocity, the k values were higher in the central part of the nasal passages at all cross-sections and decreased toward the periphery (nasal walls).

In the straight septum model, the distribution of k fields was symmetrical between the right and left nasal passages. In models with NSD, various degree of side asymmetry was recorded in k distribution and intensity (Appendix 4). When compared to the straight septum model, k was almost completely reduced in NSD types 1, 2, and 7 at the most prominent site of NSD and at the sections behind it (Appendix 4). Similarly, a decrease in k intensity within narrow nasal passages was recorded in types 3 and 4 (Appendix 4). In NSD type 5, a local increase in k intensity was registered at the spur's tip (Appendix 4). In type 6, approximately similar k intensities were observed on both sides of the nasal passages but with turbulence descent toward the lower nasal meatus (Appendix 4).
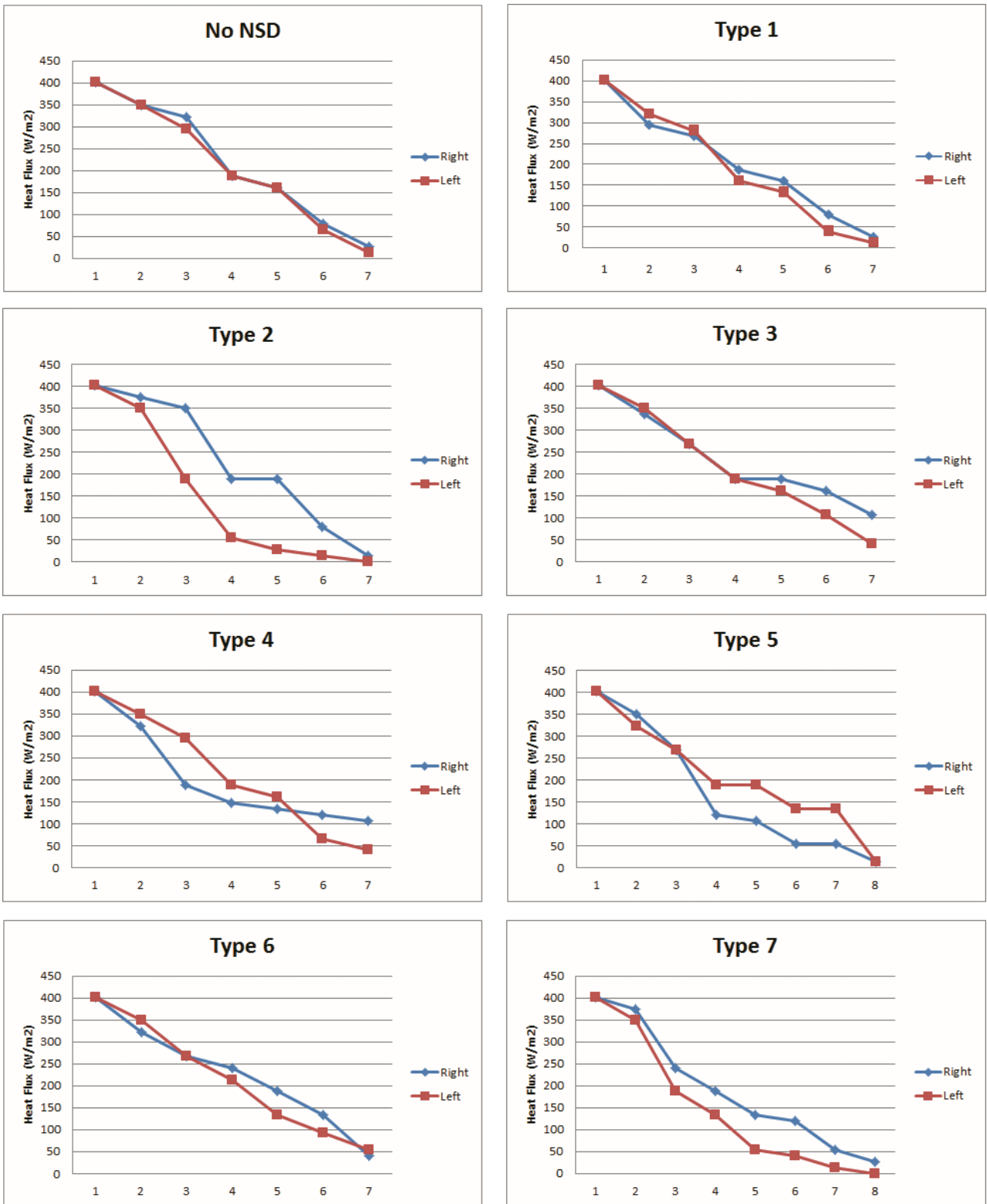
Figure 13. Comparative analysis of heat flux between the right and left nasal passage in a straight septum model and seven Mladina's NSD models. Heat flux recorded at the bony spur level in type 5, and 7 NSD is marked with the number 6.

30

4.5.8. Association between CFD-derived airflow parameters with NOSE scores

The statistical analysis detected a significant positive correlation between side differences in CFD-NR and mean NOSE scores (R=0.762, *p=0.028*). The analysis also showed a significantly negative correlation between the percent of unilateral airflow and CFD-NR (R= -0.524, *p= 0.037*).

Correlation analysis between mean NOSE scores of each NSD group, heat flux, and *k* on the narrow side only reached negative significance at the fourth cross-section (Table 13). A significant positive correlation was detected between heat flux and *k* at the level of the lower turbinate head (R=0.957, p<0.001), the middle turbinate head (R=0.910, p=0.002), and the ostiomeatal complex (R=0.731, p=0.039) on the narrow side (Table 14).

Table 13. Correlation analysis between mean NOSE scores, *k*, and heat flux recorded on the side of the NSD at selected cross-sections.

		S2	S3	S4	S5	S6	S7
		Turbulent kinetic energy					
Mean NOSE score	**R**	-0.690	-0.455	**-0.723***	-0.312	-0.094	-0.247
	p	0.058	0.257	**0.043**	0.452	0.826	0.555
		Heat flux					
Mean NOSE score	**R**	-0.282	-0.476	**-0.732***	-0.651	-0.615	-0.642
	p	0.499	0.234	**0.039**	0.081	0.105	0.086

* Correlation was significant at the 0.05 level (2-tailed)

Table 14. Correlation analysis between *k* and heat flux recorded on the narrowed side of the nasal passage at selected cross-sections.

	S2	S3	S4	S5	S6	S7
R	0.394	**0.957****	**0.910****	**0.731***	0.663	0.599
p	0.334	**<0.001**	**0.002**	**0.039**	0.073	0.116

** Correlation is significant at the 0.01 level (2-tailed)
* Correlation was significant at the 0.05 level (2-tailed)

5. DISCUSSION

Instead of developing an entirely new health-related quality of life instrument, researchers often use previously validated and published instruments that are recognized as valuable tools for self-assessment of symptom severity. Achievement of the equivalence between the original and the target version of the health-related-quality-of-life instrument is an essential and necessary step before application in a new population. According to well-established principles, this process requires translation, cross-cultural adaptation, and psychometric validation (Sousa & Rojjanasrirat, 2011; Lauffer et al., 2013). The entire process enables detection of the impact of a disease or patients' response to the applied therapy uniformly in each adopted version of the instrument. The use of standardized questionnaires allows result comparison across studies and increases the reliability of studies. Additionally, the application of validated subjective scoring instruments enables assessing the relationship between objective disease outcomes and subjective self-estimation of the symptom severity more reliably (Andre et al., 2009; Ottaviano & Fokkens, 2016).

The NOSE scale has been validated in several countries up to date (Bezerra et al., 2011, Marro et al., 2011; Mozzanica et al., 2013; Dong et al., 2014; Lachanas et al., 2014; Larrosa et al., 2015; Urbančič et al., 2016; Van Zijl et al., 2017; Amer et al., 2017). Given that the number of patients involved in these studies usually ranged from 100 to 116 (Marro et al., 2011; Lachanas et al., 2014; Larrosa et al., 2015; Urbančič et al., 2016; Amer et al., 2017), our sample size can be considered as optimal when compared with previous studies. All patients enrolled in the current study completed the NOSE-s scale without any difficulty, showing that it was not burdensome for them. The psychometric properties of the NOSE-s instrument were consistent with the original questionnaire confirming high reliability and validity of the instrument. Internal consistency of the NOSE-s scale was similar to values reported in previous studies that ranged from 0.74 to 0.97 (Stewart et al., 2004; Bezerra et al., 2011, Marro et al., 2011; Mozzanica et al., 2013; Dong et al., 2014; Lachanas et al., 2014; Larrosa et al., 2015; Urbančič et al., 2016; Van Zijl et al., 2017; Amer et al., 2017).

Among five nasal obstruction related symptoms that the NOSE scale evaluates, only trouble sleeping was close to one end of the Likert's scale (Table 5). This result could be explained by consecutive patient sampling used in our study. Patients diagnosed with the nasal septal deviation and referred to the CT examination during the sampling period were included in the study regardless of the obstruction severity. The predominance of patients with no or very mild sleeping trouble contributed to the item's low mean value. If the study group contained more patients with severe nasal obstruction and severe sleeping trouble, it would undoubtedly shift the mean score of item 4 to the greater values.

Considering a short period (5 to 14 days) during which test-retest was made, significant changes in patients' clinical status were not expected. Given that underlying patient's status did not change during this period and the fact that scores of the scale remained constant, our results demonstrated that the NOSE-s instrument measured a real state of the patient's health. Calculation of standardized response mean confirmed our expectations and showed low sensitivity to change, suggesting good stability and reproducibility of the NOSE-s scale.

The comparison between the study group and the control group showed very good inter-group discrimination. Patients with NSD had significantly higher NOSE scores than controls. This indicates that the NOSE-s scale is sensitive to detect the presence or absence of the nasal obstruction, which is consistent with the original NOSE instrument (Stewart et al., 2004) and other validation studies (Stewart et al., 2004; Bezerra et al., 2011, Marro et al., 2011; Mozzanica et al., 2013; Dong et al., 2014; Lachanas et al., 2014; Larrosa et al., 2015; Urbančič et al., 2016; Van Zijl et al., 2017; Amer et al., 2017). Construct validity of the NOSE-s questionnaire was also in

accordance with the original version of the instrument (Stewart et al., 2004) as well as with other validation studies (Bezerra et al., 2011; Marro et al., 2011; Larrosa et al., 2015). All items correlated significantly with each other and with the total score, except the "trouble sleeping" with the "nasal congestion or stuffiness" and the "nasal blockage or obstruction." Additionally, our results demonstrated that the NOSE-s scale is also sensitive to detect a change in the health status in patients treated with septoplasty.

The prevalence of NSD in the adult population varies between different studies. In our sample, the prevalence of the NSD was slightly higher in comparison to previous studies. Similar inter-study differences in the NSD prevalence also exist concerning gender and Mladina's types of NSD. A few authors have reported a slightly higher NSD prevalence in males (Rao et al., 2005; Mladina et al., 2008; Wee et al., 2012). However, in our study, NSD was more commonly encountered in femaales (60.4%), although this gender difference was not statistically significant. This could be due to the higher number of females in the study sample because participants were consecutively enrolled as they came to the CT examination. Our results also showed a predominance of Mladina's type 7, type 5, and type 3 NSD in decreasing order (Table 7 and 8). By contrast, an international study conducted by Mladina et al. found type 3 as the most prevalent (20.4%), followed by type 2 (16.4%) and type 1 (16.2%). Type 7 in their sample was the least frequent. However, type 1 NSD has been the most frequently diagnosed in Saudi Arabs, Indians, and Koreans (Daghistani, 2002; Rao et al., 2005; Wee et al., 2012).

Potential reasons for the significant discrepancy in NSD frequencies between studies might be due to different techniques used to diagnose NSD and inter-study differences in target populations. Techniques such as anterior rhinoscopy and endoscopy were frequently used diagnostic tools for NSD. The disadvantage of anterior rhinoscopy is that posterior parts of the nasal septum cannot be fully visualized, and consequently, some posterior deviations might be omitted. Therefore, it could be expected that studies in which anterior rhinoscopy was an examination technique of choice underestimate real prevalence of NSD. Although endoscopy allows visualization of the complete nasal septum, the angle of the NSD could not be measured with great accuracy and repeatability (Lee et al., 2013; Aziz et al., 2014). Concerning the types of NSD, Mladina pointed out that type 5 can be easily overlooked by anterior rhinoscopy (Mladina et al., 2008). A higher percentage of type 5 NSD in our sample could be explained by a more comprehensive evaluation of the nasal septum by CT.

Although CT is not recommended for routinely NSD diagnosis and evaluation due to relatively high radiation dose, this technique is superior to anterior rhinoscopy and nasal endoscopy because it visualizes the whole septum in three planes. Thus, NSD morphology can be examined comprehensively, the angle of NSD can be precisely measured, and none of the seven types of NSD can be misjudged. Moreover, an accurate measurement of the nasal valve angle is allowed, which is essential for the differentiation between Mladina's type 1 and 2 NSD. The CT-based assessment of the nasal valve angle in our study could be the reason for a different frequency of Mladina's type 1 and type 2 in comparison to other studies.

Previous studies that investigated NSD prevalence were conducted in ENT clinics where the number of patients that suffer from NSD can be significantly enlarged. Furthermore, it might falsely present harsh nasal obstruction symptoms in the majority of patients with NSD. However, it is well known that not all patients with NSD have nasal obstruction symptoms (Savovic et al., 2014; Van Egmond et al., 2015). Out of 225 patients in the current study, symptomatic NSD was recorded in 167 (74.2%) patients. Therefore, we focused on a normal unbiased population, who presented with a wide range of NOSE scores and CT morphology of the nasal septum. Patients were selected at the Department of Diagnostic Radiology in order to target the most general population. This way, a more representative sample was obtained by omitting ENT clinics and implementing well-defined

exclusion criteria. Therefore, it was possible to investigate accurately the real presence and severity of NSD induced NAO and its relationship with the different morphological characteristics of NSD.

According to NOSE scores, there were measurable differences in NAO severity between seven Mladina's types of NSD. Patients with type 2 NSD reported the worst NOSE scores. Since this result was obtained from only two patients, it could not be simply extrapolated to the general population. However, these were not the only cases with type 2 NSD. Almost one-third of the type 7 NSD cases consisted of type 2 and other types of NSD (23/77 patients). Their NOSE scores were also relatively high, but the mean NOSE score for type 7 NSD was lower. Our finding was in accordance with previous clinical studies as well as the airflow dynamics analysis of the INV region (Daghistani, 2002; Liu et al., 2012). Many authors argue that deviation in the INV area is critical for nasal obstruction and causes the most burdensome NAO symptoms. The mechanism behind this was revealed in studies that evaluated nasal airflow resistance in experimental nasal models. Namely, it has been found that constriction in the INV region results in a higher increase in airflow resistance than narrowing in the middle of the nasal cavity (Cole et al., 1988). If there is a combined narrowing in the INV region and the middle nasal cavity (type 7 NSD in Mladina's classification system), the INV deviation usually has a more significant impact on nasal obstruction (Cole et al., 1988; Mlynski, 2013). Similar to type 2, the INV angle is also changed in type 1. Patients with this NSD type also reported more severe symptoms than other NSD types (Table 8). However, observed differences in NOSE scores between Mladina's types of the NSD did not statistically confirm as significant. Such a result could be a consequence of a relatively low number of patients with type 1 and 2 NSD compared to the percentage of other NSD types. This finding may reflect a true low prevalence of isolated types 1 and 2 in the Serbian population and/or their coexistence with other types that constitute type 7 NSD.

Only a few studies investigated the connection between CT-assessed morphology of NSD and subjective NAO perception in the up-to-date literature. Ardeshirpour et al. (2016) found out that the angle of deviation measured at the anterior, middle, and posterior part of the nasal septum, as well as maximal angle, poorly correlate with NOSE scores. The same author also noticed a poor connection between the more obstructed side of the nose and the side of the deviation (Ardeshirpour et al., 2016). Lee and his team (2013) provided the opposite conclusion pointing out that the angle of NSD measured at the ostiomeatal unit level has a significant impact on the subjective sensation of NAO. However, the same author failed to detect any connection between INV angle and NAO symptoms (Lee et al., 2013). According to Savovic et al. (2014), an NSD angle greater than 10° has a significant effect on the difficulty of breathing through the deviated side of the nose. In our study, the NSD angle ranged from 2.5° to 22.6°, but regression analysis did not show its significant effect on NAO. The fact that a slightly higher mean and maximum NSD angle was measured in patients without NAO symptoms supports this conclusion (Table 5).

Despite contradictory results, previous studies primarily observed NSD through the angle of deviation. However, many NSD classification systems are described in the literature, each focusing on some different characteristics of NSD (Table 1). Additionally, it has not been determined yet which NSD components are responsible for the onset of NAO symptoms and, as such, are the most relevant for inspection and measurement.

In the current study, we applied five different classification systems, each focusing on the different aspects of the NSD in order to detect any specific morphological characteristic that could predict NAO severity. After a thorough analysis of the morphological aspects of NSD, a particular NSD morphological characteristic or type (within any classification system) that could predict NAO symptom severity was not identified (Table 10 and 11).

In general, the clinical impact of spurs on the NAO severity had been underinvestigated. Wee et al. (2012) reported that, after Mladina's NSD type 1 and 2, patients with type 5 NSD

frequently complained of NAO, but the symptom severity was not quantified. Simmen et al. (1999) observed turbulent flow in an experimental cadaveric model of the nose behind the spur. In the computational model of the nasal cavity, Liu et al. (2012) found complicated airflow and velocity distribution associated with a spur, but the results were not presented in the paper. Although it seems that Mladina's NSD type 5 is also important for the NAO severity in our patients (Table 8), the presence of spurs as well as whether they divide nasal passages or not showed no predictive effect on NOSE score (Table 10 and 11).

We have to emphasize that frequently used statements in radiological reports "mild (or moderate, or severe) deviation of the nasal septum" does not necessarily reflect the NAO symptom severity. A burdensome of NSD is generally evaluated by notifying how complicated the nasal septum shape looks like and how much the septum is deflected from the midline. However, it is a well-known fact that not all people with NSD have severe NAO symptoms. Moreover, some septal deviations are not symptomatic at all, and radiological diagnosis of NSD is usually an incidental finding. Our results pointed out that complicated shapes of NSD, e.g. Mladina's type 7, do not correlate with severe NAO. Some patients with this type of deviation did not have any trouble breathing through the nose (Table 8). Likewise, some patients with the NSD angle < 10˚ had severe NAO symptoms, whereas patients with NSD angles greater than 15˚ experienced less severe NAO (Table 8). Therefore, observing an anatomical aspect of NSD solely cannot be the criterion in the objective estimation of the NAO severity.

The NOSE scale in the current study detected that all patients with anterior NSD experienced some trouble with nose breathing (Table 8). This can indicate that the INV region is crucial for the emergence of NAO symptoms. However, it was not confirmed statistically that these particular types of NSD are more likely prone to cause severe NAO symptoms than other NSD types (Tables 10 and 11).

The current study demonstrated that any CT grading of NSD could not objectively confirm NAO severity. Hence, we could not recommend CT as a diagnostic tool of choice for an objective selection of septal surgery candidates. This indicates that third-party payors' current attitude to mandate CT examination prior to septoplasty just for an objective confirmation that nasal obstruction severity is not justified at all. Moreover, unnecessary radiation exposure, the extra cost of the examination, and the unjustified spending of patients' health insurance money could be considered as medical equipment overuse.

This study was the first to analyze the nasal airflow patterns thoroughly in various Mladina's NSD types by the CFD method and the impact of CFD-derived airflow parameters on NAO symptom severity. The presence of NSD alters all components of the nasal airflow dynamics that may contribute to the onset and severity of NAO symptoms. In this study, we identified particular CFD parameters that were directly associated with the NAO symptom severity in patients with different NSD types. These CFD parameters are side asymmetry in NR, turbulent kinetic energy, and heat flux. NSD-related changes in these airflow parameters activate different pathophysiological mechanisms that simultaneously contribute to the NAO perception.

Nasal airflow in the right and left nasal cavity is normally asymmetrical in the healthy nose. This phenomenon, known as the nasal cycle, occurs due to spontaneous periodic fluctuations in NR that alternate air to flow from one nasal cavity to the other (Pendolino et al., 2018). During a "working phase" of the nasal cycle, unilateral decongestion of erectile tissue in the nasal mucosa increases nasal width and decreases NR allowing the air to flow predominantly through this nasal cavity (Pendolino et al., 2018). Simultaneously, the opposite side of the nose is in a "resting phase" characterized by erectile tissue congestion, nasal width reduction, NR increase, and consequent less air volume flowing through this side (Pendolino et al., 2018). After several hours, the mucosal

congestion and decongestion change sides allowing the resting side of the nasal cavity to start "work" and become dominant for breathing, while the previously working side is "resting." During the nasal cycle, unilateral NR may vary greatly, but the total NR remains relatively constant (Cole, 1989).

In a patient without NSD, a cyclic shifting of mucosal congestion/decongestion and consequent nasal airflow alteration between the right and left nasal cavity occurs without any sensation. This function is under the control of the autonomic nervous system and exists even in the absence of the nasal airflow, for example, after laryngectomy (Fisher et al., 1994; Williams & Eccles, 2016). The patient, therefore, is not aware of the unilateral periodic changes of the NR as long as there is a minimal side difference in NR that stays relatively constant over time (Eccles, 1996). In general, patients are not aware of the function of any organ regulated by the autonomic nervous system, for example, the heartbeat, until it becomes abnormal, such as in the case of arrhythmia. Similarly, if NR becomes highly asymmetrical between nasal passages for any reason, in this case, due to NSD, this may result in troublesome nasal breathing.

The current study revealed various degrees of side asymmetry in pressure drop and CFD-NR related to the NSD type. Based on our results, the highest side differences in CFD-NR exist in NSD located in the INV region (types 1, 2, 4, and 7). These differences were accompanied by the unequal side distribution of nasal airflow (Table 12), which was lower on the narrow side. Such a result is not unexpected since the INV area is the narrowest segment in the entire nasal cavity. Even a small narrowing in the INV area may increase NR and, consequently, worse NAO (Cole et al., 1988; Dinis & Haider, 2002; Mlynski, 2013). Relatively small side differences in CFD-NR (slightly higher than the straight septum model) in types 6, 3, and 5 could be explained by NSD morphology. Types 3 and 5 are located in the posterior parts of the nasal cavity. Since the cross-sectional area in this part is much higher than in the anterior nasal cavity, inhaled air has enough space to bypass the narrow segment. Configuration of type 6 in our case did not cause significant side differences in the cross-sectional area and, subsequently, no significant effect on the NR side difference. More importantly, we demonstrated that NSD related side asymmetry in CFD-NR could be responsible for the subjective sensation of NAO severity.

Although experimental and clinical studies periodically reported side asymmetry in NR in patients with NSD (Cole et al., 1988; Ree et al., 2011; Rhee et al., 2012; Haavisto & Sipila, 2013; Radulesco et al., 2019), the clinical significance of this asymmetry has not been considered at all in the context of the NAO. Haavisto & Sipila (2013) found that patient satisfaction following septoplasty coincided with a unilateral decrease in RMM-derived NR on the previously narrowed side. When looking at their results, one could notice a great side asymmetry in the mean RMM-derived NR before septoplasty that reduced significantly after surgery. Recent CFD studies of Rhee et al. (2011; 2012) on pre and post-surgery NSD models contained similar findings. They found a great side asymmetry in CFD-NR in NSD models that normalized after septoplasty. The initial side asymmetry in airflow distribution showed the same trend after septoplasty. However, neither the side difference in CFD-NR was mentioned, nor its clinical impact on the NAO symptoms was discussed. More recently, Radulesco et al. (2019) reported side differences in NR and airflow rate in patients with NSD without further interpretation or correlation with NAO symptoms. In light of our results, it seems that reduced side asymmetry in NR after septoplasty may better explain symptom improvement than an isolated decrease in unilateral NR on the narrow side.

Side differences in CFD- NR in the current study were obtained when airflow was simulated through both nasal passages simultaneously. Unlike previous CFD studies, we minimized the effect of the nasal cycle to NR by applying nasal decongestants before CT imaging. In fact, the presence of the nasal cycle might worse NAO symptoms. NR at the narrow side is always high regardless of the nasal cycle phase. Moreover, cyclic changes in NR at the narrow side related to the mucosal congestion and decongestion are of reduced amplitude. When the narrow side is in the "working" phase, NR is insusceptible to the mucosal decongestion and remains high. Simultaneous mucosal

congestion on the opposite wide nasal passage normally increases NR that results in bilaterally high NR and consequently reduced patency of both nasal passages. Conversely, mucosal decongestion decreases NR on the wide side, allowing it to become dominant for breathing, whereas high NR at the narrow side is now even more accentuated due to mucosal congestion. The later would result in a more significant airflow reduction at the narrow side than normally expected in the "resting" phase of the nasal cycle. Besides, this would result in periodic fluctuations of the total NR that could contribute to the subjective sensation of the NAO.

In general, the greatest warming of inspired air takes place in the anterior nasal cavum. The sudden expansion of the airspace from the nasal isthmus to the head of the middle turbinate promotes the transition from laminar to turbulent airflow (Mlynski et al., 2001). The local presence of turbulence enables intense contact of inhaled air with mucosa and subsequent heat exchange (Cole, 2000; Mlynski et al., 2001). Behind the anterior nasal cavum, heat exchange gradually decreases. Studies that investigated the role of turbinates in inhaled air conditioning concluded that their heating capacity is limited. The middle and the inferior turbinate participate with 12% and 16% in air-conditioning, respectively, regardless of their relatively large mucosal surface area (Naftali et al., 2005). Although the posterior nasal cavum contributes little to the air heating process, the turbulence that is commonly present in the turbinate region is necessary to allow air-mucosa contact and consequent menthol sensitive (TRPM8) receptor stimulation (Lindemann et al., 2004; Scheithauer, 2010; Sozansky & Houser, 2014).

The current opinion about the origin of the NAO in patients with NSD is that activation of menthol sensitive (TRPM8) receptors is one of the crucial mechanisms responsible for nasal patency perception (Sozansky & Houser, 2014; Zhao et al., 2014; Sullivan et al., 2014). Despite a uniform distribution of these receptors throughout the entire nasal mucosa, Meusel et al. (2010) detected that only stimulation of menthol sensitive (TRPM8) receptors in the posterior nasal cavity correlate significantly with intranasal airflow. A similar association between CFD-derived heat flux posterior to the nasal vestibule and nasal patency was also reported by Zhao et al. (2014) and Sullivan et al. (2014). Authors considered these findings unexpected and commented that these receptors on larger post-vestibule surface areas might overpower the high receptor density in the nasal vestibule. However, our results suggest that the altered airflow turbulence profile caused by NSD could be responsible for the NAO severity.

Daily fluctuations in turbulent behavior of the inhaled air between right and left nasal passages are common phenomenon due to the nasal cycle (Lang et al., 2003). Mucosal decongestion during the "working" phase of the nasal cycle causes an increase in cross-sectional area in the anterior nasal cavum, thus promoting swirling of air and a local decrease in the airflow velocity (Lang et al., 2003). From a physiological standpoint, turbulence is necessary to ensure sufficient air-mucosa contact during an optimal time. This enables adequate heat transfer (warming) and air humidification, activation of menthol sensitive (TRPM8) receptors, and cleansing of inhaled air on its way to the lungs. Conversely, the "resting" (congested) phase results in a decreased cross-sectional area allowing predominance of the laminar airflow, while turbulent airflow may occur only at high velocities (Lang et al., 2003). Maintenance of a rhythmic change of turbulence profiles between nasal passages is crucial to prevent mucosa desiccation and the creation of micro-lesions (Beran & Petruson, 1986; Lang et al., 2003; Lindemann et al., 2003).

In order to explore and visualize turbulence profiles in their full potential in different Mladina's NSD types, we simulated the "working" phase of the nasal cycle simultaneously on both sides of the nasal cavity in all eight 3D models. This was achieved by applying intranasal decongestants before the CT examination. In comparison to the symmetrical distribution of airflow components in the straight septum model, seven NSD types showed substantial differences in turbulent kinetic energy (k) and heat flux. All NSD models demonstrated a various degree of k asymmetry between the right and left nasal passages. The greatest side asymmetry in k was

recorded in NSD types 2, 1, and 7, which were also associated with the most severe NAO symptoms. Such result is not unexpected since these three NSD types share similar morphological characteristics (curvature in the INV region). The descent of turbulence into lower nasal passages in type 6 can be explained by the fact that this type differs from other NSDs by its characteristic bilateral distortion in lower parts of the nasal cavity (intermaxillary bone wing on one side and as an anterior basal septal crest on the opposite side). In NSD type 5, disturbed laminar flow and a local increase in TKE at the spur's tip seemed to have no significant impact on NAO symptom severity.

Our study demonstrated that compromised airflow turbulence at the narrow side between the region of the inferior turbinate head and ostiomeatal complex reduces air-mucosa heat exchange significantly. Heat flux lines of the straight septum model were symmetrical and gradually decreased through the nasal cavity. Although the greatest heat transfer occurred in the anterior part of the nasal cavity up to the head of the middle turbinate, continuous heat transfer in the rest of the nasal cavity is of functional significance for nasal patency perception. Normally, when already warmed air (temperature range from 22˚C to 27˚C) reaches the turbinate region, it should have enough capacity to stimulate menthol sensitive (TRPM8) receptors (Liu et al., 2015). If for any reason, the air is warmer than it should be (temperature exceeds 27˚C), receptors will not be activated. In addition, the absence of turbulence will cause the same effect concerning that compromised mixing of the air would disable the contact of the mucosa with the cool air from the airstream center.

In our study, the greatest discrepancy in heat flux along the nasal cavity was recorded before and after the head of the middle turbinate in NSD models. Reduction of heat flux and k at this level was significantly associated with worse NOSE scores. The greatest side asymmetry in the heat flux was recorded in type 2 NSD. Steep heat flux line on the narrow side, as well as the absence of turbulence in this NSD type, suggest more prompt warming up of the inhaled air in the anterior segments of the nasal cavity. Behind the head of the middle turbinate, the heat flux was small, suggesting almost a negligible heat transfer in this region despite its relatively large mucosal surface area. This means that the air that reached the turbinate region was already quite warmed up and could not receive more heat. The air conditioned in such a way exceeds the optimal temperature range for receptor activation and consequently causes the subjective sensation of NAO.

Wall shear stress is a physical phenomenon caused by airflow that has an essential role in the conditioning and cleaning of the inhaled air. Air heating and humidification occur via the water-reach mucus layer on the nasal epithelium surface. The mucus is also involved in the air cleaning by trapping and removing airborne particles via mucociliary clearance (Williams et al., 1996). As demonstrated in the experimental in vitro studies on cell cultures, wall shear stress has a significant mechanical impact on the nasal epithelium function by regulating mucus secretion (Even-Tzur et al., 2008; Even-Tzur Davidovich et al., 2011). Epithelial goblet cells increase mucus secretion in response to wall shear stress in a magnitude-dependent manner (Even-Tzur et al., 2008; Even-Tzur Davidovich et al., 2011).

Previous CFD investigations of various nasal geometries showed a tendency of the WSS distribution to accumulate on the INV walls. This has been explained by the airflow direction change from vertical to horizontal, thus causing the high WSS (Wen et al., 2008). The maximum WSS values in CFD models with simplified NSD ranged between 0.2 and 1.6 Pa (Elad et al., 2006; Doorly et al., 2008; Wang et al., 2012) with the higher values registered in the narrow nasal passage. Some authors also found that NSD-related narrowing induces a relatively high WSS to distribute over a larger nasal wall area including the region around the head of the inferior and the middle turbinate (Bailie et al, 2008; Kim et al, 2014).

In the current study, the distribution and magnitude of the WSS in the normal nasal cavity and the Mladina's NSD types were in line with the data from the literature. Relatively lower maximum WSS values registered in our models in relation to the abovementioned WSS range could

be due to simulated quite nasal breathing (airflow velocity of 125 mL/s), concerning that the WSS magnitude is directly dependent on the airflow velocity. Noticeable side differences in the WSS magnitude and distribution observed in all NSD models could be an additional contributing factor to the NAO perception. Increased WSS distributed over the broader area in the anterior nasal cavum will result in excessive heating of the inhaled air in the narrowed nasal passage. When such overheated air reaches the nasal turbinate region, it has no or reduced potential to stimulate the menthol sensitive (TRPM8) receptors. Bearing in mind the reduction or the absence of the turbulence in the narrowed nasal cavity, these two CFD parameters may mutually contribute to the severity of the NAO symptoms.

6. CONCLUSIONS

The Serbian version of the NOSE scale is valid, reliable, user-friendly, and sensitive to assess the presence and the level of nasal obstruction symptom severity.

The prevalence of the nasal septal deviation in the Serbian population is 92.7%. The most common Mladina's type of the nasal septal deviation was type 7 (34.9%), while the least frequent was type 2 (0.6%). The mean angle value of the nasal septal deviation was $8.6° \pm 3.4$.

Patients with various NSD types differed in NAO severity. Generally, deviations affecting the anterior part of the nasal septum have more severe NAO symptoms. Paradoxically, patients with asymptomatic NSD have slightly higher NSD angle values. In symptomatic patients, higher NSD angle values are accompanied by less severe NAO symptoms. Observed differences were not confirmed as statistically significant. Our analysis did not identify any particular NSD type (within any classification system) that was more likely prone to cause nasal obstruction symptoms. The absolute value of the NSD angle and the angle-based NSD classification could not predict the severity of the NAO symptoms. The presence of septal spurs and whether they divide nasal passages did not show a predictive effect on NAO severity. Therefore, observation of a morphological aspect of NSD solely cannot be the criterion in the objective estimation of the NAO symptom severity.

The presence of NSD causes differences in nasal airflow patterns in relation to the NSD type.

Patients with different Mladina's NSD types have asymmetrical flow partitioning between right and left nasal passages, independent of the nasal cycle. The greatest asymmetry in flow partitioning is associated with Mladina's type 2 NSD.

Regardless of the presence and type of NSD, the airflow velocity inside nasal passages is similar, being the highest in the internal nasal valve area. In the nasal cavity with a straight septum, the main airstream flows symmetrically through the central part of the nasal passages at the middle meatus level. The presence of NSD induces a various degree of side asymmetry in airflow velocity profile with the redirection of airstream toward the inferior nasal meatus in the majority of NSD types. During calm breathing, the predominant airflow pattern is laminar in nasal cavities with and without NSD.

The INV region in all 3D models was subjected to the highest wall shear stress. While nasal cavity without NSD had symmetrical side distribution and the magnitude of the wall shear stress, NSD induced various side discrepancies in its magnitude. NSD-related narrowing of the nasal passage resulted in an ipsilateral elevation of the wall shear stress, being the most accentuated in the NSD type 7.

Transnasal pressure drop in the nasal cavity with a straight septum is similar in both nasal passages with a minimal side difference in CFD-NR. Different NSD types cause side asymmetry in pressure drop patterns and CFD-NR. Deviations that affect the anterior segment of the nasal septum (Mladina's NSD type 1, 2, 4, and 7) exhibit the largest side differences in the mean pressure values and CFD-NR. The presence of a bony spur does not affect pressure values.

Compared with bilaterallysimilarheat flux values in the nasal cavity with a straight septum, NSD causes more or less pronounced side asymmetry in heat flux depending on the NSD type. Mladina's type 2 NSD induces the largest side difference in heat flux.

The nasal cavity with a straight septum has a symmetrical turbulent kinetic energy profile between the right and left nasal passage, whereas the presence of NSD causes side differences in distribution and intensity of turbulent kinetic energy. NSD-related narrowing of the nasal passage

was associated with a partial or complete reduction in turbulent kinetic energy. The presence of a bony spur causes a local increase in turbulent kinetic energy at the spur's tip.

Our study revealed possible mechanisms by which NSD-induced alterations in nasal airflow patterns may contribute to the NAO severity. The most important airflow parameters responsible for the NAO severity are the side asymmetry in CFD-NR, wall shear stress, heat flux, and the turbulent kinetic energy in the narrowed nasal passage. Our results suggest that NAO perception will be absent in nasal cavities in which the side difference in NR is constant regardless of the nasal cycle phase, and the total NR remains unchanged over time. By contrast, the subjective sensation of NAO will occur when NSDs induce unstable side differences in NR during the nasal cycle phase shifting, subsequently causing pronounced periodic fluctuations of the total NR.

Subjective sensation of NAO may also be provoked by the absence of turbulence and consequent reduction of heat flux in the narrowed nasal passage. Compromised mixing of the air prevents the colder air from the airstream center to reach the mucosa and stimulates menthol sensitive (TRPM8) receptors. The lack of the "cold" stimulus to these receptors will lead to the NAO perception. As evidenced by locally elevated wall shear stress inside the narrowed nasal passage, the mucosa's cooling effect could be additionally diminished by NSD-induced excessive heating of the inhaled air in the anterior nasal cavum. When such overheated air meets the menthol sensitive (TRPM8) receptors reach mucosa, it has no potential for their activation and consequently contributes to the NAO perception.

From the clinical perspective, the results of this study strongly support the application of a multidisciplinary approach in diagnosing NSD-related NAO that should include radiologists, ENT specialists, and mechanical engineers dealing with fluid mechanics. Considering the impact of the NSDs affecting the INV region on the nasal airflow dynamics and NAO symptoms severity, a more detailed analysis of this region by radiologists would be of particular clinical importance. We suggest the inclusion of Mladina's NSD classification in the radiological report due to its easy applicability and necessity for the INV angle measurement. Based on the confirmed association between NSD-related NAO and specific nasal airflow parameters in a large sample, future studies should focus on a patient-specific approach to diagnosing NSD-related NAO. This concept would require the standardized CFD application in daily ENT practice, the definition of normative ranges of CFD parameters, CFD-assisted confirmation of NAO in NSD patients, and CFD-based estimation of a possible surgical treatment outcome.

7. REFERENCES

1. Aday LA. Defining and clarifying the survey variables. Designing and conducting health surveys: a comprehensive guide, 2nd ed., San Francisco: Jossey-Bass Publishers; 1996, p. 48-80.

2. Amer MA, Kabbash IA, Younes A, Elzayat S, Tomoum MO. Validation and cross-cultural adaptation of the Arabic version of the Nasal Obstruction Symptom Evaluation scale. Laryngoscope 2017; doi:10.1002/lary.26640.

3. Andre RF, Vuyk HD, Ahmed A, Graamans K, Nolst Trenite GJ. Correlation between subjective and objective evaluation of the nasal airway. A systematic review of the highest level of evidence. Clin Otolaryngol 2009; 34: 518-525.

4. Ardeshirpour F, McCarn KE, McKinney AM, Odland RM, Yueh B, Hilger PA. Computed tomography scan does not correlate with patient experience of nasal obstruction. Laryngoscope 2016; 126: 820-825.

5. Aziz T, Biron VL, Ansari K, Flores-Mir C. Measurement tools for the diagnosis of nasal septal deviation: a sistematic review. J Otolaryngol Head Neck Surg 2014; 43: 11.

6. Bailie N, Gallagher G, Cole J, Watterson J. Computational fluid dynamics in the investigation and treatment of the nasal obstruction. WIT Transactions on State of the Art in Science and Engineering, 2008; 35: doi:10.2495/978-1-84564-096-5/07.

7. Baraniuk JN. Subjective nasal fullness and objective congestion. Proc Am Thorac Soc 2011; 8: 62-69.

8. Barrett KE, Barman SM, Boitano S, Brooks HL. Ganong's review of medical physiology, 25th ed., New York: McGraw-Hill Education; 2016.

9. Baumann I. Quality of life before and after septoplasty and rhinoplasty. GMS Cur Top Otorhinolaryngol Head Neck Surg 2010; 9: doi:10.3205/cto000070.

10. Beaton DE, Bombardier C, Guillemin F, Ferraz MB. Guidelines for the process of cross-cultural adaptation of self-report measures. Spine 2000; 25: 3186-3191.

11. Becker SS, Dobratz EJ, Stowell N, Barker D, Park SS. Revision septoplasty: review of sources of persistent nasal obstruction. Am J Rhinol 2008; 22: 440-444.

12. Behrbohm H. The nose as an aerodynamic body, In: The NOSE - Revision & Reconstruction. Manual and Casebook, Stuttgard: Thieme, 2015.

13. Beran M, Petruson B. Occurrence of epistaxis in habitual nose-bleeders and analysis of some etiological factors. ORL 1986; 48: 297-303.

14. Bermuller C, Kirsche H, Rettinger G, Riechelmann H. Diagnostic accuracy of peak nasal inspiratory flow and rhinomanometry in functional rhinosurgery. Laryngoscope 2008; 118: 605-610.

15. Beule AG. Physiology and pathophysiology of respiratory mucosa of the nose and the nose and the paranasal sinuses. GMS Curr Top Otorhinolaryngol Head Neck Surg 2010; 9.

16. Bezerra TF, Padua FG, Pilan RR, Stewart MG, Voegels RL. Cross-cultural adaptation and validation of a quality of life questionnaire: the Nasal Obstruction Symptom Evaluation questionnaire. Rhinology 2011; 49: 227-231.

17. Bhattacharyya N. Ambulatory sinus and nasal surgery in the United States: demographic and perioperative outcomes. Laryngoscope 2010; 120: 635-638.

18. Borojeni AAT, Garcia GJM, Moghaddam MG, Frank-Ito DO, Kimbell JS, Laud PW, et al. Normative ranges of nasal airflow variables in healthy adults. Int J Comput Assist Radiol Surg 2020; 15(1): 87-98.

19. Cakmak O, Celik H, Cankurtaran M, Ozluglu LN. Effects of anatomical variations of the nasal cavity on acoustic rhinometry measurements: a model study. Am J Rhinol 2005; 19: 262-268.

20. Cankurtaran M, Celik H, Coskun M, Hizal E, Cakmak O. Acoustic rhinometry in healthy humans: accuracy of area estimates and ability to quantify certain anatomic structures in the nasal cavity. Ann Otol Rhinol Laryngol 2007; 116: 906-916.

21. Cauna N. Blood and nerve supply of the nasal lining. In: Proctor DF, Anderson IB, editors. The nose. Amsterdam: Elsevier Biomedical Press; 1982, p.45-70.

22. Chen XB, Lee HP, Chong VFH, Wang DY. Assessment of septal deviation effects on nasal air flow: a computational fluid dynamics model. Laryngoscope 2009; 119: 1730-1736.

23. Clement PAR. Committee report on standardisation of rhinomanometry. Rhinology 1984; 22: 151-155.

24. Clement P, Gordts F. Consensus report on acoustic rhinometry and rhinomanometry. Rhinology 2005; 43: 169-179.

25. Cole P, Chaban R, Naito K, Oprysk D. The obstructive nasal septum. Effect of simulated deviations on nasal airflow resistance. Arch Otolaryngol Head Neck Surg 1988; 114(4): 410-412.

26. Cole P. Stability of nasal airflow resistance. Clin Otolaryngol Allied Sci 1989; 14: 177-182.

27. Cole P. Biophysics of nasal airflow: a review. Am J Rhinol 2000; 14: 245-249.

28. Courtiss EH, Goldwyn RM. The effects of nasal surgery on airflow. Plast Reconstr Surg 1983; 72: 9-19.

29. Cuddihy PJ, Eccles R. The use of nasal spirometry as an objective measure of nasal septal deviation and the effectiveness of septal surgery. Clin Otolaryngol 2003; 28: 325-330.

30. Daghistani KJ. Nasal septal deviation in Saudi patients: a hospital based study. J Kau Med Sci 2002; 10: 39-46.

31. Daniel WW. Biostatistics: A Foundation for Analysis in the Health Sciences, 7th ed., New York: John Wiley & Sons; 1999.

32. Delaney SW. Evolution of the septoplasty: maximizing functional and aestetic outcomes in nasal surgery. M J Otol 2018; 1(1): 004.

33. Dinis PB, Haider H. Septoplasty: Long-term evaluation of results. Am J Otolaryngol 2002; 23: 85-90.

34. Dong D, Zhao Y, Stewart MG, Sun L, Cheng H, Wang J, et al. Development of the Chinese nasal obstruction symptom evaluation (NOSE) questionnaire. Zhonghua Er Bi Yan Hou Tou Jing Wai Ke Za Zhi 2014; 49: 20-26.

35. Doorly DJ, Taylor DJ, Schroter RC. Mechanics of airflow in the human nasal airways. Respir Physiol Neurobiol 2008; 163: 100-110.

36. Eccles R. A role for the nasal cycle in respiratory defence. Eur Respir J 1996; 9: 371-376.

37. Elad D, Naftali S, Rosenfeld M, Wolf M. Physical stress at the air-wall interface of the human nasal cavity during breathing. J Appl Physiol 2006; 100: 1003-1010.

38. Even-Tzur N, Kloog Y, Wolf M, Elad D. Mucus secretion and cytoskeletal modifications in cultured nasal epithelial cells exposed to wall shear stress. Biophysical Journal 2008; 95: 2998-3008.

39. Even-Tzur Davidovich N, Kloog Y, Wolf M, Elad D. Mechanophysical stimulation of Mucin Secretion in Cultures of Nasal Epithelial Cells. Biophys J 2011; 100: 2855-2864.

40. Fisher EW, Liu M, Lung VJ. The nasal cycle after deprivation of airflow: a study of laryngectomy patients using acoustic rhinometry. Acta Otolaryngol 1994; 114: 443-446.

41. Garcia GJM. Visualization of nasal airflow patterns in a patient affected with atrophic rhinitis using particle image velocimetry. J Physics: Conference Series. 2007; 85(1): 012032-7.

42. Goubergrits L, Schaller J, Kertzscher U, van den Bruck N, Poethkow K, Petz Ch, et al. Statistical wall shear stress maps of ruptured and unruptured middle cerebral artery aneurysms. J R Soc Interface 2012; 9(69): 677–688.

43. Goubergrits L, Mevert R, Yevtushenko P, et al. The impact of MRI based inflow for the hemodynamic evaluation of aortic coarctation. Ann Biomed Eng 2013; 41(12): 2575–2587.

44. Grutzenmacher S, Robinson DM, Grafe K, Lang C, Mlynski G. First findings concerning airflow in noses with septal deviation and compensatory turbinate hypertrophy - a model study. ORL 2006; 68: 199-205.

45. Gunbey E, Karabulut H. The relationship between the migraine and obstructive nasal pathologies. Acta Med Mediterr 2014; 30: 1249-1253.

46. Guyuron B, Uzzo CD, Scull H. A practical classification of septonasal deviation and an effective guide to septal surgery. Plast Reconstr Surg 1999; 104: 2202-2209.

47. Haavisto LE, Sipila JI. Acoustic rhinometry, rhinomanometry and visual analogue scale before and after septal surgery: a prospective 10-year follow-up. Clin Otolaryngol 2013; 38(1): 23-29.

48. Hall RL. Energetics of nose and mouth breathing, body size, body composition, and nose volume in young adult males and females. Am J Hum Biol 2005; 17(3): 321-330.

49. Hildebrandt T, Goubergrits L, Heppt WJ, Bessler S, Zachow S. Evaluation of the intranasal flow field through computational fluid dynamics. Facial Plast Surg 2013; 29: 93-98.

50. Hinderer KH. Fundaments of Anatomy and Surgery of the Nose, London: Aesculapius Publishing Co; 1971, p.1-3.

51. Juretic F. cfMesh user guide. Document version: 1.1, Creative Fields, Zagreb, 2015 http://cfmesh.com/wp-content/uploads/2015/09/User_Guide-cfMesh_v1.1.pdf

52. Kahveci OK, Miman MC, Yucel A, Yucedag F, Okur E, Altuntas A. The efficiency of Nose Obstruction Symptom Evaluation (NOSE) scale on patients with nasal septal deviation. Auris Nasus Larynx 2012; 39: 275-279.

53. Kayser R. Die exacte Messung der Luftdurchgängigkeit der Nase. Arch Laryngol. 1895; 3: 101-120.

54. Kim SK, Heo GE, Seo A, Na Y, Chung SK. Correlation between nasal airflow characteristics and clinical relevance of nasal septal deviation to nasal airway obstruction. Respir Rhysiol Neurobiol 2014; 192: 95-101.

55. Kimbell JS, Garcia GJM, Frank DO, Cannon DE, Pawar SS, Rhee JS. Computed nasal resistance compared with patient-reported symptoms in surgically treated nasal airway passages: A preliminary report. Am J Rhinol Allergy 2012; 26: e94-e98.

56. Kimbell JS, Frank DO, Laud P, Garcia GJ, Rhee JS. Changes in nasal airflow and heat transfer correlate with symptom improvement after surgery for nasal obstruction. J Biomech 2013; 46(15): 2634-2643.

57. Lachanas VA, Tsiouvaka S, Tsea M, Hajiioannou JK, Skoulakis CE. Validation of the nasal obstruction symptom evaluation (NOSE) scale for Greek patients. Otolaryngol Head Neck Surg 2014; 151: 819-823.

58. Lang J. Clinical anatomy of the nose, nasal cavity and paranasal sinuses, New York: Thieme Medical Publishers; 1989.

59. Lang C, Grutzenmacher S, Mlynski B, Plontke S, Mlynski G. Investigating the nasal cycle using endoscopy, rhinoresistometry, and acoustic rhinometry. Laryngoscope 2003; 113: 284-289.

60. Larrosa F, Roura J, Dura MJ, Guirao M, Alberti A, Alobid I. Adaptation and validation of the Spanish version of the Nasal Obstruction Symptom Evaluation (NOSE) Scale. Rhinology 2015; 53: 176-180.

61. Lauffer A, Solé L, Bernstein S, Lopes MH, Francisconi CF. Practical aspects for minimizing errors in the cross-cultural adaptation and validation of quality of life questionnaires. Rev Gastroenterol Mex 2013; 78: 159-176.

62. Lebowitz RA, DoudGalli SK, Holliday RA, Jacobs JB. Nasal septal deviation: a comparison of clinical and radiological evaluation. Oper Tech Otolayngol Head Neck Surg 2001; 12(2): 104-106.

63. Lee DC, Shin JH, Kim SW, Kim SW, Kim BG, Kang JM, et al. Anatomical analysis of nasal obstruction: nasal cavity of patients complaining of stuffy nose. Laryngoscope 2013; 123: 1381-1384.

64. Leite SHP, Jain R, Douglas RG. The clinical implications of computerised fluid dynamic modeling in rhinology. Rhynology 2019; 57(1): 2-9.

65. Leong SC, Chen XB, Lee HP, Wang DY. A review of the implications of computational fluid dynamic studies on nasal airflow and physiology. Rhinology 2010; 48: 139-145.

66. Lindemann J, Leiacker R, Rettinger G, Keck T. The relationship between water vapour saturation of inhaled air and nasal patency. Eur Respir J 2003; 21: 313-316.

67. Lindemann J, Keck T, Wiesmiller K, Sander B, Brambs HJ, Rettinger G, et al. A numerical simulation of intranasal air temperature during inspiration. Laryngoscope 2004; 114: 1037-1041.

68. Liu T, Han D, Wang J, Tan J, Zang H, Wang T, et al. Effects of septal deviation on the airflow characteristics: Using computational fluid dynamics models. Acta Otolaryngol 2012; 132: 290-298.

69. Liu SC, Lu HH, Cheng LH, Chu YH, Lee FP, Wu CC, et al. Identification of the cold receptor TRPM8 in the nasal mucosa. Am J Rhinol Allergy 2015; 29: e112-e116.

70. Mamikoglu B, Houser S, Akbar I, Ng B, Corey JP. Acoustic rhinometry and computed tomography scans for the diagnosis of nasal septal deviation, with clinical correlation. Otolaryngol Head Neck Surg 2000; 123: 61-68.

71. Marro M, Mondina M, Stoll D, de Gabory L. French validation of the NOSE and Rhino QOL questionnaires in the management of nasal obstruction. Otolaryngol Head Neck Surg 2011; 144: 988-993.

72. Menter FR. Two-equation eddy-viscosity turbulence models for engineering application. AIAA Journal 1994; 32(8): 1598-1605.

73. Meusel T, Negoias S, Scheibe M, Hummel T. Topographical differences in distribution and responsiveness of trigeminal sensitivity within the human nasal mucosa. PAIN 2010; 151: 516-521.

74. Mladina R. Deformacije nosnog septuma i piramide, Zagreb: Školska knjiga; 1990.

75. Mladina R, Cujic E, Subaric M, Vukovic K. Nasal septal deformities in ear, nose, and throat patients: An international study. Am J Otolaryngol 2008; 29: 75-82.

76. Mlynski G. Physiology and pathophysiology of nasal breathing. In: Onerci M, ed. Nasal Physiology and Pathophysiology of Nasal Disorders, Heidelberg: Springer; 2013: p. 257-272.

77. Mlynski G, Beule A. Diagnostik der respiratorischen funktion der nase. HNO 2008; 56: 81-99.

78. Mlynski G, Grutzenmacher S, Plontke S, Mlynski B, Lang C. Correlation of nasal morphology and respiratory function. Rhinology 2001; 39: 197-201.

79. Mohebbi A, Ahmadi A, Etemadi M, Safdarian M, Ghourchian S. An epidemiologic study of factors associated with nasal septum deviation by computed tomography scan: a cross sectional study. BMC Ear Nose Throat Disord 2012;12: doi:10.1186/1472-6815-12-15.

80. Moukalled F, Mangani L, Darwish M. The finite volume method in computational fluid dynamics - An advanced introduction with OpenFOAM and Matlab, Springer; 2016.

81. Mozzanica F, Urbani E, Atac M, Scotta G, Luciano K, Bulgheroni C, et al. Reliability and validity of the Italian nose obstruction symptom evaluation (I-NOSE) scale. Eur Arch Otorhinolaryngol 2013; 270: 3087-3094.

82. Naftali S, Rosenfeld M, Wolf M, Elad D. The air-conditioning capacity of the human nose. Ann Biomed Eng 2005; 33(4): 545-553.

83. Naing L, Winn T, Rusli BN. Practical issues in calculating the sample size for prevalence studies. Arch Orofac Sci 2006; 1: 9-14.

84. Naito K, Cole P, Chaban R, Oprysk D. Nasal resistance, sensation of obstruction and rhinoscopic findings compared. Am J Rhinol 1988; 2: 65-69.

85. Naito K, Cole K, Humphrey D. Unilateral and bilateral nasal resistances: A supplement. Rhinology 1990; 28: 91-95.

86. Netter FH. Atlas anatomije čoveka, 2.srpsko izdanje, urednici Milisavljević M, Maliković A, Beograd: Data status; 2004.

87. O'Reilly BJ, Simpson DC, Dharmeratnam R. Recurrent epistaxis and nasal septal deviation in young adults. Clin Otolaryngol 1996; 21: 12-14.

88. Ottaviano G, Fokkens WJ. Measurements of nasal airflow and patency: a critical review with emphasis on the use of peak nasal inspiratory flow in daily practice. Allergy 2016; 71: 162-174.

89. Ozlugedik S, Nakiboglu G, Sert C, Elhan A, Tonuk E, Akyar S, et al. Numerical study of the aerodynamic effects of septoplasty and partial lateral turbinectomy. Laryngoscope 2008; 118: 330-334.

90. Pendolino AL, Lund VJ, Nardello E, Ottaviano G. The nasal cycle: a comprehensive review. Rhinology 2018; 1: 67-76.

91. Prus M, Wysocki J, Krasny M, Niemczyk K. Nasal resistance asymmetry as a predictor of satisfaction following nasal airway obstruction surgeries. Pol Otorhino Rev 2017; 6(4): 1-9.

92. Rao JJ, Kumar EC, Babu KR, Chowdary VS, Singh J, Rangamani CV. Classification of nasal septal deviations - relation to sinonasal pathology. Indian J Otolaryngol Head Neck Surg 2005; 57: 199-201.

93. Radulesco T, Meister L, Bouchet G, Varoquaux A, Giordano J, Mancini J, et al. Correlations between computational fluid dynamics and clinical evaluation of nasal airway obstruction due to septal deviation: An observational study. Clinical Otolaryngology 2019; 44(4): 603-611.

94. Reichenheim ME, Moraes CL. Operationalizing the cross-cultural adaptation of epidemiological measurement instruments. Rev Saude Publica 2007; 41: 665-673.

95. Rhee JS, Pawar SS, Garcia GM, Kimbell JS. Toward personalized nasal surgery using computational fluid dynamics. Arch Facial Plast Surg 2011; 13(5): 305-310.

96. Rhee JS, Cannon DE, Frank DO, Kimbell JS. Role of virtual surgery in preoperative planning. Assessing the individual components of functional nasal airway surgery. Arch Facial Plast Surg 2012; 14(5): 354-359.

97. Sahin-Yilmaz A, Naclerio RM. Anatomy and physiology of the of the upper airway. Proc Am Thorac Soc 2011; 8: 31-39.

98. Savovic S, Kljaic V, Buljacik Cupic M, Jovancevic LJ. The influence of nasal septum deformity degree on subjective nasal breathing assessment. Med Pregl 2014; 67: 61-64.

99. Scheithauer MO. Surgery of the turbinates and "empty nose" syndrome. GMS Curr Top Otorhinolaryngol Head Neck Surg 2010; 9: doi: 10.3205/cto000067.

100. Sedaghat AR, Kieff DA, Bergmark RW, Cunnane ME, Busaba NY. Radiographic evaluation of nasal septal deviation from computed tomography correlates poorly with physical exam findings. Int Forum Allergy Rhinol 2014; 5: 258-262.

101. Serifoglu I, Ilker I, Damar M, Buyukuysal MC, Tosun A, Tokgoz O. Relationship between the degree and direction of nasal septum deviation and nasal bone morphology. Head Face Med 2017; 13: 3.

102. Shimzu T. Mucus, Goblet Cell, Submucosal Gland. In: Onerci M, ed. Nasal Physiology and Pathophysiology of Nasal Disorders. Heidelberg: Springer; 2013, p.1-13.

103. Simmen D, Scherrer JL, Moe K, Heinz B. A dynamic and direct visualization model for the study of nasal airflow. Arch Otolaryngol Head Neck Surg 1999; 125: 1015-1021.

104. Smith KD, Edwards PC, Saini TS, Norton NS. The prevalence of concha bullosaa and nasal septal deviation and their relationship to maxillary sinusitis by volumetric tomography. Int J Dent 2010; doi: 10.1155/2010/404982.

105. Sousa VD, Rojjanasrirat W. Translation, adaptation and validation of instruments or scales for use in cross-cultural health care research: a clear and user-friendly guideline. J Eval Clin Pract 2011; 17: 268-274.

106. Sozansky J, Houser SM. The physiological mechanism for sensing nasal airflow: a literature review. Int Forum Allergy Rhinol 2014; 4: 834-838.

107. Standring S, Borley NR, Gray H. Gray's anatomy: the anatomical basis of clinical practice. 40th ed., Edinburgh: Churchill Livingstone/Elsevier, 2008, p. 547-559.

108. Stewart MG, Witsell DL, Smith TL, Weaver EM, Yueh B, Hannley MT. Development and validation of the Nasal Obstruction Symptom Evaluation (NOSE) scale. Otolaryngol Head Neck Surg 2004; 130: 157-163.

109. Stoksted P. Rhinometric measurements for determination of the nasal cycle. Acta Otolaryngol Suppl 1953; 109: 159-175.

110. Suh MW, Jin HR, Kim JH. Computed tomography versus nasal endoscopy for the measurement of the internal nasal valve angle in Asians. Acta Otolaryngol 2008; 128: 675-679.

111. Sullivan CD, Garcia GJM, Frank-Ito DO, Kimbell JS, Rhee JS. Perception of better nasal patency correlates with increased mucosal cooling after surgery for nasal obstruction. Otolaryngol Head Neck Surg 2014; 150(1): 139-147.

112. Taghiloo H, Halimi Z. The frequencies of different types of nasal septum deviation and their effect on increasing the thickness of maxillary sinus mucosa. J Dent Res Dent Clin Dent Prospects 2019; 13(3): 208-214.

113. Tarhan E, Coskun M, Cakmak O, Celik H, Cankurtaran M. Acoustic rhinometry in humans: accuracy of nasal passage area estimates, and ability to quantify paranasal sinus volume and ostium size. J Appl Physiol 2005; 99: 616-623.

114. Thomas A, Alt J, Gale C, et al. Surgeon and hospital cost variability for septoplasty and inferior turbinate reduction. Int Forum Allergy Rhinol 2016; 20: 1–6.

115. Tomkinson A, Eccles R. Comparison of the relative abilities of acoustic rhinometry, rhinomanometry, and the visual analogue scale in detecting change in the nasal cavity in a healthy adult population. Am J Rhinol 1996; 10: 161-165.

116. Urbančič J, Soklič Košak T, Jenko K, Božanić Urbančič N, Hudoklin P, Delakorda M, et al. Cross-cultural adaptation and validation of nasal obstruction symptom evaluation questionnaire in Slovenian language. Zdr Varst 2016; 56: 18-23.

117. Van Egmond MM, Rovers MM, Hendriks CT, van Heerbeek N. Effectiveness of septoplasty versus non-surgical management for nasal obstruction due to a deviated nasal septum in adults: study protocol for a randomized controlled trial. Trials 2015; 16: 500.

118. Van Zijl FV, Timman R, Datema FR. Adaptation and validation of the Dutch version of the nasal obstruction symptom evaluation (NOSE) scale. Eur Arch Otorhinolaryngol 2017; doi:10.1007/s00405-017-4486-y.

119. Wang DY, Heow PL, Bruce RG. Impacts of fluid dynamics simulation in study of nasal airflow physiology and pathophysiology in realistic human three-dimensional nose models. Clin Exp Otorhinolaryngol 2012; 5(4): 181-187.

120. Wee JH, Kim DW, Lee JE, Rhee CS, Lee CH, Min YG, et al. Classification and prevalence of nasal septal deformity in Koreans according to two classification systems. Acta Otolaryngol 2012; 132: S52-S57.

121. Wen J, Inthavong K, Tu J, Wang S. Numerical simulations for detailed airflow dynamics in human nasal cavity. Respiratory Physiology & Neurobiology 2008; 161: 125-135.

122. Williams M, Eccles R. A model for the central control of airflow patterns within the human nasal cycle. J Laryngol Otol 2016; 130: 82-88.

123. Williams R, Rankin N, Smith T, Galler D, Seakins P. Relationship between the humidity and temperature of inspired gas and the function of the airway mucosa. Crit Care Med 1996; 24: 1920-1929.

124. Wolf M, Naftali S, Schroter RC, Elad D. Air conditioning characteristics of the human nose. J Laryngol Otol 2004; 118: 87-92.

125. Wotman M, Kacker A. What are the indications for the use of computed tomography before septoplasty? Laryngoscope 2016; 126: 1268-1270.

126. Zachow S, Muigg P, Hildebrant T, Doleisch H, Hege HC. Visual Exploration of Nasal Airflow. IEEE Trans VISUAL Comput Graph 2009; 15(6): 1407-1414.

127. Zhao K, Jiang J. What is normal airflow? A computational study of 22 healthy adults. Int Forum Allergy Rhinol 2014; 4(6): 435-446.

128. Zhao K, Jiang J, Blacker K, Lyman B, Dalton P, Cowart BJ, et al. Regional peak mucosal cooling predicts the perception of nasal patency. Laryngoscope 2014; 124: 589-595.

APPENDICES

Figure 9. The nasal airflow velocity profile in a straight septum model and seven Mladina's NSD types at selected cross-sections along the nasal cavity

STRAIGHT SEPTUM MODEL

TYPE 1 NSD

S1

S2

S3

S4

S5

S6

S7

S8

S1

S2

S3

S4
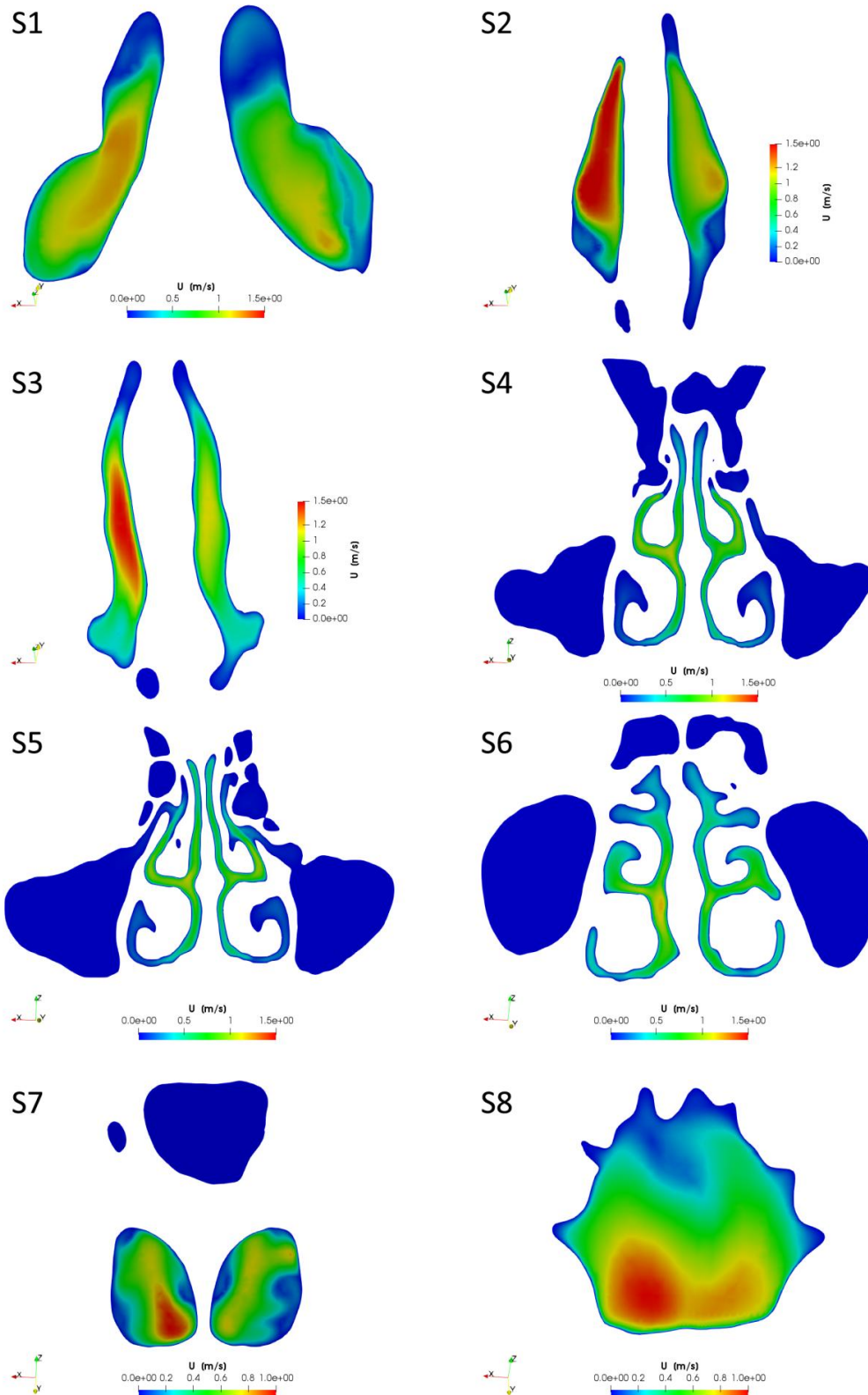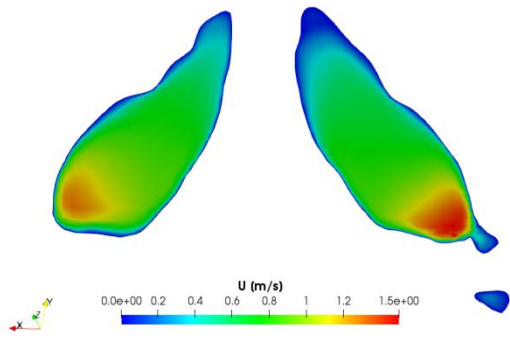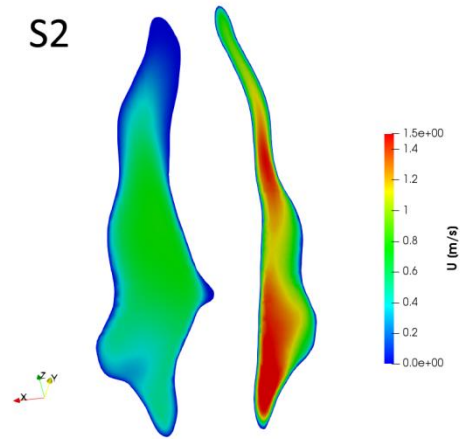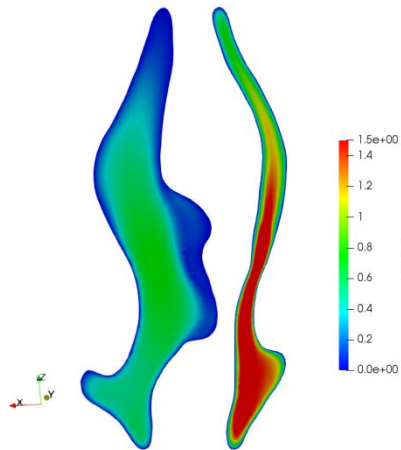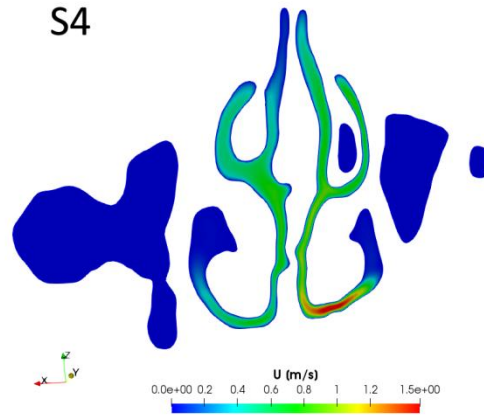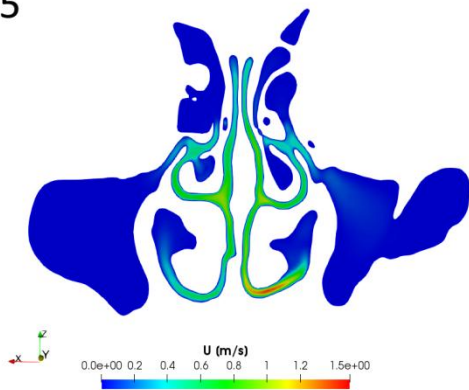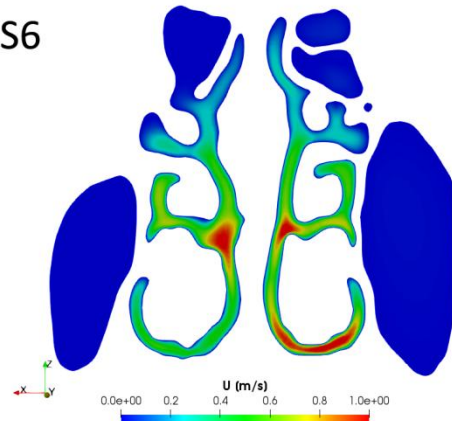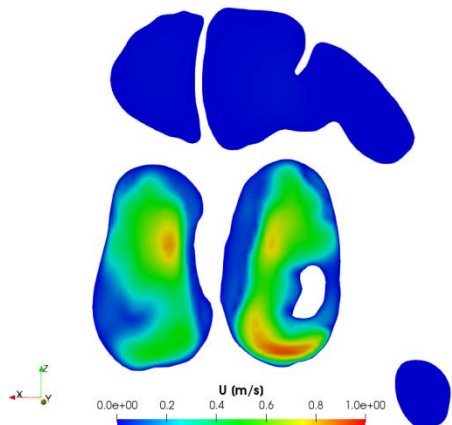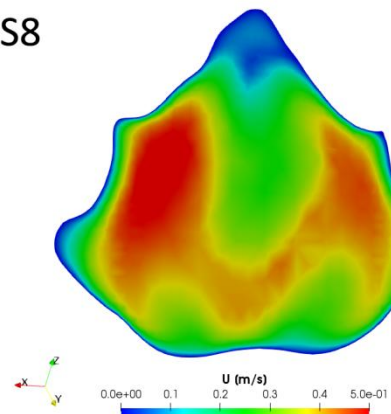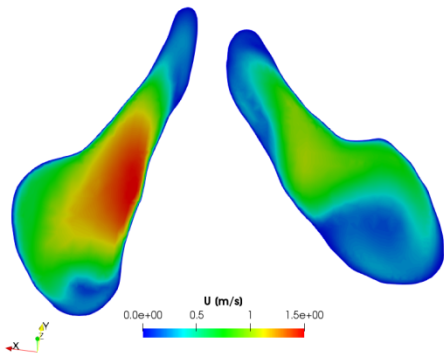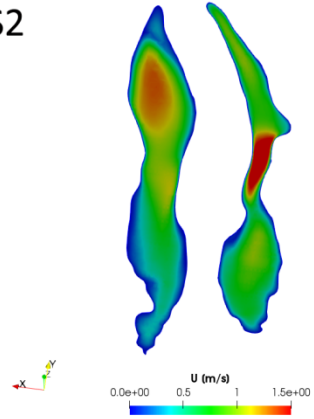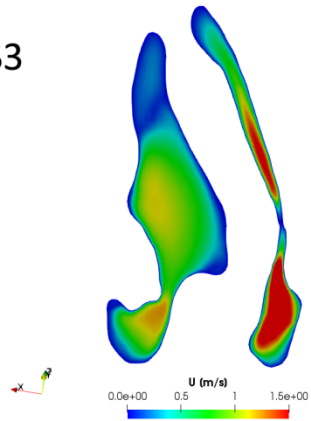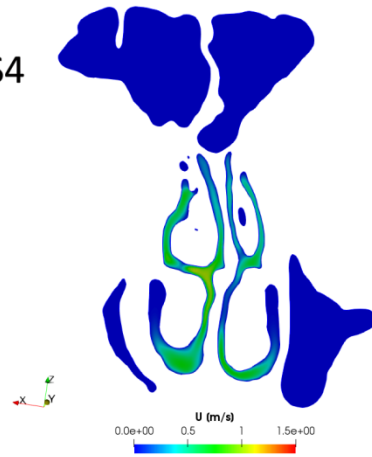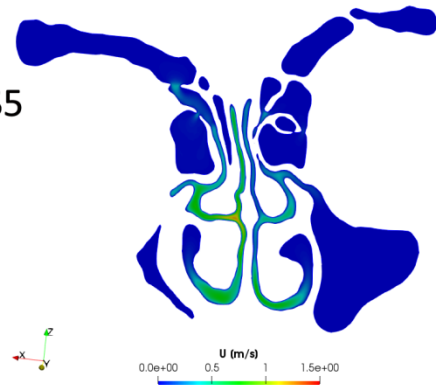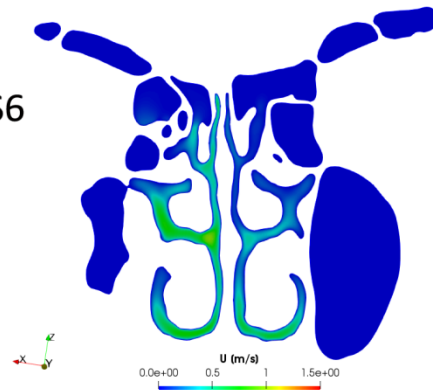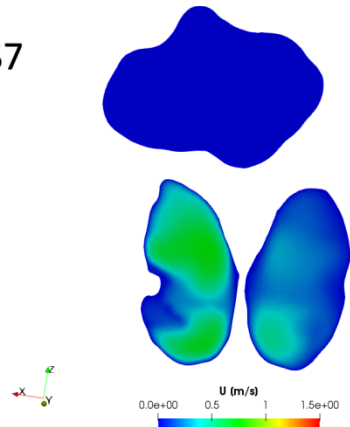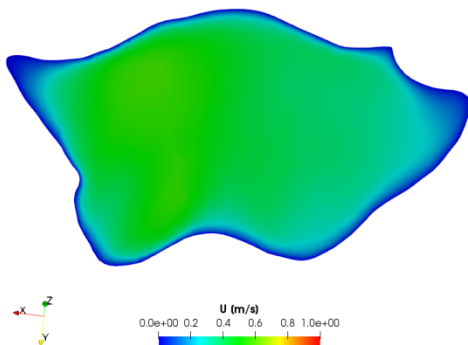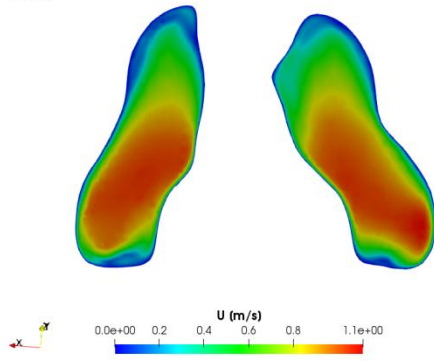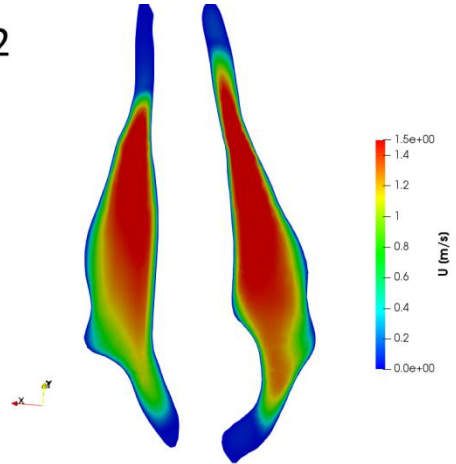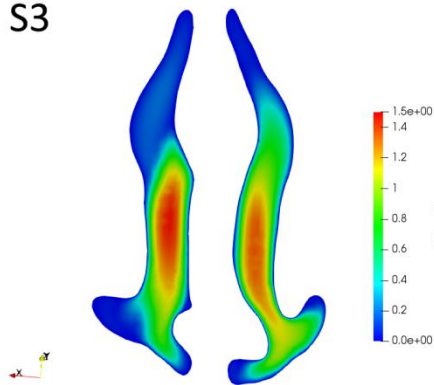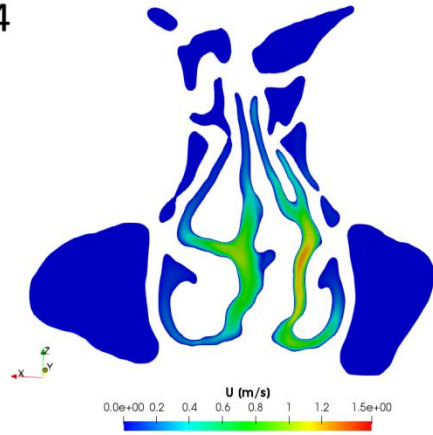
S5
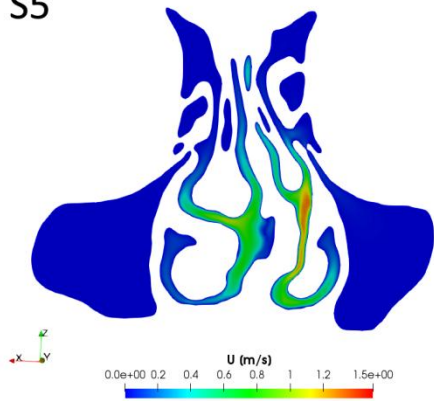
S6
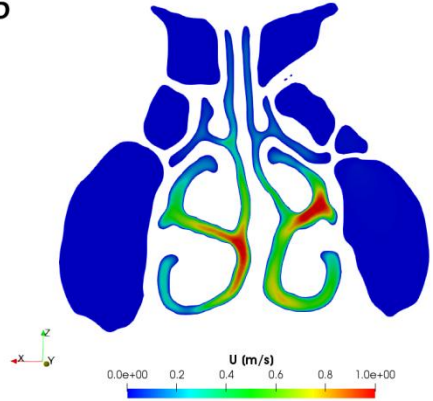
S7
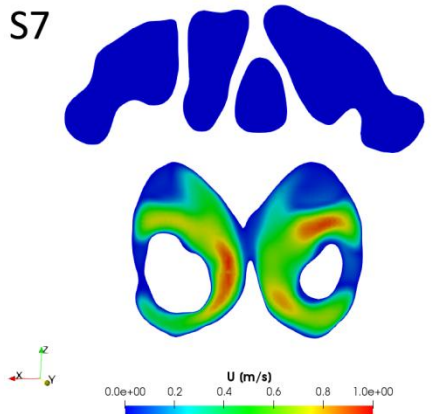
S8
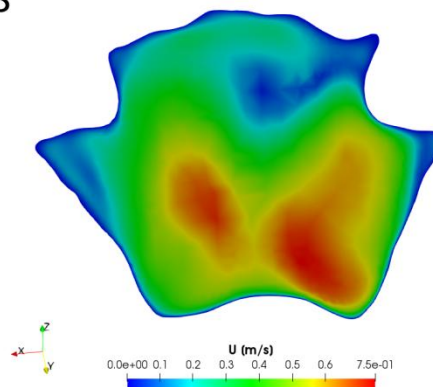
TYPE 4 NSD

S1

S2

S3

S4

S5

S6

S7

S8

55
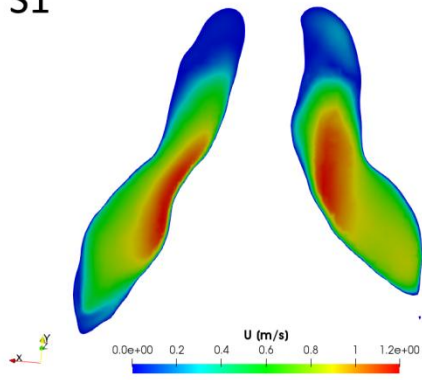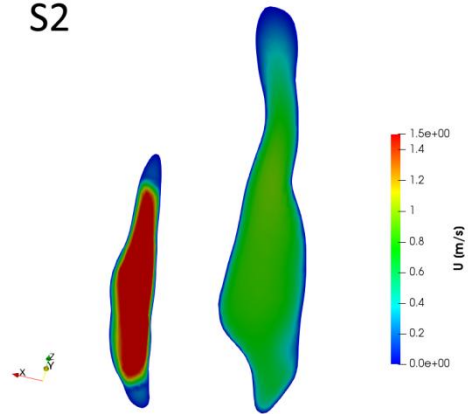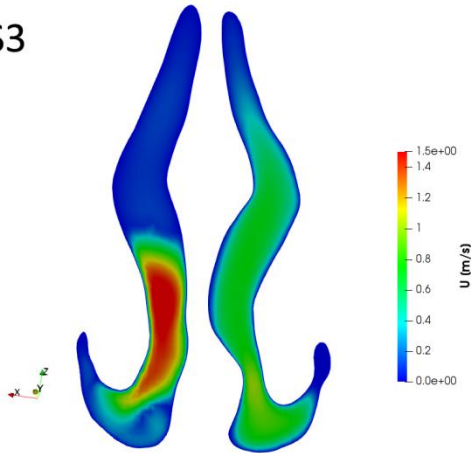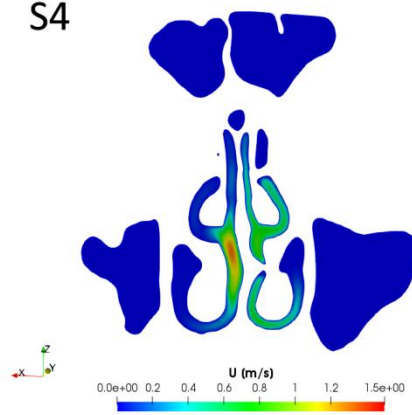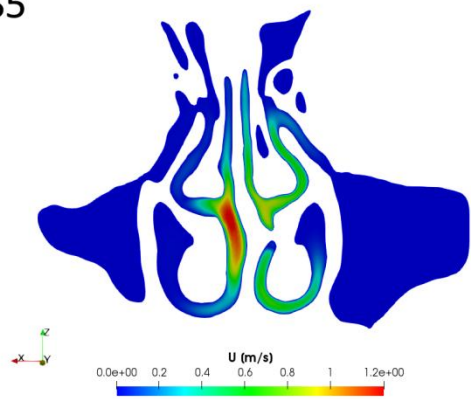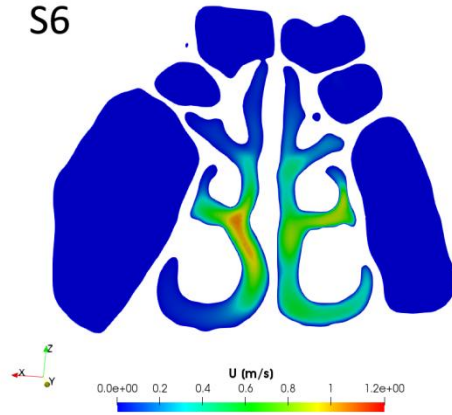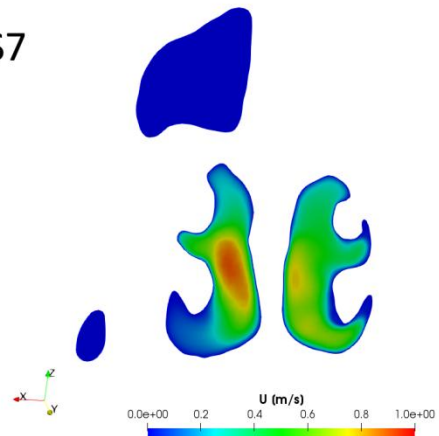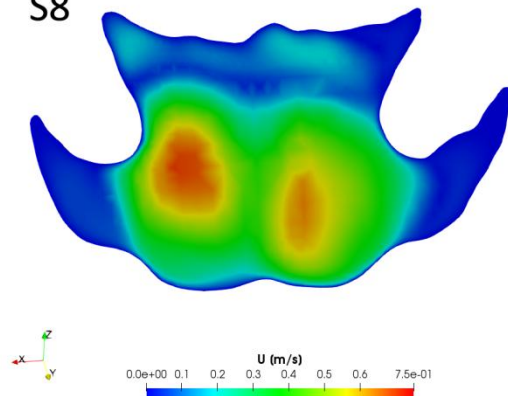
TYPE 5 NSD
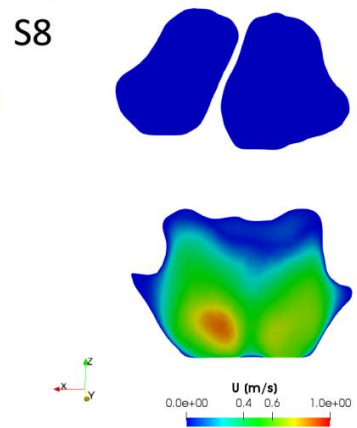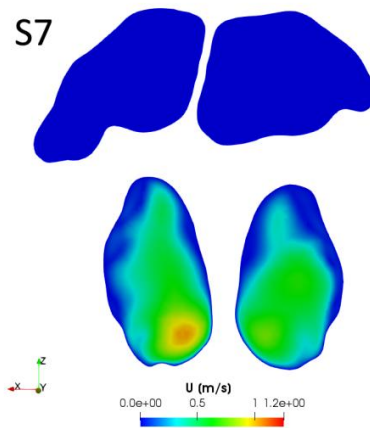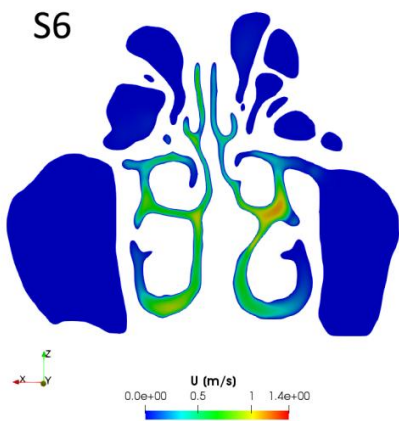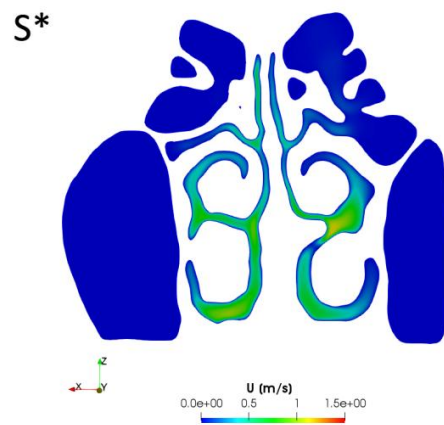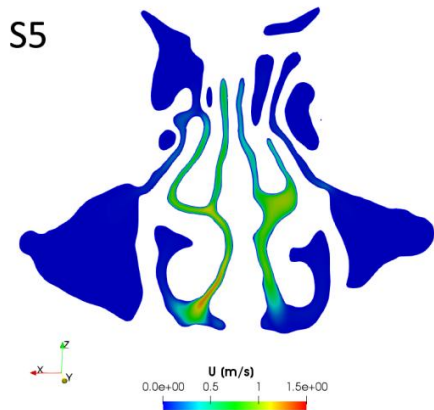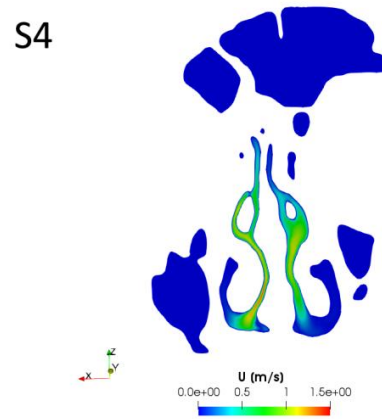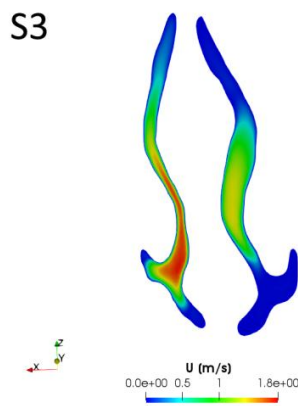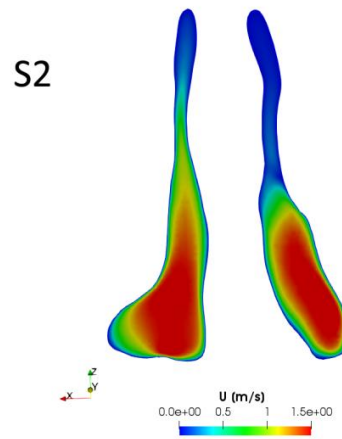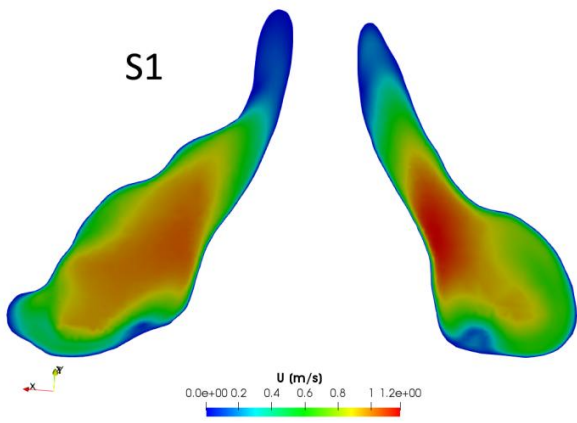
TYPE 6 NSD

S1

S2

S3

S4

S5

S6

S7

S8
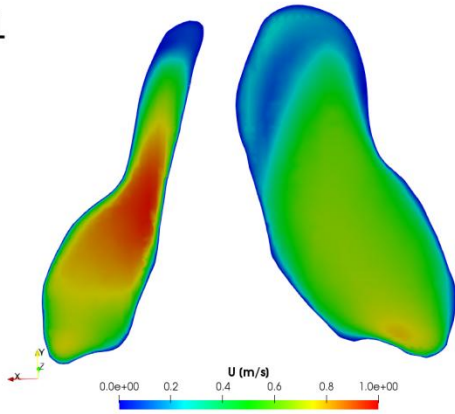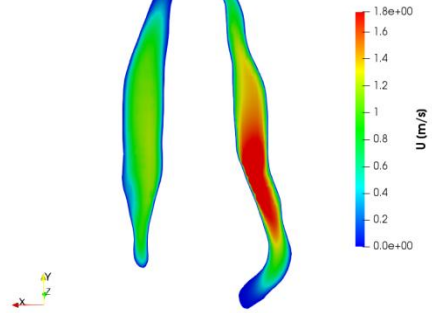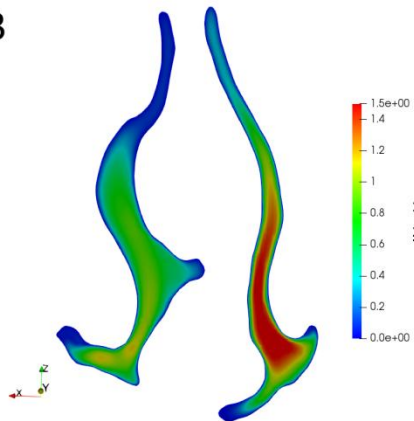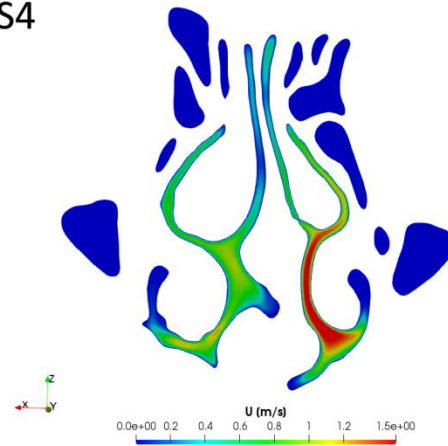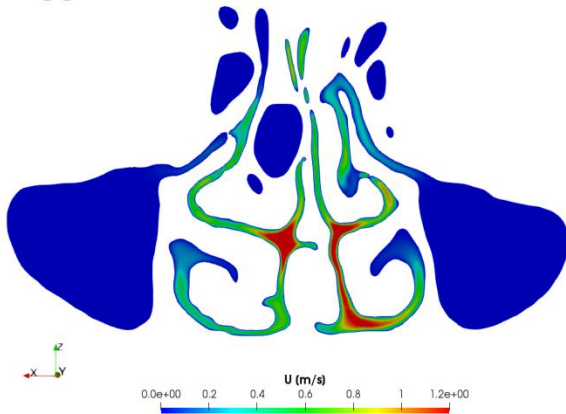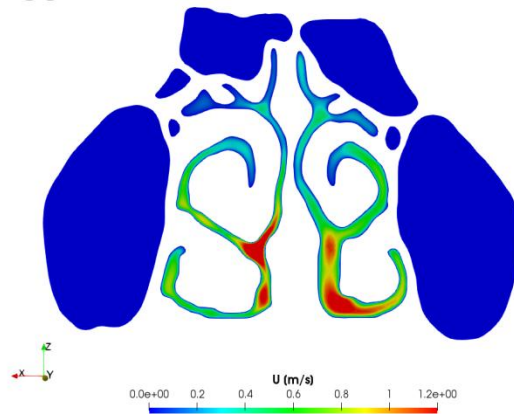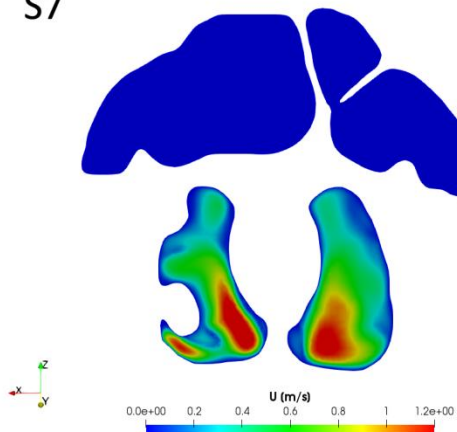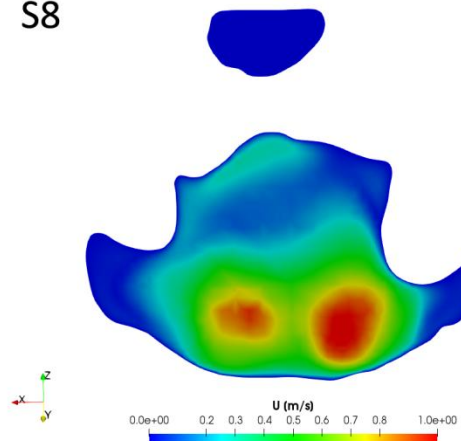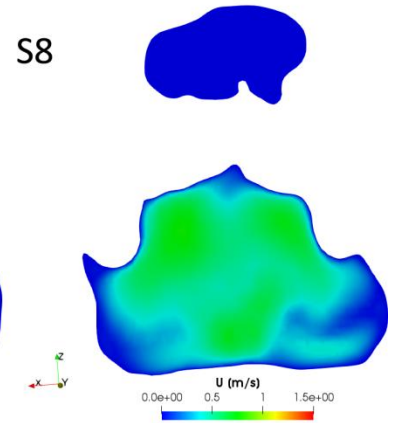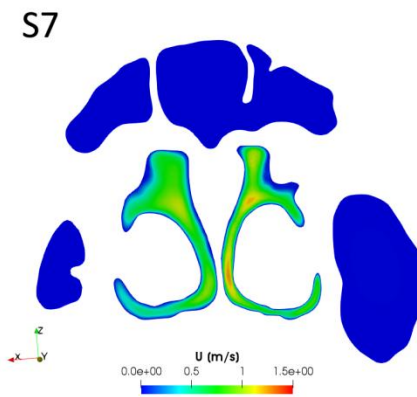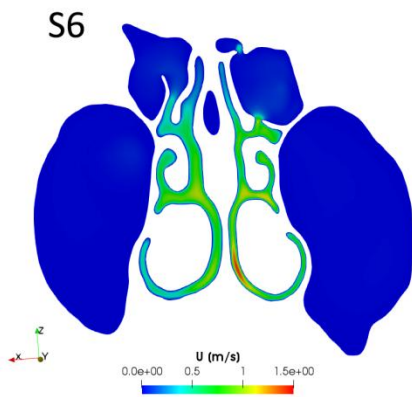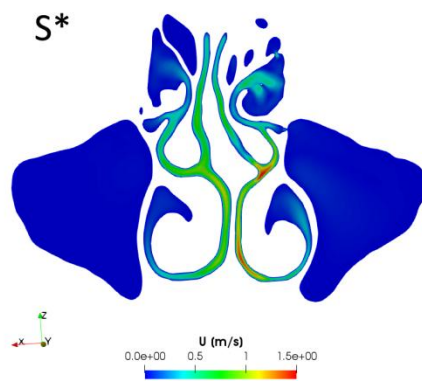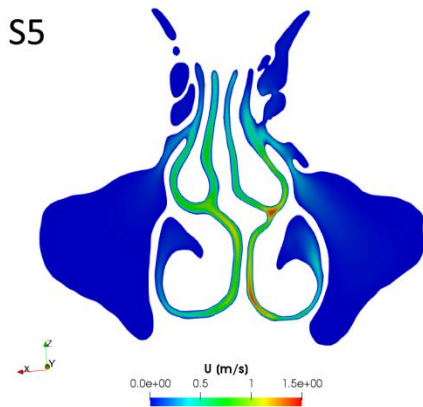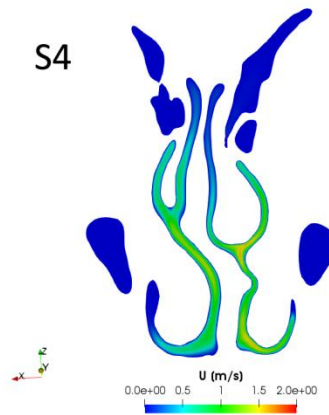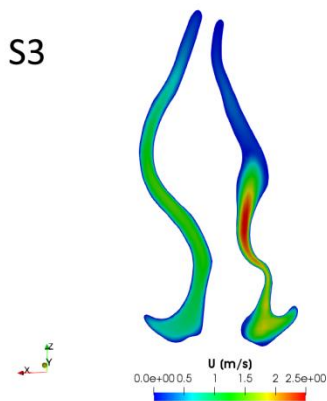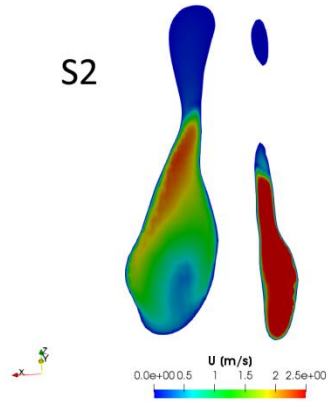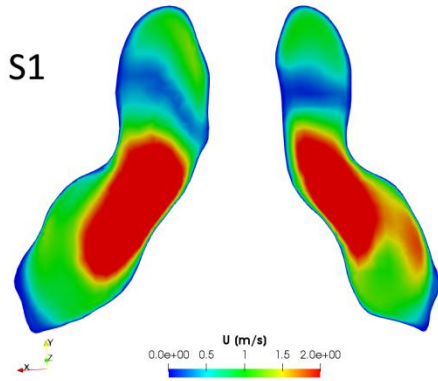
APPENDIX 2.

Figure 10. Airflow streamline distribution through the nasal cavity of a straight septum model and seven Mladina's NSD types

STRAIGHT SEPTUM MODEL

right lateral view   *left lateral view*

TYPE 1 NSD

right lateral view   *left anterolateral view*
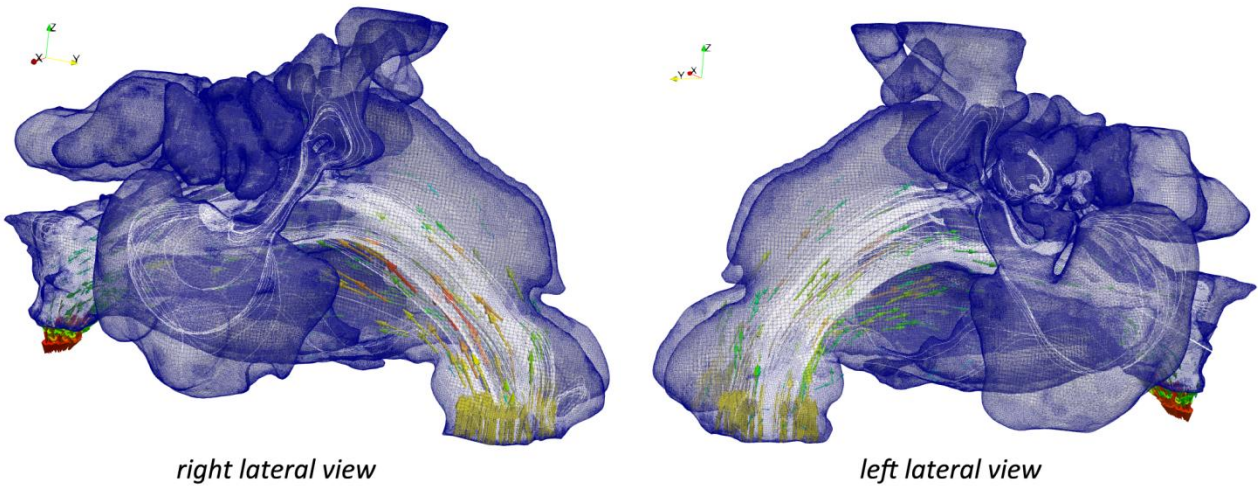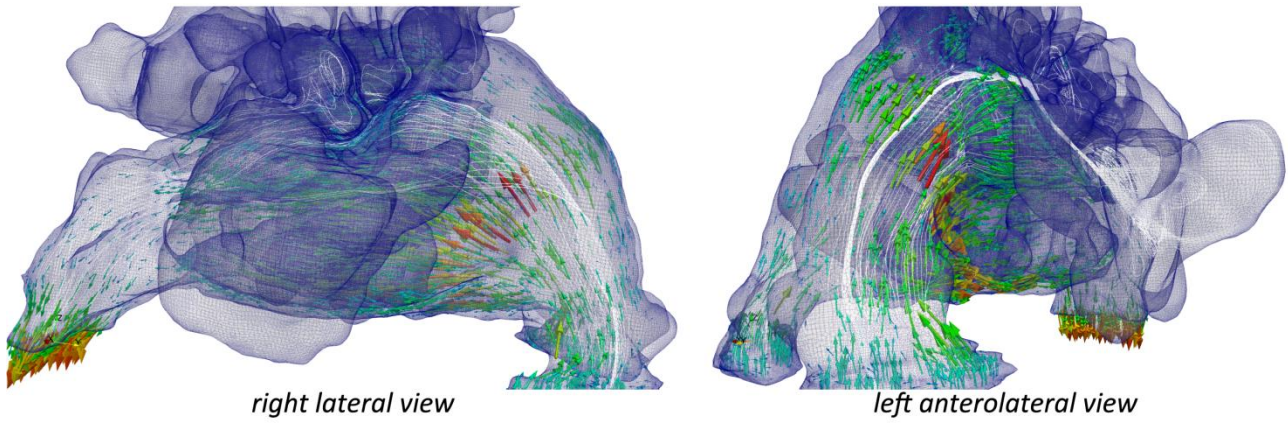
TYPE 2 NSD
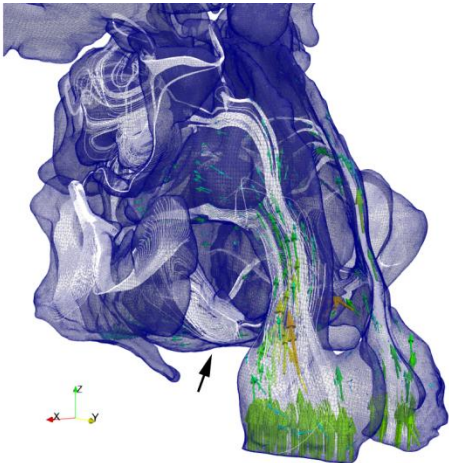
right anterolateral view
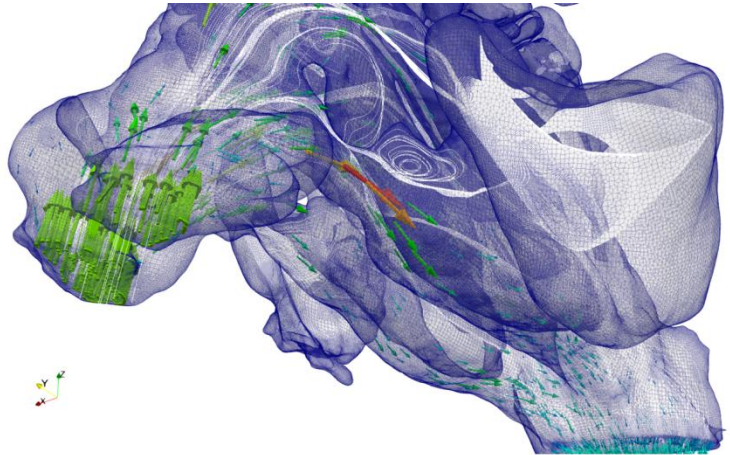
left inferolateral view
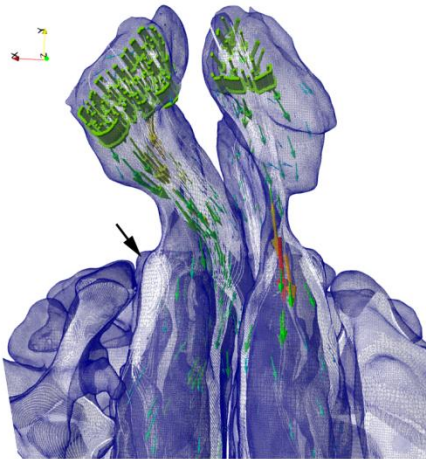
inferior view
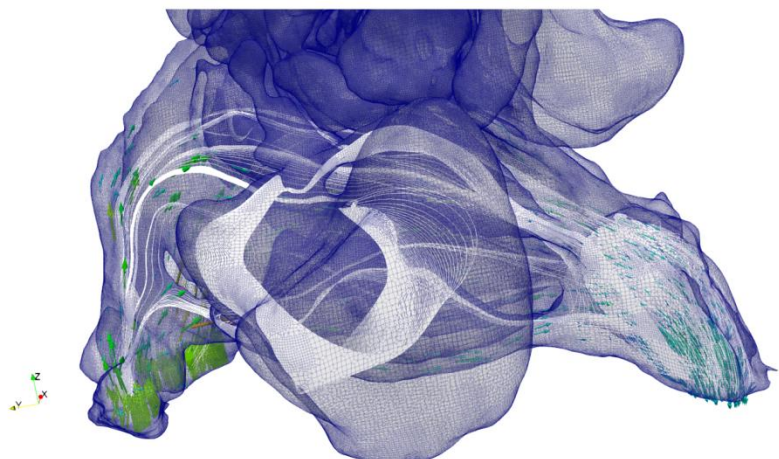
left lateral view

TYPE 3 NSD
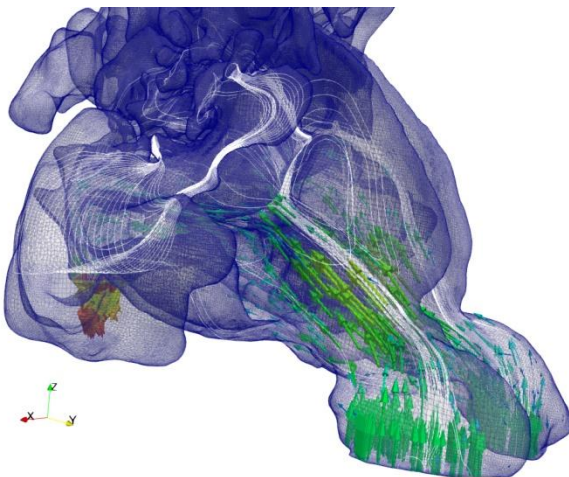
right anterolateral view
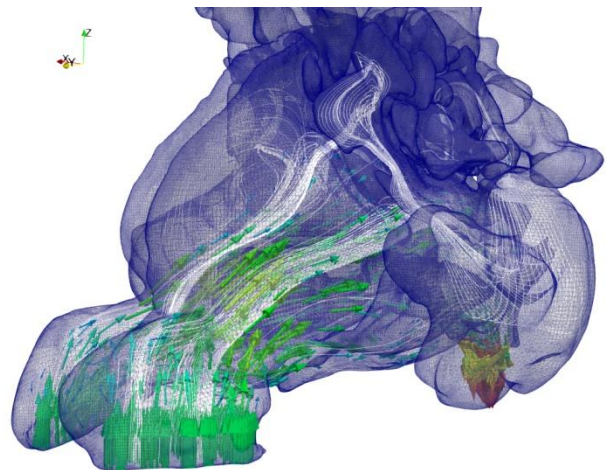
left anterolateral view

TYPE 4 NSD
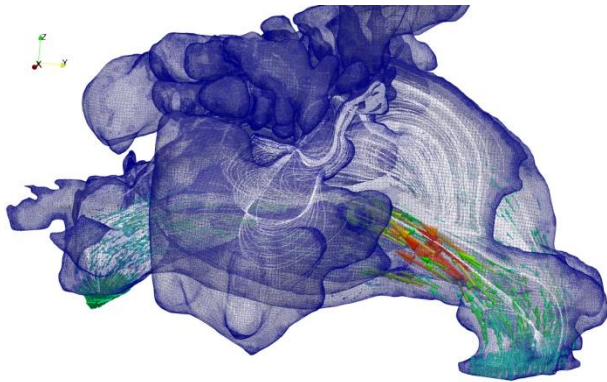
right lateral view
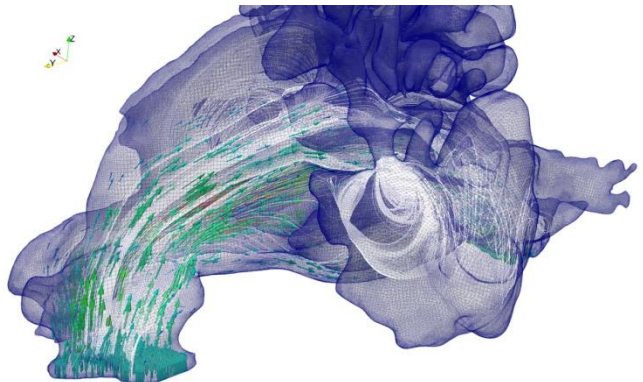
left lateral view

TYPE 5 NSD
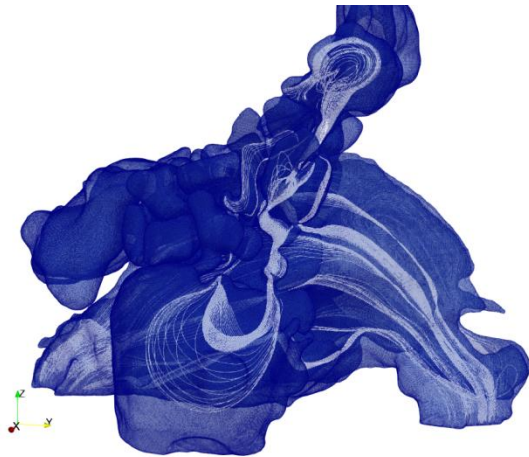
right lateral view
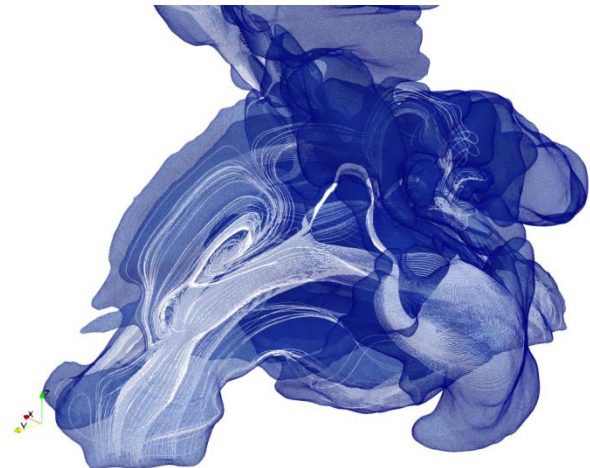
left anterolateral view
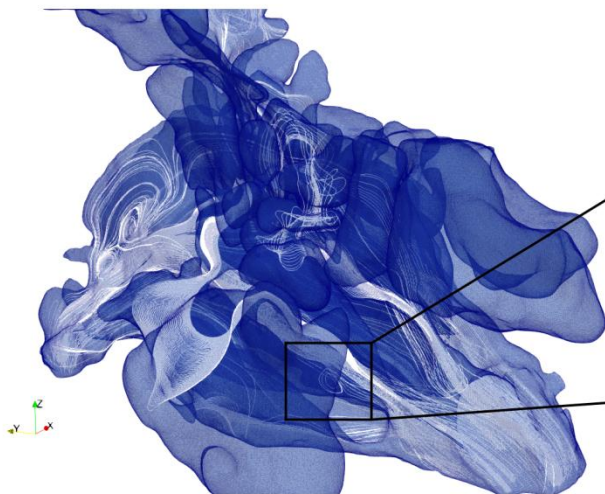
left posterolateral view
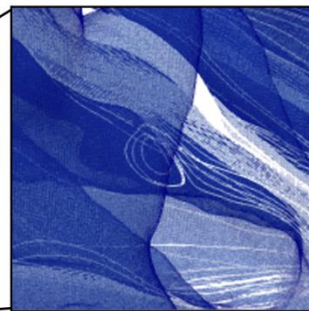
VORTEX
at the bony spur's tip

TYPE 6 NSD
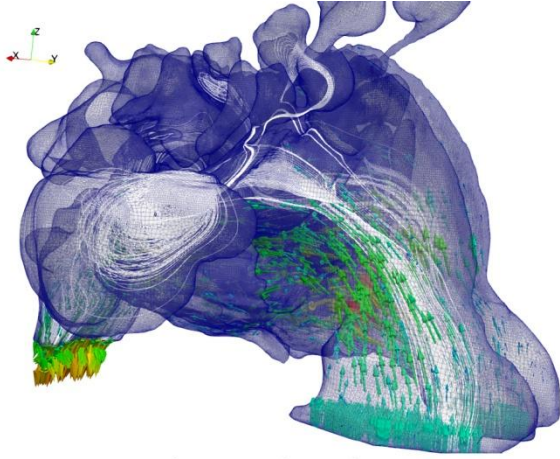
right anterolateral view
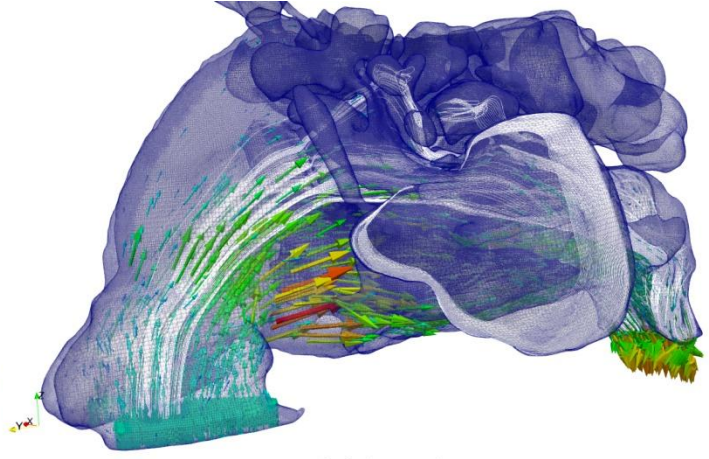
left lateral view

TYPE 7 NSD
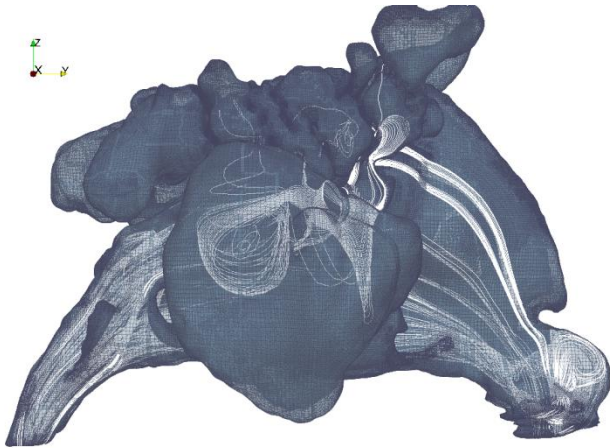
right lateral view

left lateral view

Figure 12. Distribution and magnitude of wall shear stress in a straight septum model and seven Mladina's NSD types

STRAIGHT SEPTUM MODEL

right lateral view

left lateral view

inferior view

TYPE 1 NSD

right lateral view

left lateral view

inferior view

TYPE 2 NSD

right lateral view

left lateral view

wallShearStress (Pa)

0.0e+00 0.05   0.1   0.15   0.2 2.5e-01

inferior view

TYPE 3 NSD

right lateral view

left lateral view

inferior view

wallShearStress (Pa)

2.5e-01

0.2

0.15

0.1

0.05

0.0e+00

TYPE 4 NSD

right lateral view

left lateral view

inferior view

TYPE 5 NSD

right lateral view

left lateral view

inferior view

TYPE 6 NSD

right lateral view

left lateral view

inferior view

wallShearStress (Pa)

2.5e-01
0.2
0.15
0.1
0.05
0.0e+00

TYPE 7 NSD

right lateral view

left lateral view

wallShearStress (Pa)

0.0e+00   0.1   0.15   0.2 2.5e-01

inferior view

Figure 14. Turbulent kinetic energy profile in a straight septum model and seven Mladina's NSD types at selected cross-sections along the nasal cavity

STRAIGHT SEPTUM MODEL

TYPE 1 NSD

S1

S2
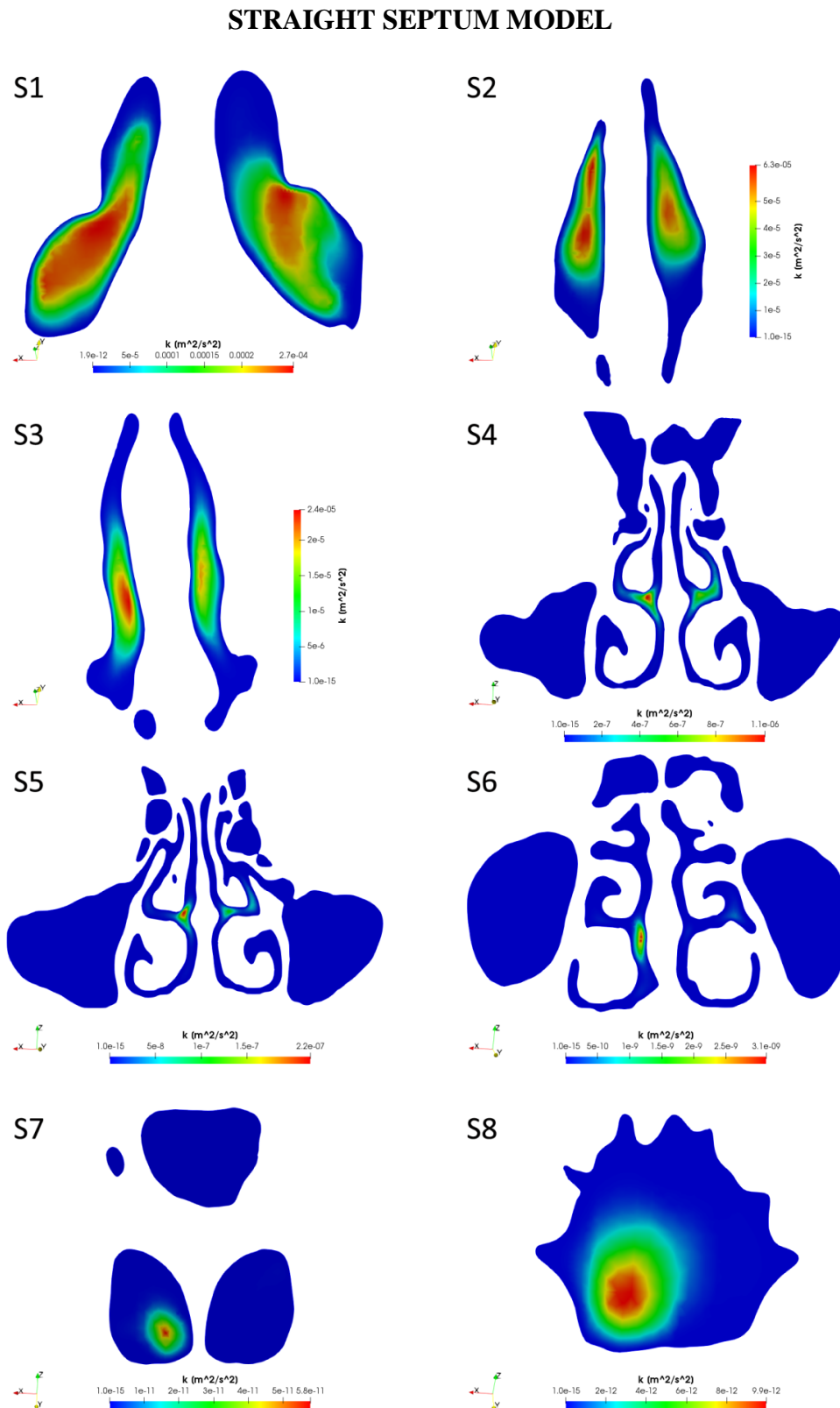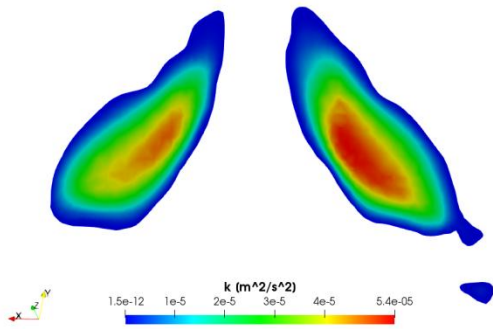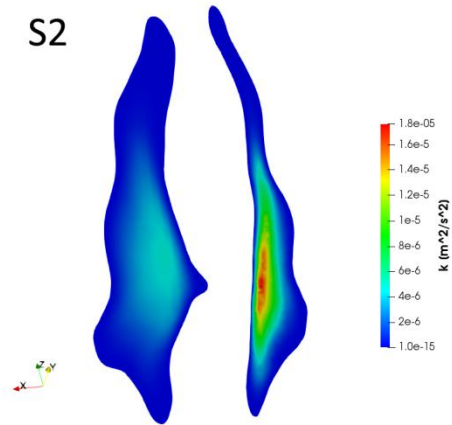
S3
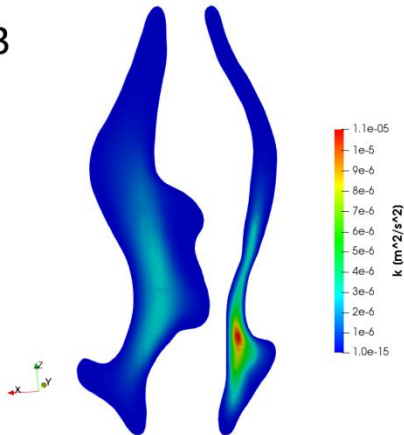
S4
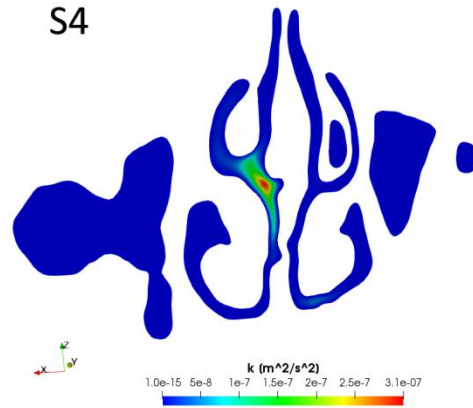
S5
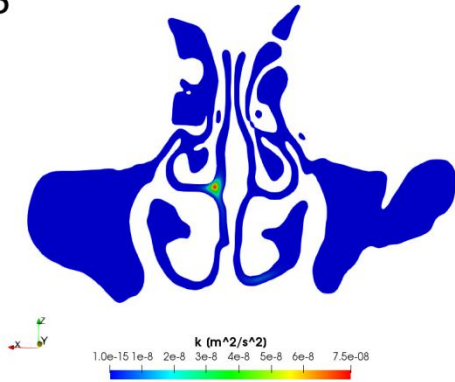
S6
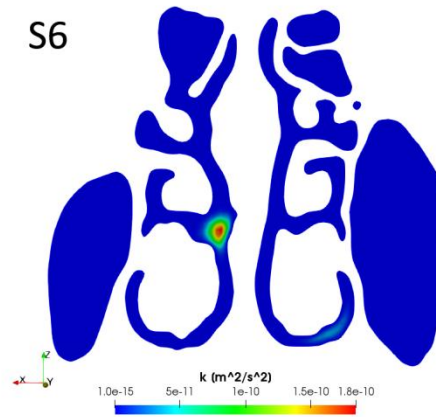
S7
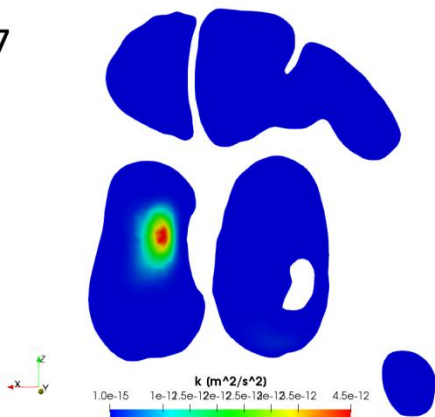
S8
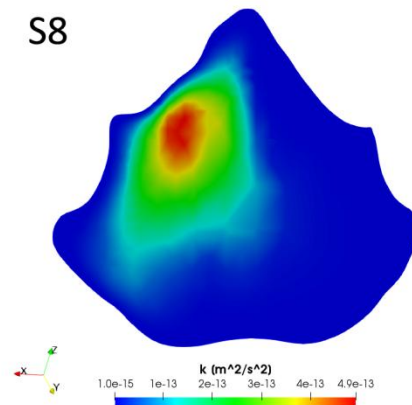
TYPE 2 NSD

S1

S2
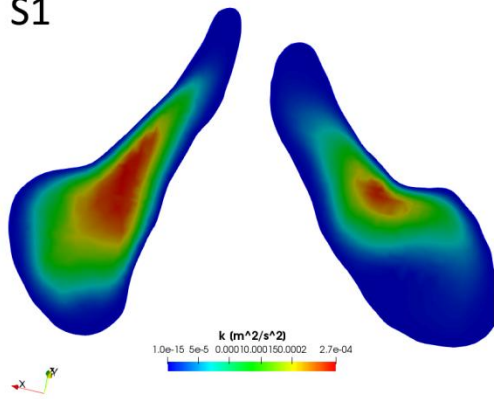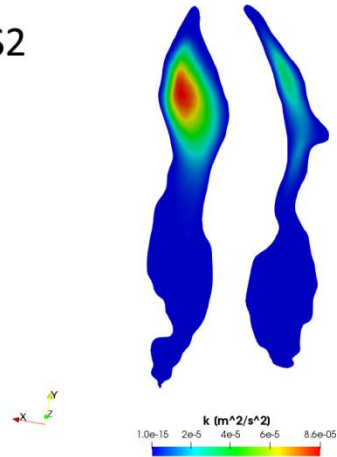
S3
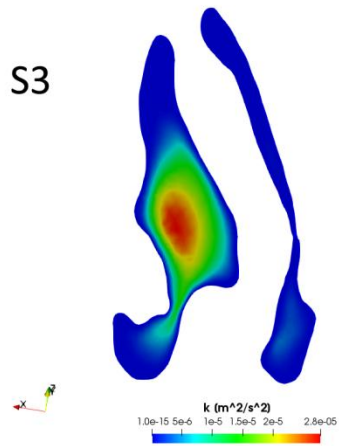
S4

S5
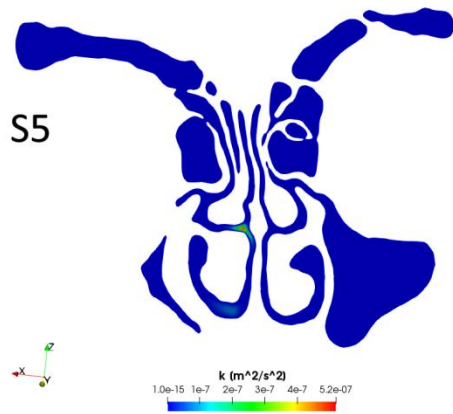
S6
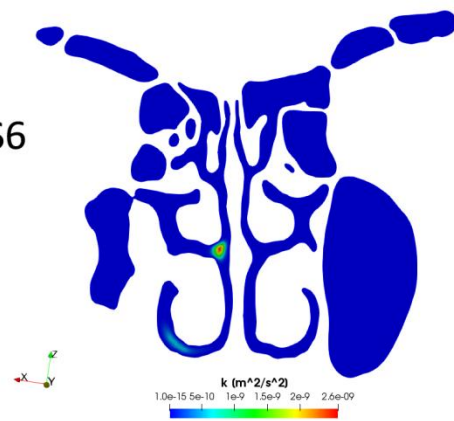
S7
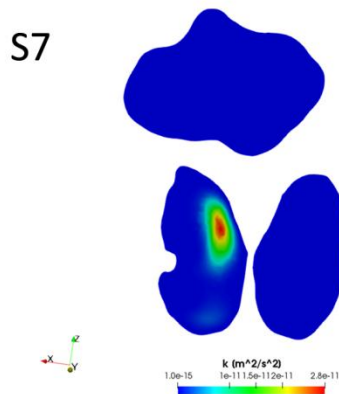
S8
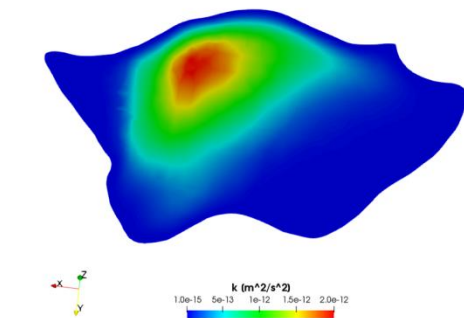
TYPE 3 NSD

S1
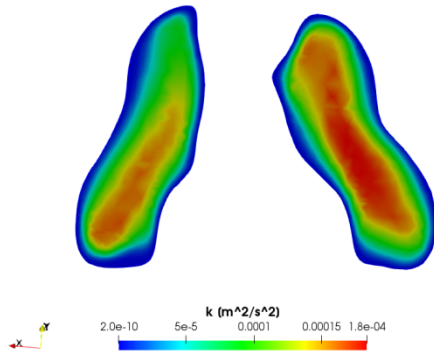
S2
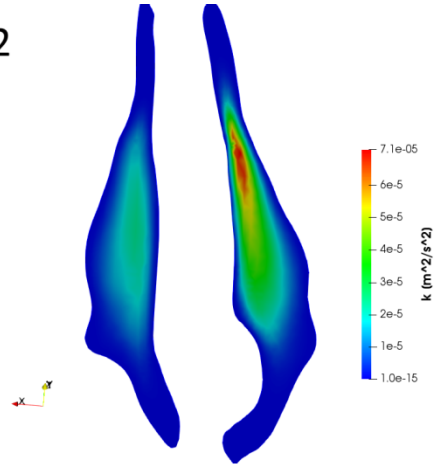
S3
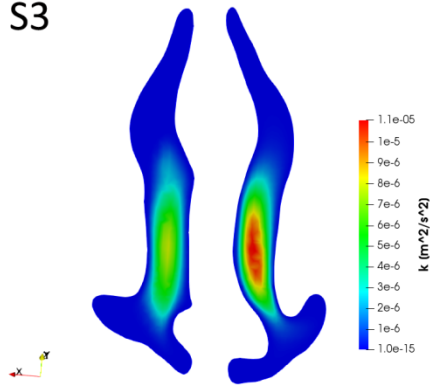
S4
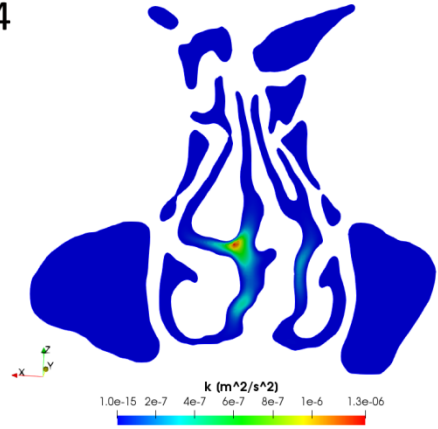
S5
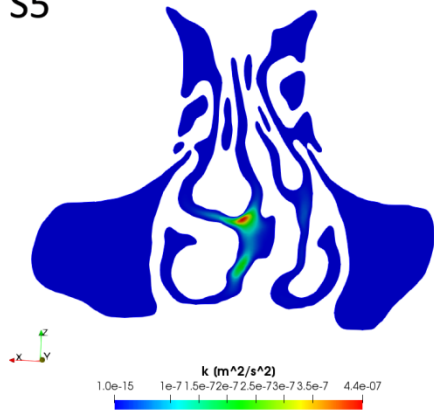
S6

S7

S8

TYPE 4 NSD

TYPE 5 NSD

S1

S2

S3

S4

S5

S*

S6

S7

S8

72
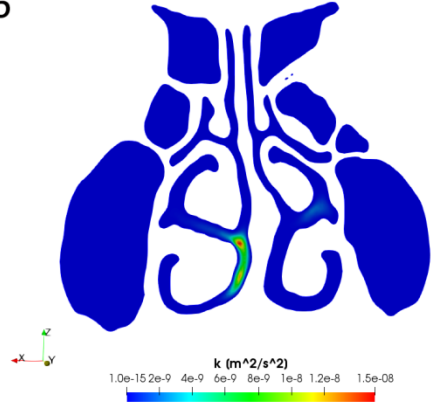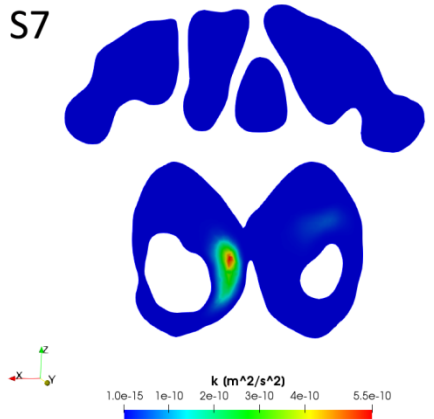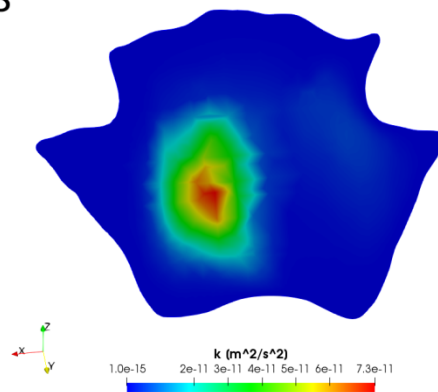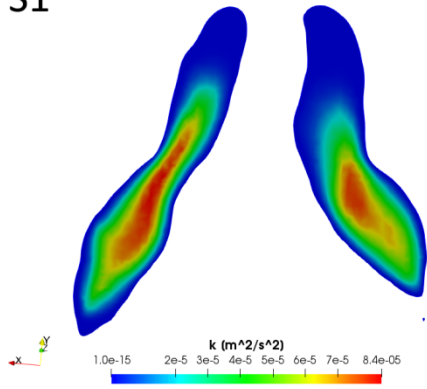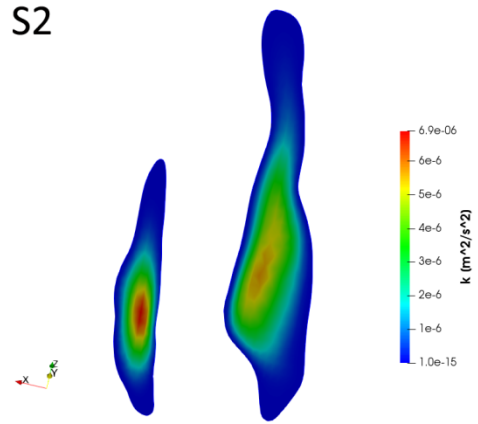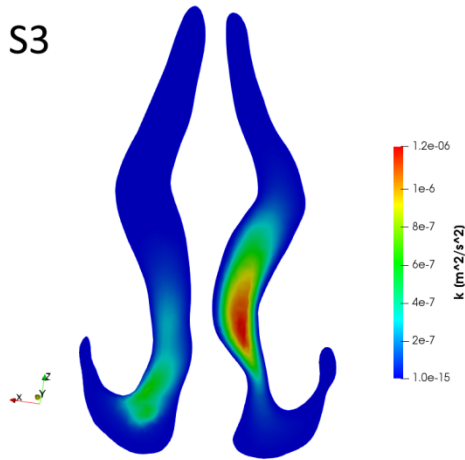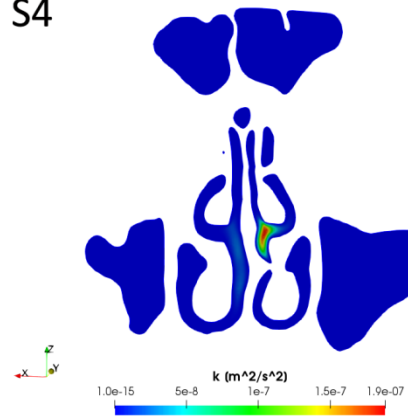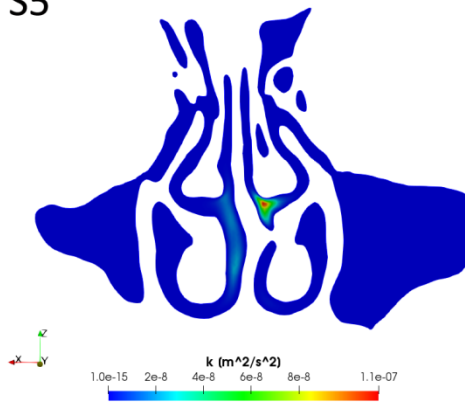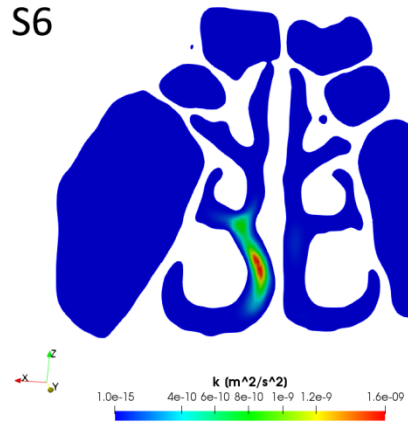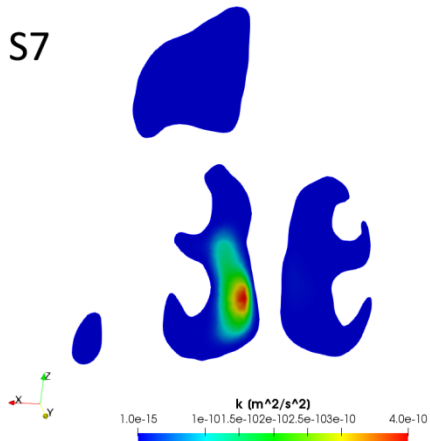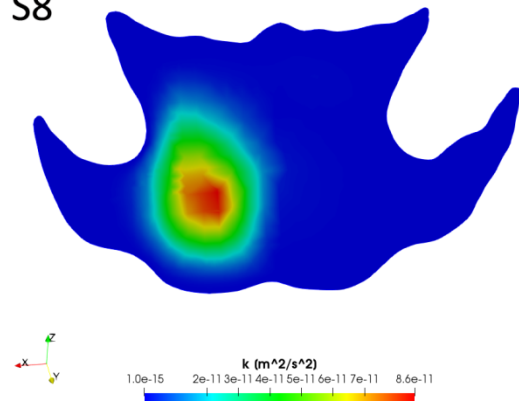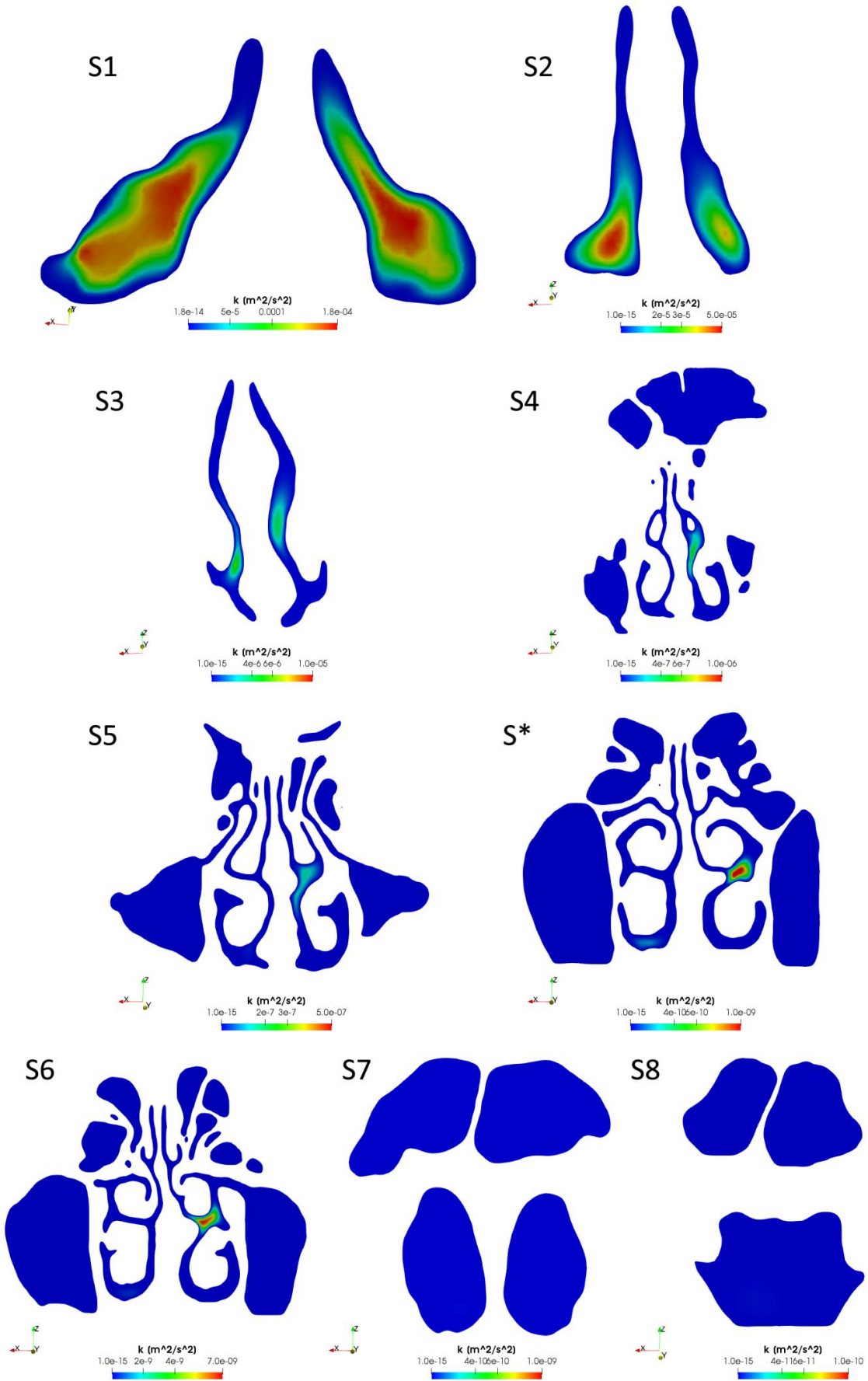
TYPE 6 NSD
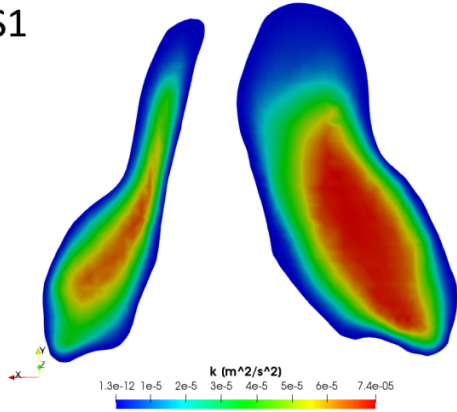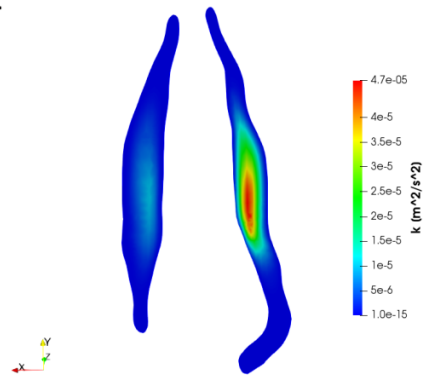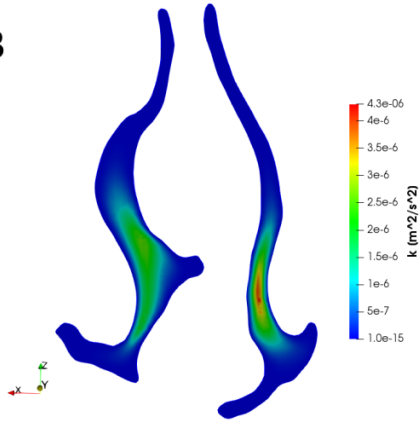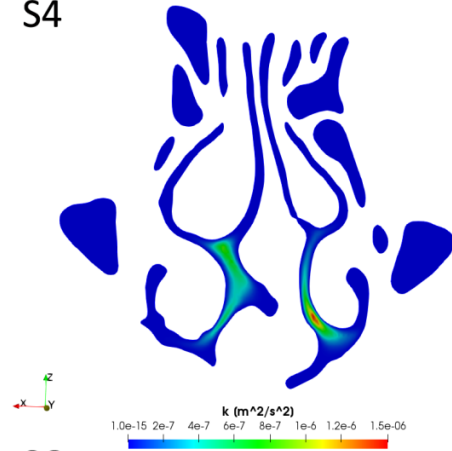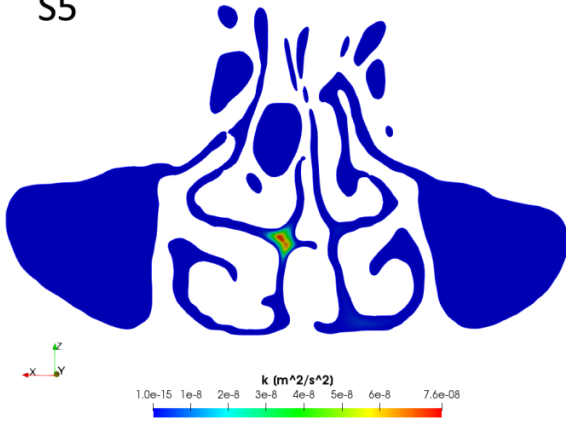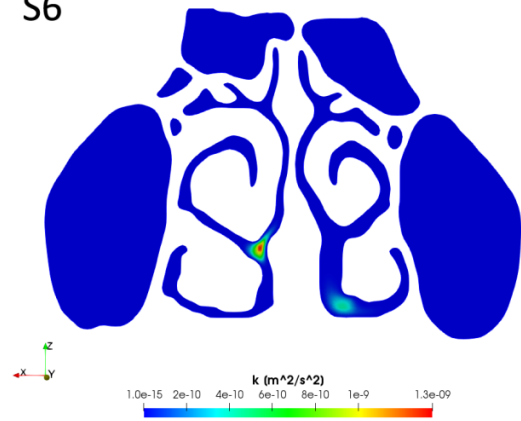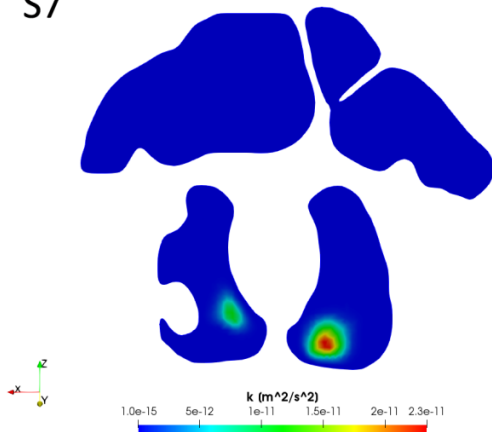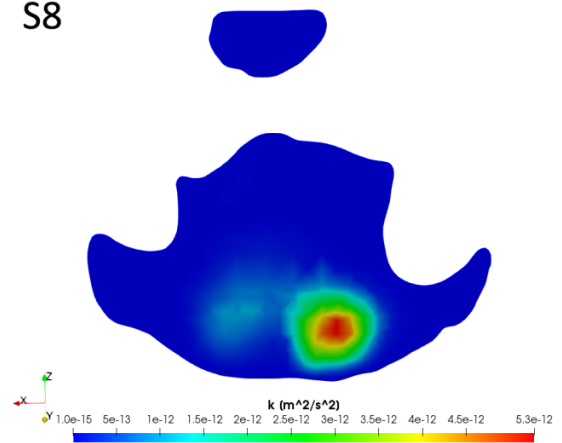
TYPE 7 NSD
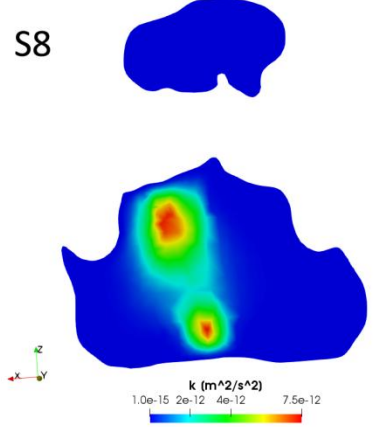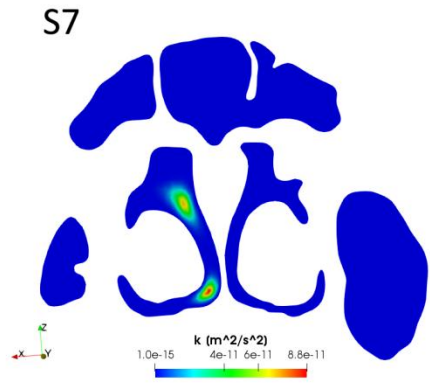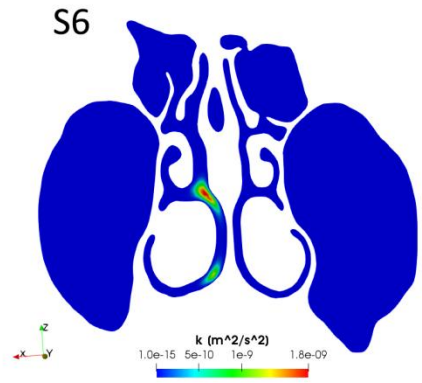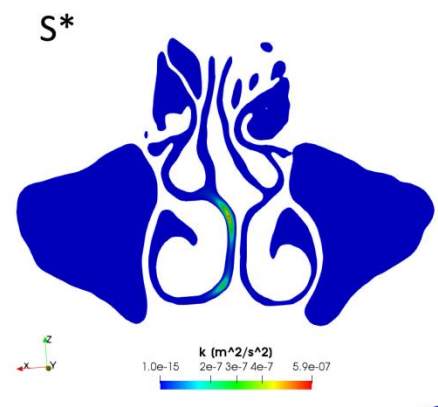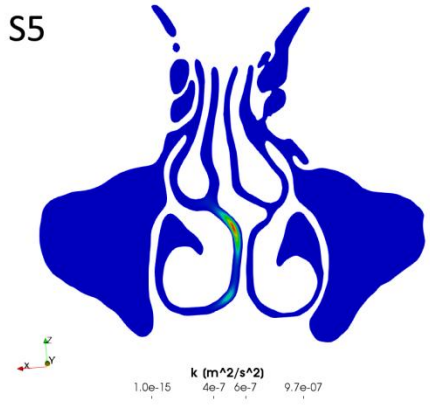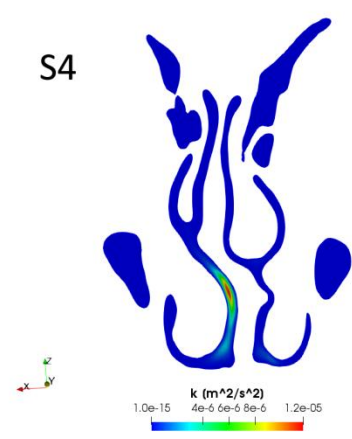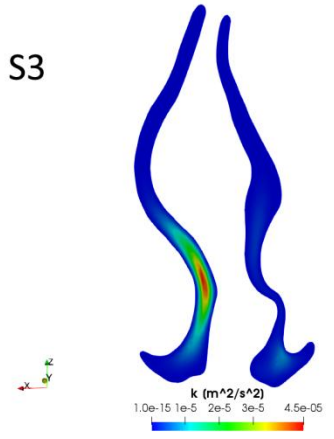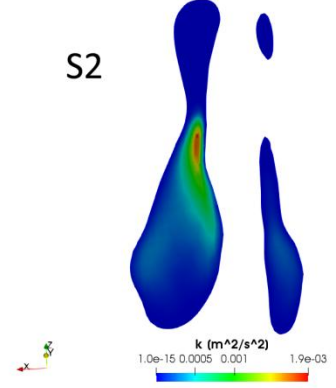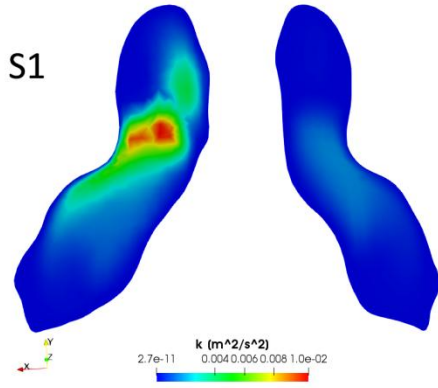
CURRICULUM VITAE

Dr. Nataša Janović (née Janjušević) was born in Belgrade on September 19th, 1985. She finished elementary school „Dušan Đurđević" in 2000 and Gymnasium in Mladenovac in 2004. In the same year, she was enrolled in the University of Belgrade - Faculty of Medicine and graduated in 2012 with GPA of 9.0/10. She was enrolled in Doctoral Studies (course: Skeletal biology) at the University of Belgrade - Faculty of Medicine in 2012/2013. In 2017, Dr. Janović was elected to the scientific position of a research associate. She participated in the DAAD scientific project between the Republic of Serbia and the Federal Republic of Germany in 2016-2017. Up to date, she published seven scientific papers as an author or co-author in peer-reviewed international journals indexed in the Journal Citation Report list. She was enrolled in a residency in diagnostic radiology at the University of Belgrade - Faculty of Medicine in 2017.

БИОГРАФИЈА КАНДИДАТА

Др Наташа Јановић (девојачко Јањушевић) рођена је 19. септембра 1985. године у Београду. Основну школу „Душан Ђурђевић“ завршила је 2000. године у Младеновцу, где је 2004. године завршила и Гимназију. Исте године се уписала на Медицински факултет у Београду. Дипломирала је 2012. године са просечном оценом 9,0 (девет). Докторске студије на Медицинском факултету у Београду, смер Биологија скелета на енглеском језику, уписала је 2012. године. Године 2017. стекла је научно звање *истраживач-сарадник*. Била је учесник ДААД пројекта у оквиру научне сарадње између Републике Србије и Савезне Републике Немачке у пројектном циклусу 2016-2017. године. Аутор је или коаутор 7 научних радова штампаних у целини у часописима индексираним у JCR листи. Специјализацију из Радиологије на Медицинском факултету у Београду започела је 2017. године.

Изјава о ауторству

Име и презиме аутора ___Наташа Јановић___

Број индекса ___DE 01/12___

Изјављујем

да је докторска дисертација под насловом

___Повезаност типова девијације носне преграде са тежином___
___опструкционих симптома и карактеристикама протока ваздуха___
___кроз носну дупљу___

- резултат сопственог истраживачког рада;
- да дисертација у целини ни у деловима није била предложена за стицање друге дипломе према студијским програмима других високошколских установа;
- да су резултати коректно наведени и
- да нисам кршио/ла ауторска права и користио/ла интелектуалну својину других лица.

Потпис аутора

У Београду, ___18. 12. 2020.___

Јановић Наташа

10

Изјава о истоветности штампане и електронске верзије докторског рада

Име и презиме аутора ___НАТАША ЈАНОВИЋ___

Број индекса ___DE 01/12___

Студијски програм ___ДОКТОРСКЕ АКАДЕМСКЕ СТУДИЈЕ МОДУЛ: БИОЛОГИЈА СКЕЛЕТА___

Наслов рада ___ПОВЕЗАНОСТ ТИПОВА ДЕВИЈАЦИЈЕ НОСНЕ ПРЕГРАДЕ СА ТЕЖИНОМ ОПСТРУКЦИОНИХ СИМПТОМА И КАРАКТЕРИСТИКАМА ПРОТОКА ВАЗДУХА КРОЗ НОСНУ ДУПЉУ___

Ментор ___Проф. др МАРИЈА ЂУРИЋ___

Изјављујем да је штампана верзија мог докторског рада истоветна електронској верзији коју сам предао/ла ради похрањивања у **Дигиталном репозиторијуму Универзитета у Београду.**

Дозвољавам да се објаве моји лични подаци везани за добијање академског назива доктора наука, као што су име и презиме, година и место рођења и датум одбране рада.

Ови лични подаци могу се објавити на мрежним страницама дигиталне библиотеке, у електронском каталогу и у публикацијама Универзитета у Београду.

Потпис аутора

У Београду, ___18.12.2020.___

Јановић Наташа

11

Изјава о коришћењу

Овлашћујем Универзитетску библиотеку „Светозар Марковић" да у Дигитални репозиторијум Универзитета у Београду унесе моју докторску дисертацију под насловом:

Повезаност типова девијације носне преграде са тежином опструкционих симптома и карактеристикама протока ваздуха кроз носну дупљу

која је моје ауторско дело.

Дисертацију са свим прилозима предао/ла сам у електронском формату погодном за трајно архивирање.

Моју докторску дисертацију похрањену у Дигиталном репозиторијуму Универзитета у Београду и доступну у отвореном приступу могу да користе сви који поштују одредбе садржане у одабраном типу лиценце Креативне заједнице (Creative Commons) за коју сам се одлучио/ла.

1. Ауторство (CC BY)

2. Ауторство – некомерцијално (CC BY-NC)

3. Ауторство – некомерцијално – без прерада (CC BY-NC-ND)

4. Ауторство – некомерцијално – делити под истим условима (CC BY-NC-SA)

5. Ауторство – без прерада (CC BY-ND)

6. Ауторство – делити под истим условима (CC BY-SA)

(Молимо да заокружите само једну од шест понуђених лиценци.
Кратак опис лиценци је саставни део ове изјаве).

Потпис аутора

У Београду, 18.12.2020.

Јанковић Наташа

12

1. **Ауторство**. Дозвољавате умножавање, дистрибуцију и јавно саопштавање дела, и прераде, ако се наведе име аутора на начин одређен од стране аутора или даваоца лиценце, чак и у комерцијалне сврхе. Ово је најслободнија од свих лиценци.

2. **Ауторство – некомерцијално**. Дозвољавате умножавање, дистрибуцију и јавно саопштавање дела, и прераде, ако се наведе име аутора на начин одређен од стране аутора или даваоца лиценце. Ова лиценца не дозвољава комерцијалну употребу дела.

3. **Ауторство – некомерцијално – без прерада**. Дозвољавате умножавање, дистрибуцију и јавно саопштавање дела, без промена, преобликовања или употребе дела у свом делу, ако се наведе име аутора на начин одређен од стране аутора или даваоца лиценце. Ова лиценца не дозвољава комерцијалну употребу дела. У односу на све остале лиценце, овом лиценцом се ограничава највећи обим права коришћења дела.

4. **Ауторство – некомерцијално – делити под истим условима**. Дозвољавате умножавање, дистрибуцију и јавно саопштавање дела, и прераде, ако се наведе име аутора на начин одређен од стране аутора или даваоца лиценце и ако се прерада дистрибуира под истом или сличном лиценцом. Ова лиценца не дозвољава комерцијалну употребу дела и прерада.

5. **Ауторство – без прерада**. Дозвољавате умножавање, дистрибуцију и јавно саопштавање дела, без промена, преобликовања или употребе дела у свом делу, ако се наведе име аутора на начин одређен од стране аутора или даваоца лиценце. Ова лиценца дозвољава комерцијалну употребу дела.

6. **Ауторство – делити под истим условима**. Дозвољавате умножавање, дистрибуцију и јавно саопштавање дела, и прераде, ако се наведе име аутора на начин одређен од стране аутора или даваоца лиценце и ако се прерада дистрибуира под истом или сличном лиценцом. Ова лиценца дозвољава комерцијалну употребу дела и прерада. Слична је софтверским лиценцама, односно лиценцама отвореног кода.